United States Nuclear Regulatory Commission

Protecting People and the Environment

NUREG/CR-7022, Vol. 1
PNNL-19418, Vol. 1

FRAPCON-3.4: A Computer Code for the Calculation of Steady-State, Thermal-Mechanical Behavior of Oxide Fuel Rods for High Burnup

Office of Nuclear Regulatory Research

AVAILABILITY OF REFERENCE MATERIALS IN NRC PUBLICATIONS

NRC Reference Material

As of November 1999, you may electronically access NUREG-series publications and other NRC records at NRC's Public Electronic Reading Room at http://www.nrc.gov/reading-rm.html. Publicly released records include, to name a few, NUREG-series publications; *Federal Register* notices; applicant, licensee, and vendor documents and correspondence; NRC correspondence and internal memoranda; bulletins and information notices; inspection and investigative reports; licensee event reports; and Commission papers and their attachments.

NRC publications in the NUREG series, NRC regulations, and *Title 10, Energy*, in the Code of *Federal Regulations* may also be purchased from one of these two sources.

1. The Superintendent of Documents
   U.S. Government Printing Office
   Mail Stop SSOP
   Washington, DC 20402–0001
   Internet: bookstore.gpo.gov
   Telephone: 202-512-1800
   Fax: 202-512-2250
2. The National Technical Information Service
   Springfield, VA 22161–0002
   www.ntis.gov
   1–800–553–6847 or, locally, 703–605–6000

A single copy of each NRC draft report for comment is available free, to the extent of supply, upon written request as follows:

Address: U.S. Nuclear Regulatory Commission
Office of Administration
Publications Branch
Washington, DC 20555-0001
E-mail: DISTRIBUTION.RESOURCE@NRC.GOV
Facsimile: 301–415–2289

Some publications in the NUREG series that are posted at NRC's Web site address http://www.nrc.gov/reading-rm/doc-collections/nuregs are updated periodically and may differ from the last printed version. Although references to material found on a Web site bear the date the material was accessed, the material available on the date cited may subsequently be removed from the site.

Non-NRC Reference Material

Documents available from public and special technical libraries include all open literature items, such as books, journal articles, and transactions, *Federal Register* notices, Federal and State legislation, and congressional reports. Such documents as theses, dissertations, foreign reports and translations, and non-NRC conference proceedings may be purchased from their sponsoring organization.

Copies of industry codes and standards used in a substantive manner in the NRC regulatory process are maintained at—

The NRC Technical Library
Two White Flint North
11545 Rockville Pike
Rockville, MD 20852–2738

These standards are available in the library for reference use by the public. Codes and standards are usually copyrighted and may be purchased from the originating organization or, if they are American National Standards, from—

American National Standards Institute
11 West 42nd Street
New York, NY 10036–8002
www.ansi.org
212–642–4900

Legally binding regulatory requirements are stated only in laws; NRC regulations; licenses, including technical specifications; or orders, not in NUREG-series publications. The views expressed in contractor-prepared publications in this series are not necessarily those of the NRC.

The NUREG series comprises (1) technical and administrative reports and books prepared by the staff (NUREG–XXXX) or agency contractors (NUREG/CR–XXXX), (2) proceedings of conferences (NUREG/CP–XXXX), (3) reports resulting from international agreements (NUREG/IA–XXXX), (4) brochures (NUREG/BR–XXXX), and (5) compilations of legal decisions and orders of the Commission and Atomic and Safety Licensing Boards and of Directors' decisions under Section 2.206 of NRC's regulations (NUREG–0750).

DISCLAIMER: This report was prepared as an account of work sponsored by an agency of the U.S. Government. Neither the U.S. Government nor any agency thereof, nor any employee, makes any warranty, expressed or implied, or assumes any legal liability or responsibility for any third party's use, or the results of such use, of any information, apparatus, product, or process disclosed in this publication, or represents that its use by such third party would not infringe privately owned rights.

United States Nuclear Regulatory Commission

Protecting People and the Environment

NUREG/CR-7022, Vol. 1
PNNL-19418, Vol. 1

FRAPCON-3.4: A Computer Code for the Calculation of Steady-State Thermal-Mechanical Behavior of Oxide Fuel Rods for High Burnup

Manuscript Completed: August 2010
Date Published: March 2011

Prepared by
K.J. Geelhood, W.G. Luscher, C.E. Beyer

Pacific Northwest National Laboratory
P.O. Box 999
Richland, WA 99352

M.E. Flanagan, NRC Project Manager

NRC Job Code N6609

Office of Nuclear Regulatory Research

Abstract

FRAPCON-3 is a Fortran 90 computer code that calculates the steady-state response of light-water reactor fuel rods during long-term burnup. The code calculates the temperature, pressure, and deformation of a fuel rod as functions of time-dependent fuel rod power and coolant boundary conditions. The phenomena modeled by the code include 1) heat conduction through the fuel and cladding to the coolant; 2) cladding elastic and plastic deformation; 3) fuel-cladding mechanical interaction; 4) fission gas release from the fuel and rod internal pressure; and 5) cladding oxidation. The code contains necessary material properties, water properties, and heat-transfer correlations. FRAPCON-3 is programmed for use on Windows-based computers, but the source code may be compiled on any computer with a Fortran 90 compiler.

The FRAPCON-3 code is designed to generate initial conditions for transient fuel rod analysis by the FRAPTRAN computer code.

This document describes FRAPCON-3.4a, which is the latest version of FRAPCON-3, released April 13, 2010.

Foreword

Computer codes related to fuel performance have played an important role in the work of the U.S. Nuclear Regulatory Commission (NRC) since the agency's inception in 1975. Formal requirements for fuel performance analysis appear in several of the agency's regulatory guides and regulations, including those related to emergency core cooling system evaluation models, as set forth in Appendix K to Title 10, Part 50, of the *Code of Federal Regulations* (10 CFR Part 50), "Domestic Licensing of Production and Utilization Facilities."

This document describes the latest version of NRC's steady state fuel performance code, FRAPTCON 3.4. This code provides the ability to accurately calculate the long-term burnup response of a single light-water reactor fuel rod, accomplishing a key objective of the NRC's reactor safety research program. The FRAPCON code serves as an independent audit tool in NRC's review of industry fuel performance codes. FRAPCON is also a companion code to the FRAPTRAN code (Geelhood et al., 2010b) developed to calculate the response of a fuel rod under transient conditions.

The latest version of FRAPCON updates material properties, incorporates a new fission gas release model that predicts grain boundary gas content for FRAPTRAN 1.4 initialization, and updates the radial power profile model for gadolinium doped fuel. These updates keep the code consistent with the most recent experimental data and industry trends.

Contents

Abstract iii
Foreword v
List of Figures ix
List of Tables xi
Executive Summary xiii
Abbreviations xv
1.0 Introduction 1.1
1.1 Objectives of the FRAPCON Series 1.1
1.2 Limitations of FRAPCON-3 ..... 1.2
1.3 Report Outline and Relation to Other Reports 1.3
2.0 General Modeling Descriptions 2.1
2.1 FRAPCON-3 Solution Scheme 2.1
2.2 Coupling of Thermal and Mechanical Models 2.2
2.3 Fuel Rod Thermal Response 2.3
2.3.1 Coolant Conditions 2.5
2.3.2 Fuel Rod Surface Temperature 2.6
2.3.3 Cladding Temperature Gradient 2.8
2.3.4 Fuel-Cladding Gap Temperature Gradient 2.8
2.3.4.1 Radiant Heat Transfer 2.8
2.3.4.2 Conduction Through the Interfacial Gas 2.9
2.3.4.3 Conduction Through Points of Contact 2.10
2.3.5 Fuel Pellet Heat Conduction Model 2.10
2.3.5.1 The Finite Difference Approach 2.11
2.3.5.2 Mesh Point Layout 2.11
2.3.5.3 Difference Approximation at Internal Mesh Points 2.13
2.3.5.4 Difference Approximation at Boundaries 2.14
2.3.5.5 Radial Power Profile 2.15
2.3.5.6 Thermal Conductivity and Iteration Procedures 2.18
2.3.5.7 The Finite Difference Temperature Calculation 2.20
2.3.6 Plenum Gas Temperature 2.20
2.3.7 Stored Energy 2.22
2.4 Fuel Rod Mechanical Response 2.23
2.4.1 The FRACAS-I Model 2.23
2.4.1.1 General Theory and Method of Solution 2.24
2.4.1.2 Rigid Pellet Cladding Deformation Model 2.33
2.4.1.3 Updated MATPRO Cladding Mechanical Properties Models 2.45
2.5 Fission Gas Release and Fuel Rod Internal Gas Pressure Response 2.53
2.5.1 Fuel Rod Internal Gas Pressure 2.53
2.5.2 Fission Gas Production 2.54
2.5.3 Fuel Rod Gas Release 2.55
2.5.3.1 ANS-5.4 Gas Release Model 2.55
2.5.3.2 Modified Forsberg-Massih Model 2.56
2.5.3.3 FRAPFGR Model 2.60
2.5.4 Nitrogen Release 2.65
2.5.5 Helium Production and Release 2.66
2.5.6 Fuel Rod Void Volumes 2.68
2.5.6.1 Pellet Dish Volume 2.68
2.5.6.2 Interface Volume 2.68

2.5.6.3 Fuel-Cladding Gap Volume 2.69
2.5.6.4 Fuel Crack Volume 2.69
2.5.6.5 Plenum Volume 2.69
2.5.6.6 Open Porosity Volume 2.69
2.5.6.7 Roughness Volume 2.70
2.5.6.8 Central Hole Volume 2.70
2.6 Waterside Corrosion and Hydrogen Pickup 2.70
2.6.1 PWR and BWR Waterside Corrosion Models 2.70
2.6.2 Hydrogen Pickup Fraction 2.73
3.0 General Code Description 3.1
3.1 Code Structure and Solution Routine 3.1
3.1.1 Code Structure 3.1
3.1.2 Solution Scheme 3.1
3.2 Code Results 3.5
3.2.1 Fuel Rod Response 3.5
3.2.2 Plot Package 3.6
3.2.3 FRAPTRAN Initialization 3.6
3.3 Features of FRAPCON-3 ..... 3.6
3.3.1 Code Solution 3.6
3.3.2 Excel Input Generator 3.6
3.3.3 Uncertainty Analysis 3.7
4.0 References 4.1
Appendix A Input Instructions for the FRAPCON-3 Code A.1
Appendix B List of Subroutines in FRAPCON-3 ..... B.1
Appendix C Instruction for using Excel Plot Routine for FRAPCON-3 ..... C.1

List of Figures

Figure 2.1 Simplified FRAPCON-3 flowchart 2.2
Figure 2.2 Flow chart of the fuel and cladding temperature calculation 2.4
Figure 2.3 Schematic of the fuel rod temperature distribution 2.5
Figure 2.4 Mesh point layout 2.12
Figure 2.5 Typical mesh points 2.12
Figure 2.6 Boundary mesh points 2.12
Figure 2.7 Typical isothermal stress-strain curve 2.25
Figure 2.8 Schematic of the method of successive elastic solutions 2.28
Figure 2.9 Cladding creep strain as a function of time and hoop stress for 630°F and flux=10^{18} n/m²/s for (a) SRA Zircaloy and (b) RXA Zircaloy 2.32
Figure 2.10 Fuel rod geometry and coordinates 2.36
Figure 2.11 Calculation of effective stress σ_e from $d\varepsilon^P$ 2.38
Figure 2.12 Idealized stress-strain behavior 2.43
Figure 2.13 Computing stress 2.45
Figure 2.14 Predicted vs. measured yield stress from the PNNL database ($293K \leq T \leq 755K$), $0 \leq \Phi \leq 14x10^{25}$ n/m^2, $0 \leq H_{ex} \leq 850$ ppm 2.49
Figure 2.15 Interpellet void volume 2.51
Figure 2.16 Power and burnup dependence of the FRAPCON-3 relocation model 2.53
Figure 2.17 Modeling the pellet high burnup rim structure in FRAPFGR 2.61
Figure 3.1 FRAPCON-3 flowchart 3.2
Figure 3.2 Calling sequence for FRAPCON-3 subroutines 3.3

List of Tables

Table 1.1 Roadmap to documentation of models and properties in NRC fuel performance codes, FRAPCON-3.4 and FRAPTRAN 1.4 ..... 1.3
Table 2.1 Fission and capture cross sections used in FRAPCON-3 ..... 2.17
Table 2.2 Summary of FRACAS-I governing equations 2.27
Table 2.3 Parameters for FRAPCON-3.4 creep equation for SRA and RXA cladding 2.31
Table 2.4 Fitting parameters for helium production in MOX 2.67
Table 3.1 Major FRAPCON-3 packages 3.1
Table 3.2 Initialization subroutines 3.3
Table 3.3 Subroutines in the time-step loop 3.4
Table 3.4 Subroutines in the gas-release loop 3.4
Table 3.5 Subroutines in the axial-node loop 3.4
Table 3.6 Subroutines in the gap conductance loop 3.5

Executive Summary

The fuel performance code, FRAPCON-3, has been developed for the U.S. Nuclear Regulatory Commission by Pacific Northwest National Laboratory for calculating steady-state fuel behavior at high burnup (up to rod-average burnup of 62 gigawatt-days per metric ton of uranium, depending on application). The code has been significantly modified since the release of FRAPCON-3 v1.0 in 1997. This document is Volume 1 of a two-volume series that describes the current version, FRAPCON-3.4. Volume 1 contains: 1) code limitations and structure; 2) fuel performance model summaries; and 3) code input instructions and features to aid the user. Volume 2 (Geelhood et al., 2010a) provides a code assessment based on comparisons of code predictions to integral performance data up to high burnups.

The FRAPCON-3 code is designed to perform steady-state fuel rod calculations and generate initial input conditions for FRAPTRAN for transient analyses. The code uses a single-channel coolant enthalpy rise model. The code also uses a finite difference heat conduction model, similar to RELAP5 and FRAPTRAN, that uses a variable mesh spacing to accommodate the power peaking at the pellet edge that occurs in high-burnup fuel.

FRAPCON-3.4 has been validated for boiling-water reactors, pressurized reactors, and heavy-water reactors. The fuels that have been validated are uranium dioxide (UO_2), mixed oxide fuel ($(U,Pu)O_2$), urania-gadolinia (UO_2-Gd_2O_3), and UO_2 with zirconium diboride (ZrB_2) coatings. The cladding types that have been validated are Zircaloy-2, Zircaloy-4, M5, and ZIRLO. FRAPCON-3.4 can predict fuel and cladding temperature, rod internal pressure, fission gas release, cladding axial and hoop strain, and cladding corrosion and hydriding. The code uses an updated version of the MATPRO material properties package (Hagrman et al., 1981) as described in a separate material properties handbook (Luscher and Geelhood, 2010) that has been updated for high-burnup conditions and advanced cladding alloys.

Abbreviations

°C	degrees Celsius
ANS	American Nuclear Society
BOL	beginning of life
BWR	boiling-water reactor
cal/mol	calorie(s) per mole
cm^2	square centimeter(s)
cm^3	cubic centimeter(s)
EM	evaluation models
FEA	finite element analysis
g	gram(s)
Gd	gadolinium
GWd/MTU	gigawatt-days per metric ton of uranium
He	helium
HWR	heavy-water reactor
IFBA	integral fuel burnable absorber
J	joule(s)
K	Kelvin
kg	kilogram(s)
kW	kilowatt(s)
LHGR	linear heat generation rate
LWR	light-water reactor
m	meter(s)
m^2	square meter(s)
m^3	cubic meter(s)
MLI	mean linear intercept
MOX	mixed oxide fuel, $(U, Pu)O_2$
MPa	megapascal(s)
n	neutron(s)
NFI	Nuclear Fuels Industries
NRC	U.S. Nuclear Regulatory Commission
Pa	pascal(s)
PNNL	Pacific Northwest National Laboratory
ppm	parts per million
psi	pounds per square inch
Pu	plutonium
PWR	pressurized-water reactor
RXA	re-crystallized annealed
s	second(s)
SHF	surface heat flux
SRA	stress relief annealed
TD	theoretical density
U	uranium
UO_2	uranium dioxide
UO_2-Gd_2O_3	urania-gadolinia
W	watt(s)
μm	micrometer(s)

1.0 Introduction

1.1 Objectives of the FRAPCON Series

The ability to accurately calculate the performance of light-water reactor (LWR) fuel rods under long-term burnup conditions is a major objective of the reactor safety research program being conducted by the U.S. Nuclear Regulatory Commission (NRC). To achieve this objective, the NRC has sponsored an extensive program of analytical computer code development, as well as both in-pile and out-of-pile experiments to benchmark and assess the analytical code capabilities. The computer code developed to calculate the long-term burnup response of a single fuel rod is FRAPCON-3. This report describes FRAPCON-3.4, the fourth released code of the FRAPCON-3 series.

FRAPCON-3 is an analytical tool that calculates LWR fuel rod behavior when power and boundary condition changes are sufficiently slow for the term "steady-state" to apply. This includes situations such as long periods at constant power and slow power ramps that are typical of normal power reactor operations. The code calculates the variation with time of all significant fuel rod variables, including fuel and cladding temperatures, cladding hoop strain, cladding oxidation, fuel irradiation swelling, fuel densification, fission gas release, and rod internal gas pressure. In addition, the code is designed to generate initial conditions for transient fuel rod analysis by FRAPTRAN, the companion transient fuel rod analysis code.

FRAPCON-3 uses fuel, cladding, and gas material properties from MAPTRO that have been recently updated to include burnup-dependent properties and properties for advanced zirconium-based cladding alloys. These properties are documented elsewhere (Luscher and Geelhood, 2010). The only material properties not included in the updated MATPRO document are fission gas release, cladding corrosion, and cladding hydrogen pickup, and these properties are described in this document. The material properties in FRAPCON-3 are contained in modular subroutines that define material properties for temperatures ranging from room temperatures to temperatures above melting and for rod-average burnup levels between 0 and 62 gigawatt-days per metric ton of uranium (GWd/MTU). Each subroutine defines only a single material property. For example, FRAPCON-3 contains subroutines defining fuel thermal conductivity as a function of fuel temperature, fuel density, and burnup; fuel thermal expansion as a function of fuel temperature; and the cladding stress-strain relation as a function of cladding temperature, strain rate, cold work, hydride content, and fast neutron fluence.

The FRAPCON-3 code was developed at Pacific Northwest National Laboratory (PNNL). FRAPCON-3 v1.0 was released first (Berna et al., 1997). Since then, seven updated versions have been released: FRAPCON-3 v1.1, FRAPCON-3 v1.2, FRAPCON-3 v1.3, FRAPCON-3 v1.3a, FRAPCON-3.2, FRAPCON-3.3, and FRAPCON-3.4.

FRAPCON-3, and specifically FRAPCON-3.4, takes a major step toward code simplification by removing extra input parameters and model selection features that cannot easily be measured and have a large impact on results. Also, reasonable default values are set for some parameters. The only model options available to the user are in the selection of the mechanical model and in the selection of the fission gas release model.

For the mechanical model, the user may select the FRACAS-I model (finite difference model) or the FEA (finite element analysis) model. The FRACAS-I model is recommended by PNNL and is the default selection. The FEA model is useful for modeling cladding axial strain in cases where there is slip between the fuel and cladding. The details of the FEA model are described elsewhere (Knuttilla, 2006). This document is posted on the FRAPCON/FRAPTRAN code users' group website at http://www.pnl.gov/frapcon3/. Only the FRACAS-1 mechanical model will be described in this document.

For the fission gas release model, the user can select the Massih model, the ANS-5.4 model (ANS, 1982), or the FRAPFGR model. The Massih model is recommended by PNNL and is the default model. The ANS-5.4 model is useful for calculating the release of short-lived radioactive gas nuclides. The FRAPFGR model is useful for initializing the transient gas release model in FRAPTRAN 1.4. The ANS-5.4 fission gas release model is incorporated as specified by the standard (ANS, 1982) and will not be described in this document. The Massih and FRAPFGR models will be described in this document.

FRAPCON-3.4 includes fuel models for uranium dioxide (UO_2), mixed oxide fuel or MOX ($(U, Pu)O_2$), integral fuel burnable absorber (IFBA) and gadolinia doped fuel, and cladding models for Zircaloy-2, Zircaloy-4, M5, and ZIRLO. Other code improvements include an Excel-based input generator, an Excel-based plot routine, and the ability to bias model predictions for uncertainty analyses.

1.2 Limitations of FRAPCON-3

The FRAPCON-3 code has inherent limitations. The major limitations are as follows:

1. The current code is limited to modeling fuel consisting of UO_2 pellets in zirconium alloy cladding with a gas gap under light and heavy water reactor conditions. Input parameters for other fuel forms (such as metal fuels) and other reactor coolants (such a liquid sodium) are not available, and model changes may be required to accommodate them. The code has been validated up to a rod-average burnup of 62 GWd/MTU, although the code should give reasonable predictions for burnup beyond this level. Also, the code is not validated beyond the fuel or cladding melting temperature. If melting of the fuel or the cladding occurs, the code will stop.

2. The thermal models of the code are based on steady-state conditions and equations, and calculate only radial heat flow. This assumption is valid for modeling a typical fuel rod (i.e., with a large length-to-diameter ratio). Similarly, the gas release models are based on steady-state and slow power ramp data and do not reflect release rates expected for rapid power changes. Therefore, time steps should be no less than 0.1 day but no greater than 50 days. (Analysis for thermal response alone can involve time steps as low as 0.001 day.) The FRAPTRAN code is recommended for modeling of transients or power ramping on the order of a few minutes or less.

3. Only small cladding deformations (< 5 percent strain) are meaningfully calculated by FRAPCON-3. All of the thermal and mechanics modeling assumes an axisymmetric fuel rod with no axial constraints. These assumptions are reasonable for modeling an LWR fuel rod.

4. The code's ability to predict cladding strains resulting from pellet-cladding mechanical interaction has been assessed against power ramp data. FRAPCON-3 has been found to

slightly overpredict cladding strain up to a burnup of about 45 GWd/MTU. The limited high burnup data suggests that FRAPCON-3 may underpredict the cladding strain during power ramps at high burnup (i.e., > 55 GWd/MTU) for hold times greater than 30 minutes.

1.3 Report Outline and Relation to Other Reports

Section 2 and Section 3 of this report deal with the modeling concepts and the code description, respectively. The material properties for fuel, gas, and cladding are fully documented in a separate report (Luscher and Geelhood, 2010). Instructions for creating an input file are discussed in Appendix A. The subroutines used in FRAPCON-3 are listed in Appendix B. The reader is cautioned that, although the thermal and mechanical models are described separately, they actually are highly interrelated. Section 2.2 is included to outline these interrelationships.

This report does not present an assessment of the code performance with respect to in-reactor data. Critical comparisons with experimental data from well-characterized, instrumented test rods are presented in Volume 2 of this series, titled "FRAPCON-3 Integral Assessment" (Geelhood et al., 2010a).

The full documentation of the steady-state and transient fuel performance codes is described in three documents. The basic fuel, cladding, and gas material properties used in FRAPCON-3.4 and FRAPTRAN 1.4 are described in the material properties handbook (Luscher and Geelhood, 2010). The FRAPCON-3.4 code structure and behavioral models are described in the FRAPCON-3.4 code description document (this document). The FRAPTRAN 1.4 code structure and behavioral models are described in the FRAPTRAN 1.4 code description document (Geelhood et al., 2010b).

Table 1.1 shows where each specific material property and model used in the NRC fuel performance codes are documented.

Table 1.1 Roadmap to documentation of models and properties in NRC fuel performance codes, FRAPCON-3.4 and FRAPTRAN 1.4

Model/Property	**FRAPCON-3.4**	**FRAPTRAN 1.4**
Fuel thermal conductivity	Material properties handbook	Material properties handbook
Fuel thermal expansion	Material properties handbook	Material properties handbook
Fuel melting temperature	Material properties handbook	Material properties handbook
Fuel specific heat	Material properties handbook	material properties handbook
Fuel enthalpy	Material properties handbook	material properties handbook
Fuel emissivity	Material properties handbook	Material properties handbook
Fuel densification	material properties handbook	NA
Fuel swelling	Material properties handbook	NA
Fission gas release	FRAPCON-3 code description	FRAPTRAN code description
Fuel relocation	FRAPCON-3 code description	FRAPTRAN code description
Fuel grain growth	FRAPCON-3 code description	NA
High burnup rim model	FRAPCON-3 code description	NA
Nitrogen release	FRAPCON-3 code description	NA
Helium release	FRAPCON-3 code description	NA

Model/Property	FRAPCON-3.4	FRAPTRAN 1.4
Radial power profile	FRAPCON-3 code description	NA (input parameter)
Stored energy	FRAPCON-3 code description	FRAPTRAN code description
Decay heat model	NA	FRAPTRAN code description
Fuel and cladding temperature solution	FRAPCON-3 code description	FRAPTRAN code description
Cladding thermal conductivity	Material properties handbook	Material properties handbook
Cladding thermal expansion	Material properties handbook	Material properties handbook
Cladding elastic modulus	Material properties handbook	Material properties handbook
Cladding creep model	Material properties handbook	NA
Cladding specific heat	Material properties handbook	Material properties handbook
Cladding emissivity	Material properties handbook	Material properties handbook
Cladding axial growth	Material properties handbook	NA
Cladding Meyer hardness	Material properties handbook	Material properties handbook
Cladding annealing	FRAPCON-3 code description	FRAPTRAN code description
Cladding yield stress and plastic deformation	FRAPCON-3 code description	FRAPTRAN code description
Cladding failure criteria	NA	FRAPTRAN code description
Cladding waterside corrosion	FRAPCON-3 code description	NA (input parameter)
Cladding hydrogen pickup	FRAPCON-3 code description	NA (input parameter)
Cladding high temperature oxidation	NA	FRAPTRAN code description
Cladding ballooning model	NA	FRAPTRAN code description
Cladding mechanical deformation	FRAPCON-3 code description	FRAPTRAN code description
Oxide thermal conductivity	Material properties handbook	Material Properties Handbook
Crud thermal conductivity	FRAPCON-3 code description	NA
Gas conductivity	Material properties handbook	Material properties handbook
Gap conductance	FRAPCON-3 code description	FRAPTRAN code description
Plenum gas temperature	FRAPCON-3 code description	FRAPTRAN code description
Rod internal pressure	FRAPCON-3 code description	FRAPTRAN code description
Coolant temperature and heat transfer coefficients	FRAPCON-3 code description	FRAPTRAN code description
Optional models and properties not developed at PNNL		
VVER fuel and cladding models	NA	NUREG/IA-0164 (Shestopalov et al., 1999)
Cladding FEA model	VTT-R-11337-06 (Knuttilla, 2006)	VTT-R-11337-06 (Knuttilla, 2006)

NA = not applicable
FEA = finite element analysis
VVER = water-cooled, water-moderated energy reactor

2.0 General Modeling Descriptions

2.1 FRAPCON-3 Solution Scheme

The FRAPCON-3 code iteratively calculates the interrelated effects of fuel and cladding temperature, rod internal gas pressure, fuel and cladding deformation, release of fission product gases, fuel swelling and densification, cladding thermal expansion and irradiation-induced growth, cladding corrosion, and crud deposition as functions of time and fuel-rod-specific power.

The calculated procedure is illustrated in Figure 2.1, a simplified flowchart of FRAPCON-3. (A detailed flowchart is provided in Section 3.) The calculation begins by processing input data. Next, the initial fuel rod state is determined through a self-initialization calculation. Time is advanced according to the input-specified time-step size, a steady-state solution is performed, and the new fuel rod state is determined. The new fuel rod state provides the initial state conditions for the next time step. The calculations are cycled in this manner for the user-specified number of time steps.

The solution for each time step consists of 1) calculating the temperature of the fuel and the cladding; 2) calculating fuel and cladding deformation; and 3) calculating the fission product generation and release, void volume, and fuel rod internal gas pressure. Each calculation is made in a separate subcode. As shown in Figure 2.1, the fuel rod response for each time step is determined by repeated cycling through two nested loops of iterative calculations until the fuel-cladding gap temperature difference and internal gas pressure converge.

For the FRACAS-I (Bohn et al., 1977) mechanical model, the fuel temperature and deformation are alternately calculated in the inner loop. On the first cycle through this loop for each time step, the gap conductance is computed using the fuel-cladding gap size from the previous time step. Then the fuel rod temperature distribution is computed. This temperature distribution feeds the deformation calculation by influencing the fuel and cladding thermal expansions and the cladding stress-strain relation. An updated fuel-cladding gap size is calculated and used in the gap conductance calculation on the next cycle through the inner loop. The cyclic process through the inner loop is repeated until two successive cycles calculate essentially the same temperature distribution.

The outer loop of calculations is cycled in a manner similar to that of the inner loop, but with the amount of internal gas being determined during each iteration. The calculation alternates between the fuel rod void volume-gas pressure calculation and the fuel rod temperature-deformation calculation. On the first cycle through the outer loop for each time step, the gas pressure from the previous time step is used. For each cycle through the outer loop, the number of gas moles is calculated and the updated gas pressure computed and fed back to the deformation and temperature calculations (the inner loop). The calculations are cycled until two successive cycles calculate essentially the same gas pressure, and then a new power-time step is begun.

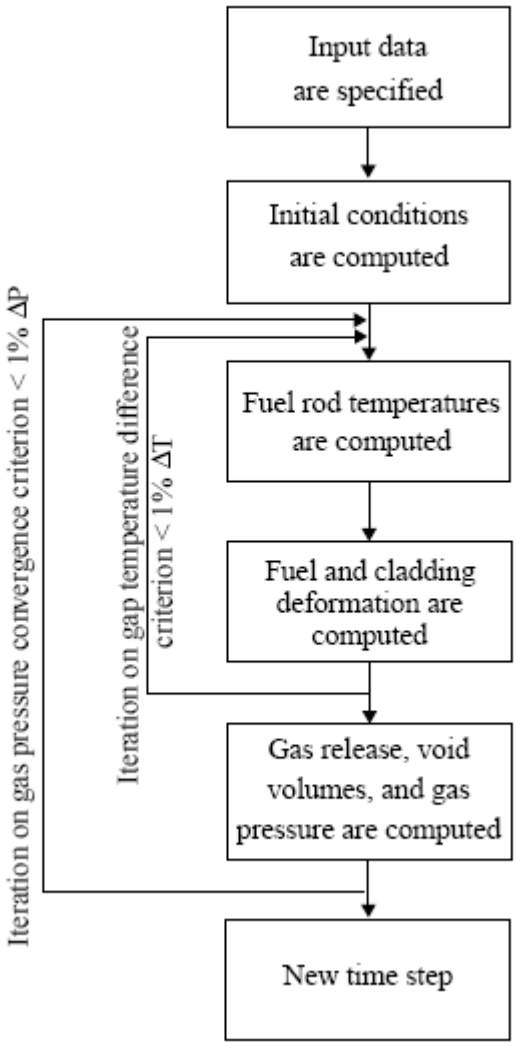

Figure 2.1 Simplified FRAPCON-3 flowchart

2.2 Coupling of Thermal and Mechanical Models

The close coupling of the thermal modeling and mechanical modeling is the result of the existence of the fuel-cladding gap. As the fuel temperature increases, the extreme stresses resulting from the large temperature gradients in the fuel cause the fuel to crack and relocate. Cracks can be circumferential or radial, but are predominantly radial. Void space, which is originally in the fuel-cladding gap, is relocated into the fuel as fragments of fuel move outwardly into the fuel-cladding gap.

As the fuel becomes hotter, the fuel expands, filling some of the voids within the fuel. However, asperities do not align exactly, thereby causing the fuel diameter to appear larger and the fuel to interact with the cladding at a lower power than that expected due to normal expansion (or contraction) mechanisms, including thermal expansion, swelling, and densification. FRACAS-I has been modified to allow 50 percent of the original fuel surface relocation to be recovered due to fuel swelling before hard contact is established between the fuel and the cladding.

The modeling of the cracked and relocated fuel, both thermally and mechanically, requires accounting for changed fuel-cladding gap size (and hence gap conductance) and the changed fuel pellet diameter as the fuel interacts with the cladding. The fuel surface relocation provides a new fuel-cladding gap size for calculating gap conductance and mechanical interactions. Also considered is the shift of voids from the fuel-cladding gap into cracks in the fuel pellet (and the resultant pressure change due to higher temperature in the cracks) and the feedback into the mechanics and thermal calculations.

FRACAS-I uses the relocated fuel-cladding gap size for the thermal calculations and makes partial use of the fuel surface relocation in the mechanics calculation (i.e., when 50 percent of the relocation is recovered, the code assumes the pellet to be a rigid structure, and, therefore, hard contact is assumed between the fuel and cladding).

2.3 Fuel Rod Thermal Response

The temperature distribution throughout the fuel and the cladding is calculated at each axial node. A simplified flowchart of the temperature distribution solution is shown in Figure 2.2. A schematic of the temperature distribution at an arbitrary axial node is shown in Figure 2.3.

The models used in the fuel rod temperature calculations assume a cylindrical fuel pellet located symmetrically within a cylindrical fuel rod surrounded by coolant. User-supplied boundary conditions (coolant inlet temperature, coolant channel equivalent heated diameter, and time coolant mass flux) and the user-supplied axial linear heat generation rate are used to calculate the coolant bulk temperature, T_b, using a single-channel coolant enthalpy rise model. A film temperature rise, ΔT_f, is then calculated from the coolant to the surface of the fuel rod through any crud layer which may exist. The cladding inside surface temperature, T_{ci}, is found by calculating the temperature rise across the zirconium oxide and the cladding using Fourier's law. The temperature rise to the fuel surface is determined from an annular gap conductance model, thereby establishing the fuel surface temperatures, T_{fs}. Finally, the temperature distribution in the fuel is calculated, accounting for fuel cracking effects using the fuel surface temperature and assumed symmetry at the centerline as boundary conditions.

The models used in the temperature calculations involve assumptions and limitations. The most important are as follows:

1. Heat conduction in the axial direction is considered negligible relative to radial heat conduction and is ignored due to the large length-to-diameter ratio.

2. Heat conduction in the azimuthal direction is ignored (axisymmetric analysis).

3. Constant boundary conditions are maintained during each time step.

4. Steady-state heat flow is assumed.

5. The fuel rod is a right circular cylinder surrounded by water coolant.

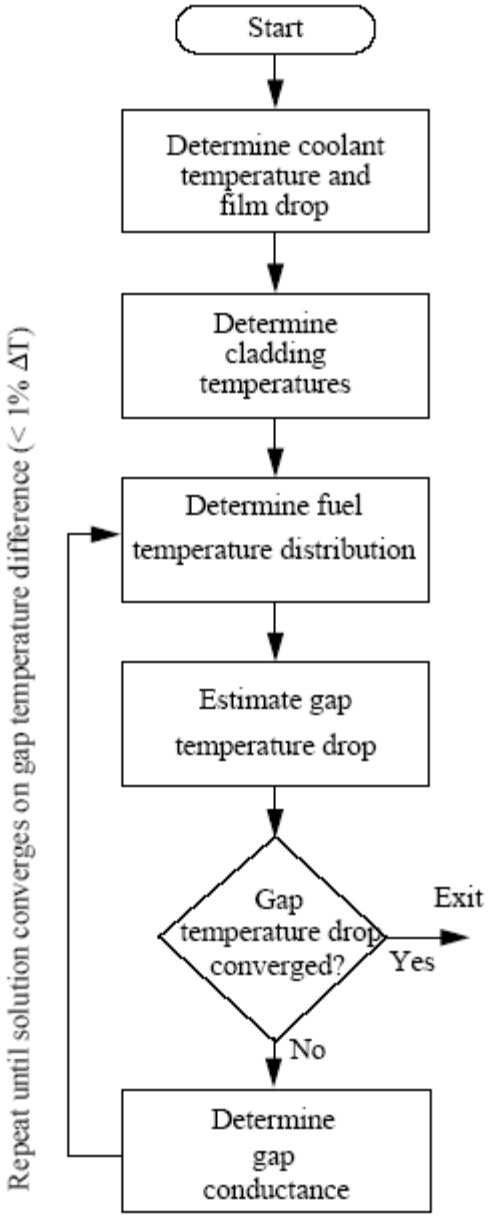

Figure 2.2 Flow chart of the fuel and cladding temperature calculation

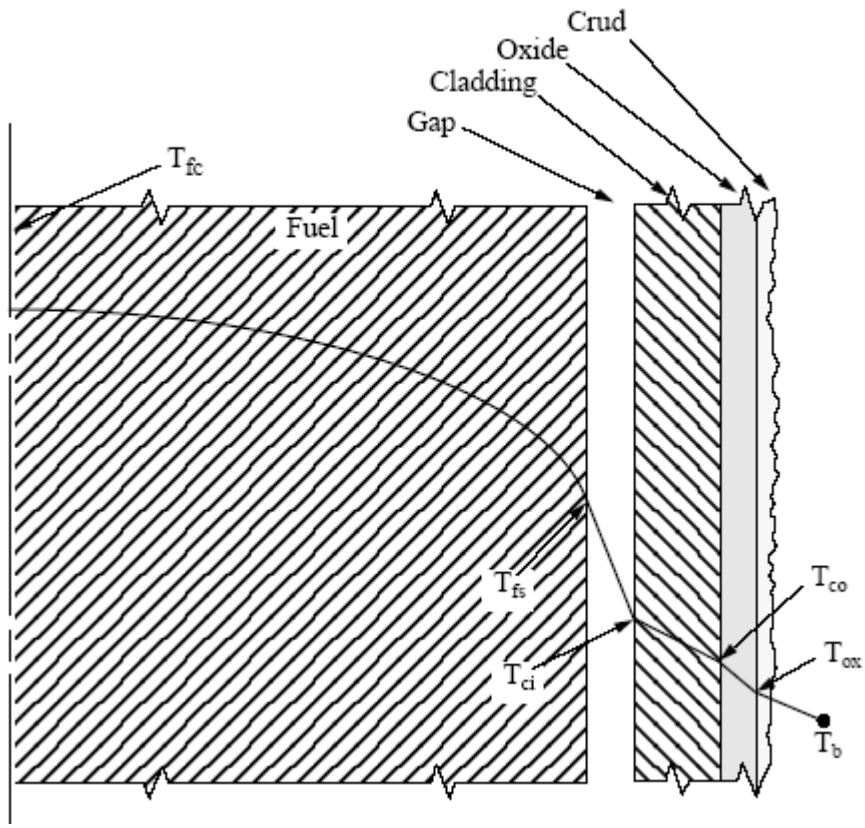

Figure 2.3 Schematic of the fuel rod temperature distribution

2.3.1 Coolant Conditions

FRAPCON-3 calculates bulk coolant temperatures assuming a single, closed coolant channel according to

$$T_b(z) = T_{in} + \int_0^z \left[\frac{(\pi D_0)\, q''(z)}{C_p G A_f} \right] dz \tag{2-1}$$

where

$T_b(z)$	=	bulk coolant temperature at elevation z on the rod axis (K)
T_{in}	=	inlet coolant temperature (K)
$q''(z)$	=	rod surface heat flux at elevation z on the rod axis (W/m^2)
C_p	=	heat capacity of the coolant (J/kg-K)
G	=	coolant mass flux (kg/s-m^2)
A_f	=	coolant channel flow area (m^2)
D_o	=	outside cladding diameter (m)

Coolant heat capacity for water is calculated using the following relationships:

$$C_p = 2.39 \times 10^5 \text{ for } T_b(z) < 544\text{K}$$
$$C_p = 2.39 \times 10^5 [1 + 7.73 \times 10^{-4} (1.8 T_b(z) - 979.4)] \text{ for } 544\text{K} <= T_b(z) < 583\text{K} \quad (2\text{-}2)$$
$$C_p = 2.39 \times 10^5 [1 + 2.95 \times 10^{-3} (1.8 T_b(z) - 1031)] \text{ for } T_b(z) >= 583\text{K}$$

Coolant channel hydraulic diameter is calculated from rod pitch and diameter using the following relationship:

$$D_e \frac{4.0\left[P_{pit}^2 - \frac{\pi}{4} D_0^2\right]}{\pi D_0} \quad (2\text{-}3)$$

where

P_{pit} = rod-to-rod pitch (m)
D_o = outside cladding diameter (m)

2.3.2 Fuel Rod Surface Temperature

The cladding surface temperature at axial elevation z is taken as the minimum value of

$$T_w(z) = T_b(z) + \Delta T_f(z) + \Delta T_{cr}(z) + \Delta T_{ox}(z) \quad (2\text{-}4)$$

$$T_w(z) = T_{sat} + \Delta T_{JL} + \Delta T_{ox}(z) \quad (2\text{-}5)$$

where

$T_b(z)$ = bulk coolant temperature at elevation z on the rod axis (K)
$T_w(z)$ = rod surface temperature at elevation z on the rod axis (K)
$\Delta T_f(z)$ = forced convection film temperature drop at elevation z on the rod axis (K)
$\Delta T_{cr}(z)$ = crud temperature drop at elevation z on the rod axis (K)
$\Delta T_{ox}(z)$ = oxide layer temperature drop at elevation z
T_{sat} = coolant saturation temperature (K)
ΔT_{JL} = nucleate boiling temperature drop at elevation z on the rod axis (K), determined by the Jens-Lottes correlation (Jens and Lottes, 1951)

The choice of the minimum value is a simple means of deciding whether heat is transferred from the cladding surface to the coolant by forced convection or nucleate boiling. It also provides a smooth numerical transition from forced convection to nucleate boiling, thereby avoiding convergence problems. For forced-convection heat transfer, the temperature drop across the coolant film layer at the rod surface is based on

$$\Delta T_f(z) = q''(z) / h_f \quad (2\text{-}6)$$

where h_f is the Dittus-Boelter (Dittus and Boelter, 1930) film conductance given by

$$h_f = \left(\frac{0.023k}{D_e}\right)\mathrm{Re}^{0.8}\,\mathrm{Pr}^{0.4} \tag{2-7}$$

where

h_f	=	conductance (W/m^2-K)
k	=	thermal conductivity of the coolant (W/m-K)
D_e	=	coolant channel heated diameter (m)
Re	=	Reynolds number (dimensionless)
Pr	=	Prandtl number (dimensionless)

The temperature drop across the crud is given by

$$\Delta T_{cr}(z) = q''(z)\frac{\delta_{cr}}{k_{cr}} \tag{2-8}$$

where

δ_{cr}	=	crud thickness (m)
k_{cr}	=	crud thermal conductivity, 0.8648 (W/m-K)

For nucleate boiling heat transfer, the temperature drop across the coolant film layer at the rod surface is based on the Jens-Lottes (Jens and Lottes, 1951) formulation:

$$\Delta T_{JL}(z) = 60[q''(z)/10^6]^{0.25} / e^{(P/6.2\times10^6)} \tag{2-9}$$

where

P	=	system bulk coolant pressure (Pa)

It is assumed that the crud does not offer any resistance to heat flow during nucleate boiling; therefore, no temperature drop due to crud is calculated. The coolant is assumed to boil through the crud blanket.

The temperature drop across the zirconium oxide layer at elevation z on the rod axis is determined by

$$\Delta T_{ox}(z) = \frac{q''(z)\delta_{ox}(z)}{k_{ox}} \tag{2-10}$$

where

$\Delta T_{ox}(z)$	=	oxide temperature drop at elevation z on the rod axis (K)
$\delta_{ox}(z)$	=	oxide thickness at elevation z on the rod axis (m)
k_{ox}	=	oxide thermal conductivity (W/m–K)

2.3.3 Cladding Temperature Gradient

The cladding temperature drop for each axial location is calculated according to the following expression for steady-state heat transfer through a cylinder with uniform thermal conductivity:

$$\Delta T_c = q''(z) r_o \ln(r_o / r_i) / k_c \tag{2-11}$$

where

ΔT_c	=	cladding temperature drop (K)
r_o	=	cladding outside radius (m)
r_i	=	cladding inside radius (m)
k_c	=	temperature and material dependent thermal conductivity of the cladding (W/m-K)

2.3.4 Fuel-Cladding Gap Temperature Gradient

The fuel-cladding gap temperature drop is calculated using the fuel rod surface heat flux at elevation z and the fuel-cladding gap conductance. The fuel-cladding gap conductance is the sum of three components: the conductance due to radiation, the conduction through the gas, and the conduction through regions of solid-solid contact. The equations and models for each of these components are presented in the following sections.

$$\Delta T_{gap} = \frac{q''(z)}{h} \tag{2-12}$$

where

h	=	$h_r + h_{gas} + h_{solid}$
$q''(z)$	=	rod surface heat flux at elevation z on the rod axis (W/m^2)
h_r	=	conductance due to radiation (W/m^2-K)
h_{gas}	=	conductance of the gas gap (W/m^2-K)
h_{solid}	=	conductance due to fuel-cladding contact (W/m^2-K)

2.3.4.1 Radiant Heat Transfer

The net radiant heat transfer of heat from the fuel to the cladding is the infinite-cylinder, gray body form as derived for high-aspect-ratio small gaps from the general radiant heat transfer equation by Kreith (1964) and others:

$$\text{Net surface heat flux (SHF)} = \sigma F\left(T_{fs}^4 - T_{ci}^4\right) \tag{2-13}$$

where

F	=	$1/[e_f + (r_{fs} / r_{ci})(1/e_c - 1)]$
σ	=	Stefan-Boltzman constant = 5.6697E-8 (W/m^2-K^4)
e_f	=	fuel emissivity
e_c	=	cladding emissivity
T_{ci}	=	fuel surface temperature (K)

T_{fs} = cladding inner surface temperature (K)
r_{fs} = fuel outer surface radius (m)
r_{ci} = cladding inner surface radius (m)

The conductance due to radiation, h_r (W/m^2-K), is defined by

$$h_r(T_{fs} - T_{ci}) = \text{SHF} \tag{2-14}$$

Combining Equations (2-13) and (2-14) and dividing by (T_{fs} - T_{ci}) gives

$$h_r = \sigma F[T_{fs}^2 + T_{ci}^2][T_{fs} + T_{ci}] \tag{2-15}$$

2.3.4.2 Conduction Through the Interfacial Gas

The form of the conductance due to conductive heat transfer through the gas in the fuel-cladding gap, h_{gas} (W/m^2-K), is that applied to small annular gaps:

$$h_{gas} = \frac{k_{gas}}{\Delta x} \tag{2-16}$$

where

k_{gas} = gas thermal conductivity (W/m-K)
Δx = total effective gap width (m)

$$\Delta x = d_{eff} + 1.8(g_f + g_c) - b + d \tag{2-17}$$

where

d = value from FRACAS for open fuel-cladding gap size (m)
d_{eff} = exp (-0.00125P) (R_f+ R_c) for closed fuel-cladding gaps (m),
= (R_f+ R_c) for open fuel-cladding gaps (m)
P = fuel-cladding interfacial pressure (kg/cm^2)
R+ R_c = cladding plus fuel surface roughness (m)
(g_f + g_c) = temperature jump distances at fuel and cladding surfaces, respectively (m)
b = 1. 397x10^{-6} (m)

The quantity (g_f + g_c) is calculated from the GAPCON-2 (Beyer et al., 1975) model and is

$$(g_f + g_c) = A\left[\frac{k_{gas}\sqrt{T_{gas}}}{P_{gas}}\right]\left[\frac{1}{\sum a_i f_i / \sqrt{M_i}}\right] \tag{2-18}$$

where

A = 0.7816
k_{gas} = gas conductivity (W/m-K)
P_{gas} = gas pressure (Pa)
T_{gas} = average gas temperature (K)

a_i = accommodation coefficient of i-th gas component
M_i = gram-molecular weight of i-th gas component (g moles)
f_i = mole fraction of i-th gas component

2.3.4.3 Conduction Through Points of Contact

The contact conductance model is a modification of the Mikic-Todreas (Tondreas and Jacobs, 1973) model that preserves the roughness, conductivity, and pressure dependencies while providing a best estimate for the range of contact conductances measured by Garnier and Begej (1979). The FRACAS-I model uses expressions for h_{solid} that depend on both the fuel-cladding interfacial pressure and the microscopic roughness, R, as follows:

$$h_{solid} = \frac{0.4166 K_m P_{rel} R_{mult}}{RE} \quad \text{, if } P_{rel} > 0.003$$
$$h_{solid} = \frac{0.00125 K_m}{RE} \quad \text{, if } 0.003 > P_{rel} > 9\text{x}10^{-6} \qquad (2\text{-}19)$$
$$h_{solid} = \frac{0.4166 K_m P_{rel}^{0.5}}{RE} \quad \text{, if } P_{rel} < 9\text{x}10^{-6}$$

where

P_{rel} = ratio of interfacial pressure to cladding Meyer hardness (approximately 680 MPa)
K_m = geometric mean conductivity (W/m-K)
= $2K_f K_c/(K_f + K_c)$
R = $\sqrt{R_f^2 + R_c^2}$ (m), where R_f and R_c are the roughnesses of the fuel and cladding (m)
R_{mult} = 333.3 P_{rel}, if $P_{rel} \leq 0.0087$
= 2.9 , if $P_{rel} > 0.0087$
K_c = cladding thermal conductivity (W/m-K)
K_f = fuel thermal conductivity (W/m-K)
E = $\exp[5.738 - 0.528 \ln(3.937 \times 10^7 R_f)]$

The above comes from a fit to Ross and Stoute (1962) data plus that by Rapier et al. (1963) using the Todreas (Tondreas and Jacobs, 1973) model. The contact conductance model provides a relatively smooth transition between the open and closed gap conductance that helps to eliminate non-convergence in the code caused by oscillating between an open and closed gap situation.

2.3.5 Fuel Pellet Heat Conduction Model

This section describes the steady-state fuel pellet heat conduction model. The model is developed based on the finite difference heat conduction models used in RELAP5 and FRAPTRAN. First, an overview of the fuel pellet heat conduction model used in FRAPCON-3 is provided. Next, the requirements for the fuel pellet heat conduction model are given. The development of the finite difference approach begins in Section 2.3.5.1, and subsequent sections provide specific applications of the steady-state heat conduction equation that will lead to the final form of the heat conduction model.

A schematic of a representative temperature distribution at an arbitrary axial node is shown in Figure 2.3. The fuel surface temperature, T_{fs}, is used as one of the boundary conditions to feed

into the finite difference heat conduction model. The new finite difference model calculates the temperature profile in the fuel pellet and has fine mesh capabilities at the fuel surface that will handle fuel pellets with burnup to 75 megawatt-days per kilogram of uranium.

2.3.5.1 The Finite Difference Approach

Finite differences will be used to calculate the temperature distribution in the fuel region. Variable mesh spacing will be used, and the spatial dependence of the internal heat source is allowed to vary over each mesh interval.

The steady-state integral form of the heat conduction equation is

$$\iint_S k(T,\bar{x})\vec{\nabla}T(\bar{x}) \bullet \vec{n}ds = \iiint_V S(\bar{x})dV \tag{2-20}$$

where

k	=	thermal conductivity (W/m-K)
s	=	surface of the control volume (m^2)
$\vec{n}$	=	the surface normal unit vector
S	=	internal heat source (W/m^3)
T	=	temperature (K)
V	=	control volume (m^3)
$\bar{x}$	=	the space coordinates (m)

The following assumptions were made to develop this heat conduction model:

- fixed geometry
- symmetrical geometry
- negligible heat conduction in the axial direction
- negligible heat conduction in the azimuthal direction
- steady-state
- mesh point averaged thermal conductivity (discussed in the following sections)

Two boundary conditions are needed to calculate the temperature profile in the fuel. The boundary conditions are the symmetry condition, $\left.\frac{\partial T}{\partial \bar{x}}\right|_{\bar{x}=0} = 0$, at the center of the fuel pellet and a prescribed temperature at the surface of the fuel.

2.3.5.2 Mesh Point Layout

Figure 2.4 illustrates the placement of mesh points at which temperatures are to be calculated. The mesh point spacing is positive in the radial direction. The first mesh point is placed at the fuel centerline or at the inner annular surface of the fuel. Variable mesh spacing is used to determine the placement of interior mesh points. The mesh placement does not provide constant volume nodes, but is consistent with the radial power and burnup distribution model, TUBRNP (Lassman et al., 1994; and Lassman et al., 1998), developed at the Institute for Transuranium Elements, Karlsruhe, incorporated in FRAPCON-3. This scheme places more nodes near the

surface of the pellet to account for the rim effects. The last mesh point is placed on the surface of the fuel.

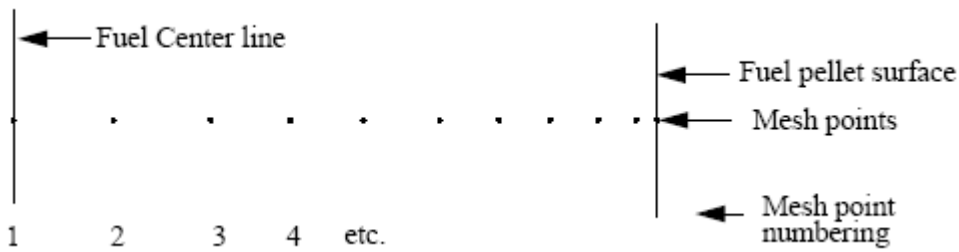

Figure 2.4 Mesh point layout

Figure 2.5 represents three typical mesh points. The subscripts are space indexes indicating the mesh point number; and l and *r* (if present) designate quantities to the left and right, respectively, of the mesh point. The δ's indicate mesh point spacing. Between mesh points, the thermal conductivity, *k*, and the source term, *S*, are assumed spatially constant; but k_{lm} is not necessarily equal to k_{rm} and similarly for *S*.

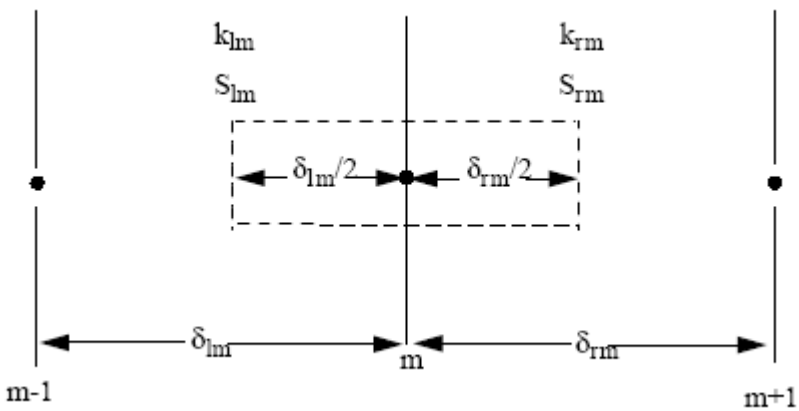

Figure 2.5 Typical mesh points

To obtain the spatial-difference approximation for the m-th interior mesh point, a form of Equation (2-20) applicable to radial heat conduction in cylindrical coordinates is applied to the volume and surfaces indicated by the dashed line shown in Figure 2.5. To obtain the spatial difference approximation at the boundaries, Equation (2-20) is applied to the volumes and interior surfaces indicated by the dashed lines shown in Figure 2.6.

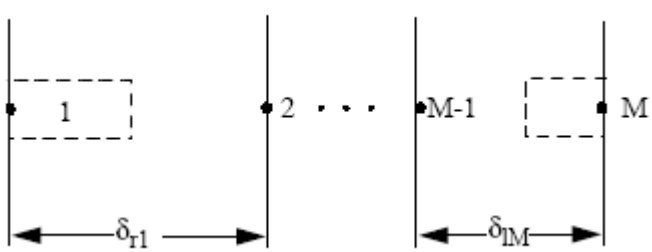

Figure 2.6 Boundary mesh points

The spatial finite-difference approximations use approximate expressions for the space and volume factors and simple differences for the gradient terms. To condense the expressions defining the numerical approximations, the following quantities are defined.

$$\delta_{lm}^{v} = 2\pi \frac{\delta_{lm}}{2}\left(x_m - \frac{\delta_{lm}}{4}\right),\ \delta_{rm}^{v} = 2\pi \frac{\delta_{rm}}{2}\left(x_m - \frac{\delta_{rm}}{4}\right)$$
$$\delta_{lm}^{s} = \frac{2\pi}{\delta_{lm}}\left(x_m - \frac{\delta_{lm}}{2}\right),\ \delta_{rm}^{s} = \frac{2\pi}{\delta_{rm}}\left(x_m - \frac{\delta_{rm}}{2}\right) \tag{2-21}$$
$$\delta_{m}^{b} = 2\pi x_m$$

The superscripts, *v* and *s*, refer to volume and surface-gradient weights. The δ_m^b is a surface weight used at exterior boundaries and in heat-transfer-rate equations.

2.3.5.3 Difference Approximation at Internal Mesh Points

The first term of Equation (2-20) for the surfaces of Figure 2.5 is approximated by

$$\iint_s k(T,\bar{x})\vec{\nabla}T(\bar{x}) \bullet \vec{n}ds \approx (T_m - T_{m-1})k_{lm}\delta_{lm}^{s} + (T_m - T_{m+1})k_{rm}\delta_{rm}^{s} \tag{2-22}$$

Note that the volume in Figure 2.5 is divided into two sub-volumes by the interface line. When the surface integrals of these sub-volumes are added, the surface integrals along the common interface cancel because of the continuity of heat flow.

The source term in Equation (2-20) is represented by

$$S(x) = P_f PQ(x) \tag{2-23}$$

where

P_f	=	the axial power factor that relates *P* to a particular axial node
P	=	the power function derived from the linear heat generation rate
$Q(x)$	=	the radial position dependent function (as determined by the TUBRNP model and subroutine)

The value of $Q(x)$ is assumed constant over a mesh interval, but each interval can have a different value. The third term of Equation (2-20) is then approximated as

$$\iiint_V S(\bar{x},t)dV \approx P_f P(Q_{lm}\delta_{lm}^{v} + Q_{rm}\delta_{rm}^{v} \tag{2-24}$$

Gathering the approximations of terms in Equation (2-20), the basic difference equation for the m-th mesh point is

$$(T_{m-1} - T_m)k_{lm}\delta_{lm}^{s} + (T_{m+1} - T_m)k_{rm}\delta_{rm}^{s} = P_f P(Q_{lm}\delta_{lm}^{v} + Q_{rm}\delta_{rm}^{v}) \tag{2-25}$$

Writing Equation (2-25) in abbreviated form, the difference approximation for the m-th interior mesh point is

$$a_m T_{m-1} + b_m T_m + c_m T_{m+1} = d_m \tag{2-26}$$

$$a_m = -(k_{lm}\delta^s_{lm}) \tag{2-27}$$

$$b_m = -a_m - c_m \tag{2-28}$$

$$c_m = -(k_{rm}\delta^s_{rm}) \tag{2-29}$$

$$d_m = P_f P(Q_{lm}\delta^v_{lm} + Q_{rm}\delta^v_{rm}) \tag{2-30}$$

2.3.5.4 Difference Approximation at Boundaries

To obtain the difference approximations for the mesh points at the boundaries, Equation (2-20) is applied to the volumes of Figure 2.6. The first boundary condition evaluated is the symmetry condition, $\left.\frac{\partial T}{\partial \bar{x}}\right|_{\bar{x}=0} = 0$. The symmetry condition is applied at mesh point 1. The first term of Equation (2-20) is approximated by

$$\iint_s k(T,\bar{x})\vec{\nabla}T(\bar{x}) \bullet \vec{n}ds = k_{rl}(T_2 - T_1)\delta^s_{rl} \tag{2-31}$$

The complete basic expression for mesh point 1 (located at the symmetry boundary) becomes

$$k_{rl}(T_2 - T_1)\delta^s_{rl} = P_f P(t) Q_{rl}\delta^v_{rl} \tag{2-32}$$

Thus, for the symmetry boundary

$$b_1 T_1 + c_1 T_2 = d_1 \tag{2-33}$$

$$b_1 = -c_1 \tag{2-34}$$

$$c_1 = -k_{rl}\delta^s_{rl} \tag{2-35}$$

$$d_1 = P_f(P) Q_{rl}\delta^v_{rl} \tag{2-36}$$

For the fuel surface boundary at mesh point *M*, a known fuel surface temperature is applied, giving

$$a_M T_{M-1} + b_M T_M = d_M \tag{2-37}$$

$$a_M = 0 \tag{2-38}$$

$$b_M = 1 \tag{2-39}$$

$$d_M = T_{fs} d_M = T_{fs} \tag{2-40}$$

2.3.5.5 Radial Power Profile

The radial power profile within a fuel pellet is a function of fuel type, reactor type, and burnup. FRAPCON-3 uses the TUBRNP (Lassman et al., 1994; and Lassman et al., 1998) model to calculate the radial power profile in UO_2 and MOX under LWR and heavy-water reactor (HWR) conditions as a function of burnup.

The TUBRNP model is not currently able to calculate the radial power profile of urania-gadolinia (UO_2-Gd_2O_3) fuel. For this fuel type, FRAPCON-3 interpolates from look-up tables for LWR and HWR conditions while the gadolinium (Gd) isotopes with high cross section are burning out. After these high-cross-section Gd isotopes have burnt out, FRAPCON-3 uses the radial power profiles calculated using TUBRNP. The look-up tables were created using the neutronics code, WIMS, for a standard fuel design at various Gd_2O_3 loadings under LWR and HWR conditions.

The neutron flux distribution (r) within the fuel pellet is described in TUBRNP by the solution of one-group, one-dimensional diffusion theory applied to cylindrical fuel:

$$\phi(r) = C I_0(\kappa r) \tag{2-41}$$

for solid pellets, and

$$\phi(r) = C\left(I_0(\kappa r) + \left[\frac{I_1(\kappa r_0)}{K_1(\kappa r_0)} \right] K_0(\kappa r) \right) \tag{2-42}$$

for annular pellets

where

$$\kappa = \sqrt{\Sigma_a / D}\ ,\ \Sigma_a = \sum_k \sigma_{a,i} \overline{N}_i\ ,\ D = \frac{1}{3\Sigma_s} = \frac{1}{3\sigma_s \overline{N}_{tot}}$$

and

I,K	=	modified Bessel functions
C	=	a constant
σ_a, σ_s	=	absorption and scattering cross sections
$\overline{N}$	=	pellet-average atom concentration
r_0	=	the pellet outer radius
i	=	subscript indicating all U and Pu isotopes

The evolution of average uranium and plutonium isotope concentrations in the fuel through time can be described as a coupled set of differential equations, which are coupled because the loss of

one isotope by neutron capture leads in some cases to some production of the next higher isotope. These equations are summarized as follows:

$$\frac{d\overline{N}_{235}}{dt} = -\sigma_{a,235}\overline{N}_{235}\phi \tag{2-43}$$

$$\frac{d\overline{N}_{238}}{dt} = -\sigma_{a,238}\overline{N}_{238}\phi \tag{2-44}$$

$$\frac{d\overline{N}_{j}}{dt} = -\sigma_{a,j}\overline{N}_{j}\phi + \sigma_{c,j-1}\overline{N}_{j-1}\phi \tag{2-45}$$

where

j	=	^{239}Pu, ^{240}Pu, ^{241}Pu, and ^{242}Pu
σ_a, σ_c	=	absorption and capture cross sections

Because, in fuel performance codes, the linear heat generation rate (LHGR) and time step duration are input values, the burnup increment for the time step is prescribed and can be related to the flux, the fission cross sections, and the concentrations of fissile isotopes. Thus, flux-time increment, *dt*, can be replaced by the burnup increment, *dbu*, via the relation

$$dbu = \frac{q'''dt}{\rho_{fuel}} = \frac{\alpha}{\rho_{fuel}}\sum_{k}\sigma_{f,k}\overline{N}_{k}\phi dt \tag{2-46}$$

where

q'''	=	volumetric heat generation rate
ρ_{fuel}	=	fuel density
σ_f	=	fission cross section
α	=	a conversion constant

Furthermore, the distribution of plutonium production is described by an empirical function, $f(r)$, the parameters for which are to be selected based on code-data comparisons on plutonium concentrations as a function of burnup. Thus, the equations for isotope distribution $N(r)$ become

$$\frac{dN_{235}(r)}{dbu} = -\sigma_{a,235}N_{235}(r)A \tag{2-47}$$

$$\frac{dN_{238}(r)}{dbu} = -\sigma_{a,238}\overline{N}_{238}f(r)A \tag{2-48}$$

$$\frac{dN_{239}(r)}{dbu} = -\sigma_{a,239}N_{239}(r)A + \sigma_{c,238}\overline{N}_{238}A \tag{2-49}$$

$$\frac{dN_j(r)}{dbu} = -\sigma_{a,j} N_j(r) A + \sigma_{c,j-1} N_{j-1} A \tag{2-50}$$

where, in this case, j = ^{240}Pu, ^{241}Pu, and ^{242}Pu,

$$A = 0.8815 \frac{\rho_{fuel}}{\alpha \sum_i \sigma_{f,i} \overline{N}_i}$$

$$f(r) = 1 + p_1 \exp\left(- p_2 (r_{out} - r)^{p_3}\right)$$

and p_1, p_2, and p_3 are empirically determined constants.

In FRAPCON-3, the following values are used:

p_1 = 3.45 (for LWR), p_1 = 2.21 (for HWR)
p_2 = 3.0 (for LWR and HWR)
p_3 = 0.45 (for LWR and HWR)

The function $f(r)$ is constrained to have a volume-averaged value of 1.0.

The fission and capture cross sections are different for LWR conditions and HWR conditions due to the difference in neutron spectrum in these reactors. The fission and capture cross sections (σ_f and σ_c, respectively) used in FRAPCON-3 are listed in Table 2.1. The absorption cross section (σ_a) is the sum of the fission cross section and the capture cross section.

Table 2.1 Fission and capture cross sections used in FRAPCON-3

Isotope	**LWR**		**HWR**	
	σ_f (barns)	σ_c (barns)	σ_f (barns)	σ_c (barns)
^{235}U	41.5	9.7	107.9	22.3
^{238}U	0.00	0.78	0.00	1.16
^{239}Pu	105	58.6	239.18	125.36
^{240}Pu	0.584	100	0.304	127.26
^{241}Pu	120	50	296.95	122.41
^{242}Pu	0.458	80	0.191	91.30

The local power density, $q'''(r)$, which is needed for the thermal analysis, is proportional to the neutron flux and the macroscopic cross section for fission,

$$q'''(r) \propto \sum_j \sigma_{f,j} N_j \phi \tag{2-51}$$

where

j = ^{235}U, ^{238}U, ^{239}Pu, ^{240}Pu, ^{241}Pu, and ^{242}Pu

Equation (4-51) can be used to obtain a normalized radial power profile across the pellet. This normalized radial power profile is used as $Q(x)$ in Equation (2-23).

At the end of each time step, the isotope concentrations are updated based on the burnup increment, using the above equations. These equations are solved and the concentrations evaluated at every input radial boundary. Because the flux and plutonium deposition distribution functions are prescribed, and the solutions are carried out at ring boundaries, the solution is independent of the radial nodalization scheme; it is also quite stable with respect to time-step size, within the limits dictated by other processes, such as cladding creep and fission gas release.

2.3.5.6 Thermal Conductivity and Iteration Procedures

The thermal conductivity, *k*, is considered a function of temperature and burnup.

The fuel thermal conductivity model in FRAPCON-3 is based on the expression developed by the Nuclear Fuels Industries (NFI) model (Ohira and Itagaki, 1997) with modifications. This model applies to UO_2 and UO_2-Gd_2O_3 fuel pellets at 95% of theoretical density (TD).

$$K_{95} = \frac{1}{A + a \cdot gad + BT + f(Bu) + \left(1 - 0.9\exp(-0.04Bu)\right)g(Bu)h(T)} + \frac{E}{T^2}\exp\left(-\frac{F}{T}\right) \tag{2-52}$$

where

K_{95}	=	thermal conductivity for 95% TD fuel (W/m-K)
T	=	temperature (K)
Bu	=	burnup (GWd/MTU)
$f(Bu)$	=	effect of fission products in crystal matrix (solution)
$f(Bu)$	=	0.00187•Bu (2-53)
$g(Bu)$	=	effect of irradiation defects
$g(Bu)$	=	$0.038 \cdot Bu^{0.28}$ (2-54)
$h(T)$	=	temperature dependence of annealing on irradiation defects
		$h(T) = \frac{1}{1 + 396e^{-Q/T}}$ (2-55)
Q	=	temperature dependence parameter ("Q/R") = 6380 K
A	=	0.0452 (m-K/W)
a	=	constant = 1.1599
gad	=	weight fraction of gadolinia
B	=	2.46E-4 (m-K/W/K)
E	=	3.5E9 (W-K/m)
F	=	16361 (K)

As applied in FRAPCON-3, the above model is adjusted for as-fabricated fuel density (in fraction of TD) using the Lucuta recommendation for spherical-shaped pores (Lucuta et al., 1996), as follows:

$$K_d = 1.0789 * K_{95} * [d/\{1.0 + 0.5(1-d)\}] \tag{2-56}$$

where

d = density (fraction of TD)
K_{95} = as-given conductivity (reported to apply at 95% TD)

The factor 1.0789 adjusts the conductivity back to that for 100% TD material.

For MOX fuel ($(UO_2, Pu)O_2$), the same equation as shown in Equation (2-52) is used with A and B replaced by functions of the oxygen to metal ratio and several other fitting coefficients changed as follows:

$$K_{95(MOX)} = \frac{1}{A(x) + a \cdot gad + B(x)T + f(Bu) + \left(1 - 0.9\exp(-0.04Bu)\right)g(Bu)h(T)} + \frac{C}{T^2}\exp\left(-\frac{D}{T}\right) \tag{2-57}$$

where

$K_{95(MOX)}$ = thermal conductivity for 95% TD MOX fuel (W/m-K)
x = 2.00 – O/M (i.e., oxygen-to-metal ratio)
$A(x)$ = 2.85x + 0.035 (m-K/W)
$B(x)$ = (2.86 - 7.15x)*1E-4 (m/W)
C = 1.5E9 (W-K/m)
D = 13,520 (K)

All others are as previously defined.

As with the formula for UO_2 conductivity, the MOX conductivity can be adjusted for different pellet densities using Equation (2-56).

These thermal properties are obtained for each interval by using the average of the mesh point temperatures bounding the interval.

$$k_{l,m} = k\left(\frac{T_{m-1} + T_m}{2}\right) = k_{r,m-1} \tag{2-58}$$

$$k_{r,m} = k\left(\frac{T_m + T_{m+1}}{2}\right) = k_{l,m+1} \tag{2-59}$$

Prior to the calculation of the temperature distribution in the fuel pellet, this model uses assumed thermal conductivity values based on an estimated temperature profile. The existing FRAPCON-3 gap conductance iteration scheme (Figure 2.2) will be used to converge on temperature and thermal conductivity in the fuel.

2.3.5.7 The Finite Difference Temperature Calculation

The difference approximation for the mesh points [Equations (2-26), (2-33), and (2-37)] lead to a tri-diagonal set of M simultaneous linear equations.

$$\begin{bmatrix} b_1 & c_1 & & & & \\ a_2 & b_2 & c_2 & & & \\ & \bullet & \bullet & & & \\ & & \bullet & \bullet & \bullet & \\ & & & a_{M-11} & b_{M-1} & c_{M-1} \\ & & & & a_M & b_M \end{bmatrix} \begin{bmatrix} T_1 \\ T_2 \\ \bullet \\ \bullet \\ T_{M-1} \\ T_M \end{bmatrix} = \begin{bmatrix} d_1 \\ d_2 \\ \bullet \\ \bullet \\ d_{M-1} \\ d_M \end{bmatrix} \tag{2-60}$$

Rows 1 and M correspond to the fuel centerline and fuel surface mesh points, respectively, and rows 2 through M-1 correspond to the interior mesh points. The coefficient matrix would normally be symmetric, but is not because of the right boundary condition that specifies the fuel surface temperature. The corresponding off-diagonal element is zero in the last row. The solution to the above equation is obtained by

$$E_1 = \frac{c_1}{b_1} \text{ and } F_1 = \frac{d_1}{b_1} \tag{2-61}$$

$$E_j = \frac{c_j}{b_j - a_j E_{j-1}} \quad F_j = \frac{c_j - a_j F_{j-1}}{b_j - a_j E_{j-1}} \text{ for } j = 2, 3, ..., M\text{-}1 \tag{2-62}$$

$$g_M = \frac{d_M - a_M F_{M-1}}{b_M - a_M E_{M-1}} \tag{2-63}$$

$$g_j = -E_j g_{j+1} + F_j \text{ for } j = M\text{-}1, M\text{-}2, ..., 3, 2, 1 \tag{2-64}$$

$$T_j = g_j \text{ for all } j \tag{2-65}$$

Equations (2-61) through (2-65) were derived by applying the rules for Gaussian elimination. This method of solution introduces little roundoff error, if the off-diagonal elements are negative and the diagonal is greater than the sum of the magnitudes of the off-diagonal elements. From the form of the difference equations for a fuel pellet, these conditions are satisfied for any values of the mesh point spacing, and thermal conductivity.

2.3.6 Plenum Gas Temperature

The plenum gas temperature is calculated based on energy transfer between the top of the pellet stack and the plenum gas, between the coolant channel and the plenum gas, and between the spring and the plenum gas. A discussion of these contributions follows.

Natural convection from the top of the fuel stack is calculated based on heat transfer coefficients from McAdams (1954) for laminar or turbulent natural convection from flat plates.

The heat transfer coefficient is calculated from

$$h_p = \frac{kNu}{D} \tag{2-66}$$

where

h_p	=	the heat transfer coefficient from the top of the pellet stack to the plenum gas (W/m^2-K)
Nu	=	Nusselt number
D	=	inside diameter of the cladding of the top node (m)
k	=	conductivity of the plenum gas (W/m-K)

The Nusselt number is calculated using

$$Nu = C(Gr\,\mathrm{Pr})^m \tag{2-67}$$

where

Gr	=	the Grashof number
Pr	=	the Prandtl number

and for

$Gr\mathrm{Pr} \leq 2.0\text{x}10^7$, $C = 0.54$ and $m = 0.25$,

or

$Gr\mathrm{Pr} > 2.0\text{x}10^7$, $C = 0.14$ and $m = 0.33$.

The overall effective conductivity from the coolant to the plenum is defined as the inverse of the sum of the individual heat flow resistances. The three resistances are a) the resistance across the inside surface film, b) the resistance across the cladding, and c) the resistance across the outside surface film. The overall conductivity is therefore found as

$$U_c = \frac{1.0}{\dfrac{2.0}{Dh_f} + \dfrac{\ln\left(\dfrac{D_o}{D_i}\right)}{k_{clad}} + \dfrac{2.0}{D_o(1.0+\alpha\Delta T)h_{DB}}} \tag{2-68}$$

where

U_c	=	overall effective conductivity from the coolant to the plenum gas (W/m-K)
D	=	hot-state inside cladding diameter (m)
h_f	=	cladding inside surface film coefficient (W/m^2-K)

D_o = cold-state outside cladding diameter (m)
D_i = cold-state inside cladding diameter (m)
k_{clad} = temperature- and material-dependent thermal conductivity of the cladding (W/m-K)
α = coefficient of thermal expansion of the cladding (1/K)
ΔT = temperature difference between cladding average temperature and datum temperature for thermal expansion (K)
h_{DB} = heat transfer coefficient between the coolant and the cladding (W/m^2-K)

Gamma heating in the hold down spring is calculated assuming a volumetric heating rate of 3.76 W/m^3 for every W/m^2 of rod average heat flux. The expression is

$$Q_{sp} = 3.76\dot{q}''V_s \tag{2-69}$$

where

Q_{sp} = energy generated in the spring due to gamma heating (W)
$\dot{q}''$ = average heat flux of the rod (W/m^2)
V_s = volume of the spring (m^3)

The plenum temperature is approximated from

$$T_{plen} = \frac{Q_{sp} + U_c \frac{V_p}{D^2} T_{BLK} + T_{pa} h_p \pi \frac{D^2}{4}}{U_c \frac{V_p}{D^2} + \frac{h_p \pi D^2}{4}} \tag{2-70}$$

where

T_{plen} = plenum temperature (K)
V_p = volume of the plenum (m^3)
T_{BLK} = bulk coolant temperature at the top axial node (K)
T_{pa} = temperature associated with the insulator or top pellet (K)

2.3.7 Stored Energy

The stored energy in the fuel rod is calculated by summing the energy of each pellet ring calculated at the ring temperature. The expression for stored energy is

$$E_s = \frac{\sum_{i=1}^{I} m_i \int_{298K}^{T_i} C_p(T)dT}{m} \tag{2-71}$$

where

E_s = stored energy (J/kg)
m_i = mass of ring segment *i* (kg)
T_i = temperature of ring segment i (K)

$C_p(T)$ = specific heat evaluated at temperature T (J/kg-K)
m = total mass of the axial node (kg)
I = number of annular rings

The stored energy is calculated for each axial node.

2.4 Fuel Rod Mechanical Response

An accurate calculation of fuel and cladding deformation is necessary in any fuel rod response analysis because the heat transfer coefficient across the fuel-cladding gap is a function of both the effective fuel-cladding gap size and the fuel-cladding interfacial pressure. In addition, an accurate calculation of stresses in the cladding is needed to accurately calculate the onset of cladding failure (and subsequent release of fission products). This section describes the default mechanical model, FRACAS-I. The optional cladding FEA model is described elsewhere (Knuutilla, 2006)

2.4.1 The FRACAS-I Model

The FRACAS-I model is available for the calculation of the small displacement deformation of the fuel and cladding. The simplified model, FRACAS-I, neglects the stress-induced deformation of the fuel, and is called the "rigid pellet model."

In analyzing the deformation of fuel rods, two physical situations are envisioned. The first situation occurs when the fuel and cladding are not in contact. Here the problem of a cylindrical shell (the cladding) with specified internal and external pressures and a specified cladding temperature distribution must be solved. This situation is called the "open gap" regime.

The second situation envisioned is when the fuel (considerably hotter than the cladding) has expanded so as to be in contact with the cladding. Further heating (thermal expansion) of the fuel "drives" the cladding outward. This situation is called the "closed gap" regime. In addition, this closed gap can occur due to fuel swelling, relocation, and the creep of the cladding onto the fuel due to a high coolant pressure.

The preceding two regimes of fuel rod deformation are characterized by small cladding strains and by the cladding retaining its essentially cylindrical shape.

The deformation analysis in FRAPCON-3 consists of a small deformation analysis that includes stresses, strains, and displacements in the fuel and cladding for the entire fuel rod. This analysis is based on the assumption that the cladding retains its cylindrical shape during deformation, and includes the effects of the following:

- fuel thermal expansion, swelling, densification, and relocation
- cladding thermal expansion, creep, and plasticity
- fission gas and external coolant pressures

As part of the small displacement analysis, the applicable local deformation regime (open gap, or closed gap) is determined. Finally, an analysis is performed to determine cladding stresses and strains.

In Section 2.4.1.1, the general theory of plastic analysis is outlined and the method of solution used in the FRACAS-I model is presented. This method of solution is used in the rigid pellet model. In Section 2.4.1.2, the equations for the rigid pellet model are described.

2.4.1.1 General Theory and Method of Solution

The general theory of plastic analysis and the method of solution are used in the rigid pellet model.

2.4.1.1.1 General Considerations in Elastic-Plastic Analysis

Problems involving elastic-plastic deformation and multiaxial stress states involve aspects that do not require consideration in a uniaxial problem. In the following discussion, an attempt is made to briefly outline the structure of incremental plasticity and to outline the method of successive substitutions (also called the method of successive elastic solutions) (Mendelson, 1968), which has been used successfully in treating multiaxial elastic-plastic problems. The method can be used for any problem for which a solution based on elasticity can be obtained. This method is used in the rigid pellet model.

In a problem involving only uniaxial stress, σ_1, the strain, ε_1, is related to the stress by an experimentally determined stress-strain curve as shown in Figure 2.7 (including the elastic strains and plastic strains, but without thermal expansion strains) so Hooke's law is taken as

$$\varepsilon_1 = \frac{\sigma_1}{E} + \varepsilon_1^P + \int \alpha dT \tag{2-72}$$

where ε_1^P is the plastic strain and E is the modulus of elasticity. The onset of yielding occurs at the yield stress, which can be determined directly from Figure 2.7. Given a load (stress) history, the resulting deformation can be determined in a simple manner. The increase of yield stress with work-hardening is easily computed directly from Figure 2.7.

In a problem involving multiaxial states of stress, however, the situation is not as clear. In such a problem, a method of relating the onset of plastic deformation to the results of a uniaxial test is required, and further, when plastic deformation occurs, some means is needed for determining how much plastic deformation has occurred and how that deformation is distributed among the individual components of strain. These two complications are taken into account by use of the so-called "yield function" and "flow rule," respectively.

A wealth of experimental evidence exists on the onset of yielding in a multiaxial stress state. Most of this evidence supports the von Mises yield criterion, which asserts that yielding occurs when the stress state is such that

$$0.5\left[(\sigma_1 - \sigma_2)^2 + (\sigma_2 - \sigma_3)^2 + (\sigma_3 - \sigma_1)^2\right] = \sigma_y \tag{2-73}$$

where the σ_i values (i = 1, 2, and 3) are the principle stresses, and σ_y is the yield stress as determined in a uniaxial stress-strain test. The square root of the left side of this equation is referred to as the "effective stress," σ_e, and this effective stress is one commonly used type of yield function.

To determine how the yield stress changes with permanent deformation, the yield stress is hypothesized to be a function of the equivalent plastic strain, ε^P. An increment of equivalent plastic strain is determined at each load step, and ε^P is defined as the sum of all increments incurred:

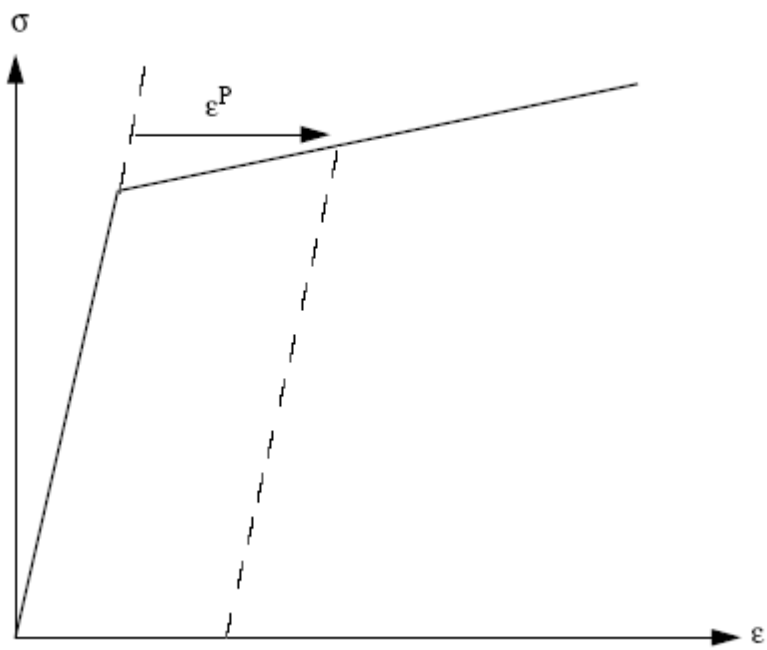

Figure 2.7 Typical isothermal stress-strain curve

$$\varepsilon^p \overset{\Delta}{=} \sum d\varepsilon^p \tag{2-74}$$

Each increment of effective plastic strain is related to the individual plastic strain components by

$$d\varepsilon^p = \frac{\sqrt{2}}{3}[(d\varepsilon_1^p - d\varepsilon_2^p)^2 + (d\varepsilon_2^p - d\varepsilon_3^p)^2 + (d\varepsilon_3^p - d\varepsilon_1^p)^2]^{1/2} \tag{2-75}$$

where the $d\varepsilon_i^P$ (i = 1, 2, and 3) are the plastic strain components in principle coordinates. Experimental results indicate that at pressures on the order of the yield stress, plastic deformation occurs with no change in volume, which implies that

$$d\varepsilon_1^p + d\varepsilon_2^p + d\varepsilon_3^p = 0 \tag{2-75}$$

Therefore, in a uniaxial test with $\sigma_1=\sigma$, $\sigma_2=\sigma_3= 0$, the plastic strain increments are

$$d\varepsilon_2^p = d\varepsilon_3^p = -\tfrac{1}{2} d\varepsilon_1^p \tag{2-77}$$

Therefore, in a uniaxial test, Equations (2-73) and (2-75) reduce to

$$\sigma = \sigma_y \tag{2-78}$$

$$d\varepsilon^p = d\varepsilon_1^p \tag{2-79}$$

Thus, when the assumption is made that the yield stress is a function of the total effective plastic strain (called the "strain-hardening hypothesis"), the functional relationship between yield stress and plastic strain can be taken directly from a uniaxial stress-strain curve by virtue of Equations (2-78) and (2-79).

The relationship between the magnitudes of the plastic strain increments and the effective plastic strain increment is provided by the Prandtl-Reuss flow rule:

$$d\varepsilon_i^p + \frac{3d\varepsilon^p}{2\sigma_e} S_i \quad i = 1, 2, 3 \tag{2-80}$$

where the S_i values are the deviatoric stress components (in principal coordinates) defined by

$$S_i = \sigma_i - \tfrac{1}{3}(\sigma_1 + \sigma_2 + \sigma_3) \quad i = 1, 2, 3 \tag{2-81}$$

Equation (2-80) embodies the fundamental observation of plastic deformation; that is, plastic strain increments are proportional to the deviatoric stresses. The constant of proportionality is determined by the choice of the yield function. Direct substitution shows that Equations (2-73), (2-75), (2-80), and (2-81) are consistent with one another.

Once the plastic strain increments have been determined for a given load step, the total strains are determined from a generalized form of Hooke's law given by

$$\begin{aligned}
\varepsilon_1 &= \frac{1}{E}\{\sigma_1 - \nu(\sigma_2 + \sigma_3)\} + \varepsilon_1^p + d\varepsilon_1^p + \int \alpha_1 dT \\
\varepsilon_2 &= \frac{1}{E}\{\sigma_2 - \nu(\sigma_1 + \sigma_3)\} + \varepsilon_2^p + d\varepsilon_2^p + \int \alpha_2 dT \\
\varepsilon_3 &= \frac{1}{E}\{\sigma_3 - \nu(\sigma_2 + \sigma_1)\} + \varepsilon_3^p + d\varepsilon_3^p + \int \alpha_3 dT
\end{aligned} \tag{2-82}$$

in which ε_1^p, ε_2^p, ε_3^p are the total plastic strain components at the end of the previous load increment and where E and ν are the modulus of elasticity and Poisson's ratio, respectively, obtained from the material properties handbook (Luscher and Geelhood, 2010).

The remaining continuum field equations of equilibrium, strain displacement, and strain compatibility are unchanged. The complete set of governing equations is presented in Table 2.2, written in terms of rectangular Cartesian coordinates and employing the usual indicial notation in which a repeated Latin index implies summation. This set of equations is augmented by an experimentally determined uniaxial stress-strain relation.

Table 2.2 Summary of FRACAS-I governing equations

Equilibrium

$$\sigma_{ji,j} + \rho f_i = 0$$

where σ = stress tensor

ρ = mass density

f_i = components of body force per unit mass

Stress strain

$$\varepsilon_{ij} = \frac{1+\nu}{E}\sigma_{ij} - \delta_{ij}\left(\frac{\nu}{E}\sigma_{kk} - \int \alpha dT\right) + \varepsilon_{ij}^{p} + d\varepsilon_{ij}^{p}$$

Compatibility

$$\varepsilon_{ij,kl} + \varepsilon_{kl,ij} - \varepsilon_{ik,jl} - \varepsilon_{jl,ik} = 0$$

Definitions used in plasticity

$$\sigma_e \overset{\Delta}{=} \sqrt{\frac{3}{2} S_{ij} S_{ij}}$$

$$S_{ij} \overset{\Delta}{=} \sigma_{ij} - \frac{1}{3}\sigma_{kk}$$

Prandtl-Reuss flow rule

$$d\varepsilon_{ij}^{p} = \frac{3}{2}\frac{d\varepsilon^{p}}{\sigma_e} S_{ij}$$

The Method of Solution—When the problem under consideration is statically determinate so that stresses can be found from equilibrium conditions alone, the resulting plastic deformation can be determined directly. However, when the problem is statically indeterminate and the stresses and deformation must be found simultaneously, the full set of plasticity equations proves to be quite formidable, even in the case of simple loadings and geometries.

One numerical procedure which has been used with considerable success is the method of successive substitutions. This method can be applied to any problem for which an elastic solution can be obtained, either in closed form or numerically. A full discussion of this technique, including a number of technologically useful examples, is contained in Knuutila (2006).

Briefly, the method involves dividing the loading path into small increments. For example, in the present application, the loads are external pressure, temperature, and either internal pressure or a prescribed displacement of the inside surface of the cladding. These loads all vary during the operating history of the fuel rod. For each new increment of the loading, the solution to all the plasticity equations listed in Table 2.2 is obtained as follows.

First, an initial estimate of the plastic strain increments, $d\varepsilon_{ij}^{P}$, is made. Based on these values, the equations of equilibrium, Hooke's law, and strain-displacement and compatibility are solved as for any elastic problem. From the stresses so obtained, the deviatoric stresses, S_{ij}, may be computed. This "pseudo-elastic" solution represents one path in the computational scheme.

Independently, through use of the assumed $d\varepsilon_{ij}^{P}$ values, the increment of effective plastic strain, $d\varepsilon^{p}$, may be computed. From this result and the stress-strain curve, a value of the effective stress, σ_e, is obtained from Equation (2-73).

Finally, a new estimate of the plastic strain increments is obtained from the Prandtl-Reuss flow rule

$$d\varepsilon_{ij}^{p} = \frac{3}{2}\frac{d\varepsilon^{p}}{\sigma_e}S_{ij} \tag{2-83}$$

and the entire process is continued until the $d\varepsilon_{ij}^{P}$ converge. A schematic of the iteration scheme is shown in Figure 2.8.

The mechanism by which improved estimates of $d\varepsilon_{ij}^{P}$ are obtained results from the fact that the effective stress obtained from $d\varepsilon^{P}$ and the stress-strain curve will not be equal to the effective stress that would be obtained with the stresses from the elastic solution. The effective stresses will only agree when convergence is obtained.

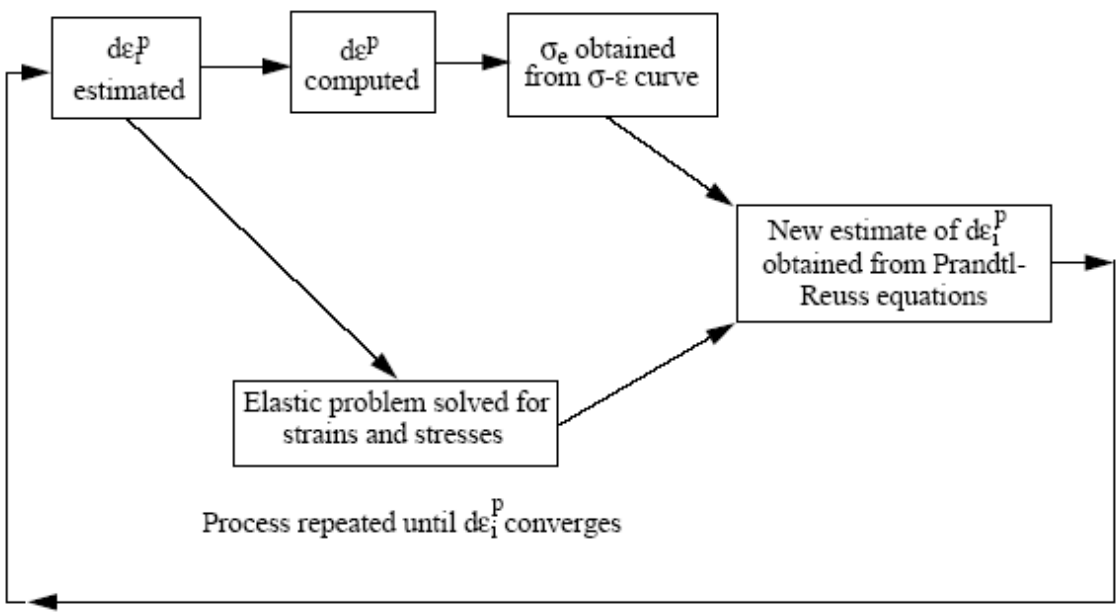

Figure 2.8 Schematic of the method of successive elastic solutions

The question of convergence is one that cannot, in general, be answered *a priori*. However, convergence can be shown to be obtained for sufficiently small load increments. Experience has shown that this technique is suitable for both steady-state and transient fuel rod analyses.

2.4.1.1.2 Extension to Creep

The method of solution described for the time-independent plasticity calculations can also be used for time-dependent creep calculations. In this context, the term "creep" refers to any time-dependent constant volume permanent deformation. Creep is a stress-driven process and is usually highly dependent on temperature.

The only change required to extend the method of successive elastic solutions to allow consideration of creep is to rewrite the Prandtl-Reuss flow rule [Equation (2-80)] as

$$
\begin{aligned}
d\varepsilon_1^c &= 1.5\frac{\dot{\varepsilon}^c \Delta t}{\sigma_e} S_1 + \frac{\dot{V}^c \Delta t}{9}\frac{(\sigma_1+\sigma_2+\sigma_3)}{\sigma_m} \\
d\varepsilon_3^c &= 1.5\frac{\dot{\varepsilon}^c \Delta t}{\sigma_e} S_2 + \frac{\dot{V}^c \Delta t}{9}\frac{(\sigma_1+\sigma_2+\sigma_3)}{\sigma_m} \\
d\varepsilon_3^c &= 1.5\frac{\dot{\varepsilon}^c \Delta t}{\sigma_e} S_3 + \frac{\dot{V}^c \Delta t}{9}\frac{(\sigma_1+\sigma_2+\sigma_3)}{\sigma_m}
\end{aligned}
\tag{2-84}
$$

The first term on the right-hand side of each of these equations computes the constant volume creep strain, whereas the second term in each equation computes the permanent change in volume. To use this form of the flow rule, two additional material property correlations must be available. The first is a correlation for constant volume creep strain, ε^c (taken in a uniaxial test), as a function of stress, time, temperature, and neutron flux; that is,

$$\varepsilon^c = f(\sigma, T, t, \phi) \tag{2-85}$$

where

σ	=	uniaxial stress (MPa)
T	=	temperature (K)
t	=	time (s)
ϕ	=	neutron flux (n/m^2-s)

In the FRACAS-I model, the strain hardening hypothesis is assumed, which implies that the strain correlation can be differentiated with respect to time and solved for creep strain rate in the form

$$\dot{\varepsilon}^c = h(\sigma, \varepsilon^c, t, T, \phi) \tag{2-86}$$

which is no longer an explicit function of time. The function "h" is contained in subroutine CREPR, and is described as follows.

A model described by Limbäck and Andersson (Limbäck and Andersson, 1996) of ABB Atom and AB Sandvik Steel, respectively, was selected for cladding irradiation creep in FRAPCON-3.4. This model uses a thermal creep model described by Matsuo (1987) and an empirical irradiation creep rate with tuned model parameters that were fit to the data set given by Franklin et al. (1983). This model was further modified by PNNL to use effective stress rather than hoop stress as an input so that the difference in creep behavior during outward and inward creep would be modeled correctly. Several of the fitting coefficients from the Limbäck paper were consequently changed to accommodate this change based on comparisons to several data sets (Franklin et al., 1983; Soniak et al., 2002; Gilbon et al., 2000; and Sontheimer and Missen, 1994). In addition, a temperature-dependent term was added to the formula for irradiation creep strain rate. This was done because creep data were used with temperature greater than the temperature of the data given by Franklin, and these data along with the Franklin data showed a dependence on temperature. This model has different parameters for stress relief annealed (SRA) and re-

crystallized annealed (RXA) cladding types, and provides reasonable creep strains in the LWR range of temperature and cladding hoop stresses that compare well to data. This model is described below.

The steady state thermal and irradiation creep rates are given by

$$\dot{\varepsilon}_{th} = A\frac{E}{T}\left(\sinh\frac{a_i\sigma_{eff}}{E}\right)^n \exp\left(\frac{-Q}{RT}\right) \tag{2-87}$$

$$\dot{\varepsilon}_{irr} = C_0 \cdot \phi^{C_1} \cdot \sigma_{eff}^{C_2} \cdot f(T) \tag{2-88}$$

where

$\dot{\varepsilon}_{th}, \dot{\varepsilon}_{irr}$ = thermal and irradiation strain rate, respectively (m/m/hr)

These rates are added together, so

$$\dot{\varepsilon}_{th+irr} = \dot{\varepsilon}_{th} + \dot{\varepsilon}_{irr} \tag{2-89}$$

The saturated primary hoop strain is given by

$$\varepsilon_p^s = 0.0216 \cdot \dot{\varepsilon}_{th+irr}^{0.109}\left(2 - \tanh(35500 \cdot \dot{\varepsilon}_{th+irr})\right)^{-2.05} \tag{2-90}$$

The total thermal strain is given by

$$\varepsilon_H = \varepsilon_p^s\left(1 - \exp\left(-52 \cdot \sqrt{\dot{\varepsilon}_{th+irr} \cdot t}\right)\right) + \dot{\varepsilon}_{th+irr} \cdot t \tag{2-91}$$

In FRAPCON-3.4, strain rate is used. Taking the derivative with respect to time of the expression above gives

$$\dot{\varepsilon}_H = \frac{52 \cdot \varepsilon_p^s \cdot \dot{\varepsilon}_{th+irr}^{\frac{1}{2}}}{2 \cdot t^{\frac{1}{2}}} \exp\left(-52 \cdot \sqrt{\dot{\varepsilon}_{th+irr} \cdot t}\right) + \dot{\varepsilon}_{th+irr} \tag{2-92}$$

where

T	=	temperature (K)
t	=	time (hours)
σ_{eff}	=	effective stress (MPa)
ϕ	=	fast neutron flux (n/m²-s)

Table 2.3 lists the parameters used in these equations for SRA and RXA cladding types. These parameters are those recommended by Limbäck and Andersson (Limbäck and Andersson, 1996), with the exception of the "A" parameter and the "f(T)" parameter, that were modified by PNNL.

Table 2.3 Parameters for FRAPCON-3.4 creep equation for SRA and RXA cladding

Parameter	Units	Values for SRA Cladding	Values for RXA Cladding
A	K/MPa/hr	1.08E9	5.47E8
E	MPA	1.149-59.9*T	
a_i	MPa^{-1}	650{1-0.56[1-exp(-1.4E-27*$\Phi^{1.3}$)]} Φ = fast neutron fluence (n/cm²)	
n	unitless	2.0	3.5
Q	kJ/mole	201	
R	kJ/mol-K	0.008314	
C_0	$(n/m^2\text{-}s)^{-C1}$ MPa^{-C2}	4.0985E-24	1.87473E-24
C_1	unitless	0.85	
C_2	unitless	1.0	
f(T)	unitless	T<570K 0.7283 570<T<625K -7.0237+0.0136T T>625K 1.4763	0.7994 -3.18562+0.00699132T 1.1840

The effective stress in the cladding is found using the principal stresses at the mid-wall radius using the thick wall formula as follows:

$$\sigma_r = \frac{P_i r_i^2 - P_o r_o^2 + \dfrac{r_i^2 r_o^2 \left(P_o - P_i\right)}{r^2}}{r_0^2 - r_i^2} \tag{2-93}$$

$$\sigma_t = \frac{P_i r_i^2 - P_o r_o^2 - \dfrac{r_i^2 r_o^2 \left(P_o - P_i\right)}{r^2}}{r_0^2 - r_i^2} \tag{2-94}$$

$$\sigma_l = \frac{P_i r_i^2 - P_o r_o^2}{r_0^2 - r_i^2} \tag{2-95}$$

where

P_i = inner pressure
P_o = outer pressure
r_i = inner radius
r_o = outer radius
r = radius within tube
σ_r = radial stress
σ_t = tangential stress
σ_l = longitudinal stress

The effective stress, σ_{eff}, is then given by

$$\sigma_{eff} = \sqrt{\tfrac{1}{2}\left(\left(\sigma_l - \sigma_t\right)^2 + \left(\sigma_t - \sigma_r\right)^2 + \left(\sigma_r - \sigma_l\right)^2\right)} \tag{2-96}$$

The correlations above are developed for SRA and RXA Zircaloy-4 and Zircaloy-2. For M5, the correlation for RXA Zircaloy is used. For ZIRLO and Optimized ZIRLO, the correlation for SRA Zircaloy reduced by a factor of 0.8 is used (Sabol et al., 1994).

A plot of the resulting creep strain is shown as a function of time and effective stress for representative flux and temperature values in Figure 2.9.

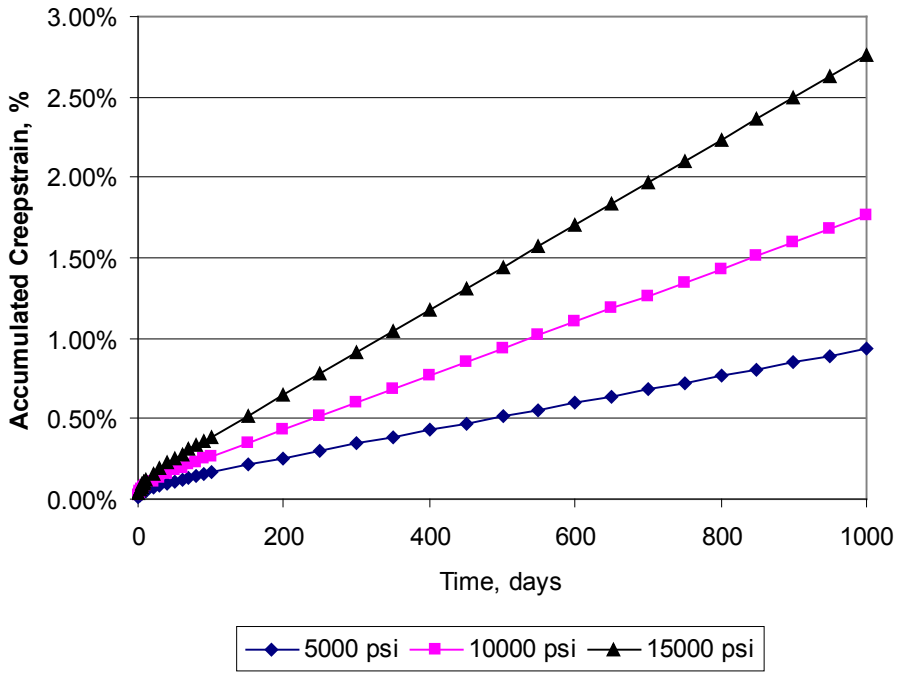

(a)

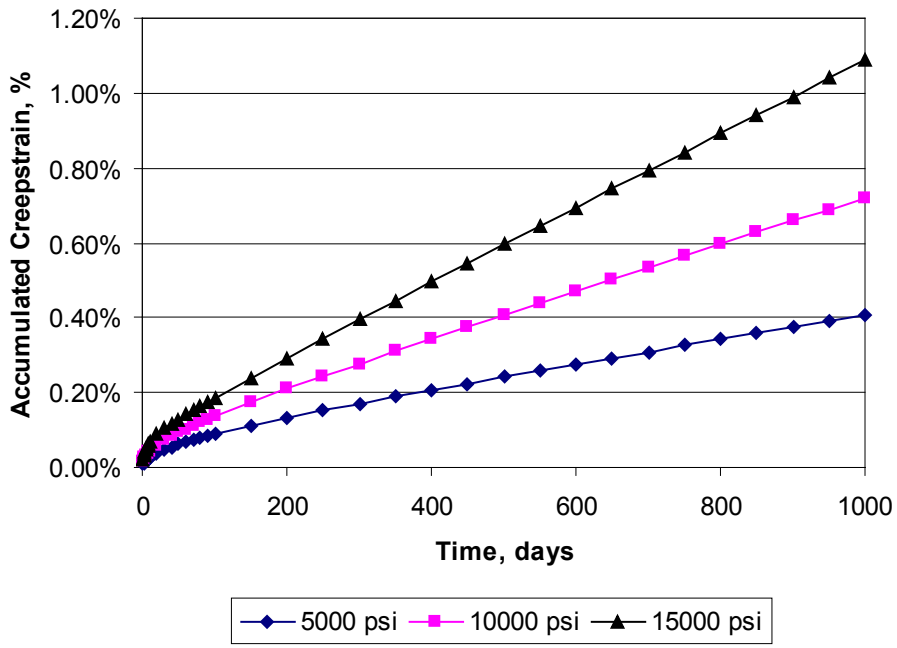

(b)

Figure 2.9 Cladding creep strain as a function of time and hoop stress for 630°F and flux=10^{18} n/m²/s for (a) SRA Zircaloy and (b) RXA Zircaloy

The second additional correlation required is a relationship between the rate of permanent volumetric strain and the applied loads; that is,

$$\dot{V}^c = g(\sigma_m, T, t, V_{avail}) \tag{2-97}$$

where

σ_m	=	$(\sigma_1+\sigma 2+\sigma 3)/3$ the mean stress (MPa)
T	=	temperature (K)
t	=	time (s)
V_{avail}	=	measure of maximum permanent volumetric change possible

The permanent volumetric strain increment dV^c is related to the creep strain increments by the equation

$$dV^c = d\varepsilon_1^c + d\varepsilon_2^c + d\varepsilon_3^c \tag{2-98}$$

As previously noted, the FRACAS-I model is the default model available for analyzing the small deformation of the fuel and cladding. The model considers the fuel pellets to be essentially rigid and to deform due to thermal expansion, swelling, and densification only. Thus, in the rigid pellet model, the displacement of the fuel is calculated independently of the deformation of the cladding. This rigid pellet analysis is performed with the FRACAS-I subcode.

2.4.1.2 Rigid Pellet Cladding Deformation Model

FRACAS-I consists of a cladding deformation model and a fuel deformation model. If the fuel-cladding gap is closed, the fuel deformation model will apply a driving force to the cladding deformation model. The cladding deformation model, however, never influences the fuel deformation model.

The cladding deformation model in FRACAS-I is based on the following assumptions:

- Incremental theory of plasticity.
- Prandtl-Reuss flow rule.
- Isotropic work-hardening.
- Thin wall cladding (stress, strain, and temperature uniform through cladding thickness).
- If fuel and cladding are in contact, no axial slippage occurs at fuel cladding interface.
- Bending strains and stresses in cladding are negligible.
- Axisymmetric loading and deformation of cladding.

The fuel deformation model in FRACAS-I is based on the following assumptions:

- Thermal expansion, swelling, and densification are the only sources for fuel deformation.
- No resistance to expansion of fuel.
- No creep deformation of fuel.
- Isotropic fuel properties.

The cladding and fuel deformation models in FRACAS-I are described below.

2.4.1.2.1 Cladding Deformation Model

The rigid pellet cladding deformation subcode (FRACAS-I) consists of four sets of models, each used independently.

Deformation and stresses in the cladding in the open gap regime are computed using a model which considers a thick wall cylindrical shell with specified internal and external pressures and a prescribed uniform temperature.

Calculations for the closed gap regime are made using a model which considers a thin cylindrical shell with prescribed external pressure and a prescribed radial displacement of the cladding inside surface. The prescribed displacement is obtained from the fuel expansion models (including swelling) described later in this section. Further, since no slippage is assumed when the fuel and cladding are in contact, the axial expansion of the fuel is transmitted directly to the cladding, and hence, the change in axial strain in the shell is also prescribed.

The decision whether the fuel-cladding gap is open or closed is made by considering the relative movement of the cladding inside surface and the fuel outside surface. At the completion of the FRACAS-I analysis, either a new fuel-cladding gap size or a new fuel-cladding interfacial pressure and the elastic-plastic cladding stresses and strains are obtained.

Two additional models are used to compute changes in yield stress with work-hardening, given a uniaxial stress-strain curve. This stress-strain curve is obtained from the updated MATPRO properties. The first model computes the effective total strain and new effective plastic strain, given a value of effective stress and the effective plastic strain at the end of the last loading increment. The second model computes the effective stress, given an increment of plastic strain and the effective plastic strain at the end of the last loading increment. Depending on the work-hardened value of yield stress, loading can be either elastic or plastic, and unloading is constrained to occur elastically. (Isotropic work-hardening is assumed in these calculations.) These four sets of models are described below.

The determination of whether or not the fuel is in contact with the cladding is made by comparing the radial displacement of the fuel surface (u_r^{fuel}) with the radial displacement that would occur in the cladding (u_r^{clad}) due to the prescribed external (coolant) pressure and the prescribed internal (fission and fill gas) pressure. The free radial displacement of the cladding is obtained using Equation (2-82). The following expression is used to determine if fuel-cladding contact has occurred:

$$u_r^{fuel} \geq u_r^{clad} + \delta \tag{2-99}$$

where

δ = as-fabricated fuel-cladding gap size (m)

If Equation (2-99) is satisfied, the fuel is in contact with the cladding. The loading history enters into this decision by virtue of the permanent plastic cladding strains which are applied to the as-fabricated geometry. These plastic strains, and total effective plastic strain, ε^P, are retained for use in subsequent calculations.

If the fuel and cladding displacements are such that Equation (2-99) is not satisfied, the fuel-cladding gap has not closed during the current step and the solution obtained by the open gap solution is appropriate. The current value of the fuel-cladding gap size is then computed and is used in the temperature calculations. The plastic strain values may be changed in the solution if additional plastic straining has occurred.

If Equation (2-99) is satisfied, however, fuel and cladding contact has occurred during the current loading increment. At the contact interface, radial continuity requires that

$$u_r^{cladl} = u_r^{fuel} - \delta \tag{2-100}$$

while in the axial direction the assumption is made that no slippage occurs between the fuel and the cladding. This state is referred to as "lockup."

Note that only the additional strain which occurs in the fuel after lockup has occurred is transferred to the cladding. Thus, if $\varepsilon_{z,o}^{clad}$ is the axial strain in the cladding just prior to contact, and $\varepsilon_{z,o}^{fuel}$ is the corresponding axial strain in the fuel, then the no-slippage condition in the axial direction becomes

$$\varepsilon_z^{clad} - \varepsilon_{z,o}^{clad} = \varepsilon_z^{fuel} - \varepsilon_{z,o}^{fuel} \tag{2-101}$$

The values of the "prestrains", $\varepsilon_{z,o}^{fuel}$ and $\varepsilon_{z,o}^{clad}$, are set equal to the values of the strains that existed in the fuel and cladding at the time of fuel-cladding gap closure and are stored and used in the cladding sequence of calculations. The values are updated at the end of any load increment during which the fuel-cladding gap is closed.

After u_r^{clad} and ε_z^{clad} have been computed, they are used in a calculation which considers a thin cylindrical shell with prescribed axial strain, external pressure, and prescribed radial displacement of the inside surface. After the solution is obtained, a value of the fuel-cladding interfacial pressure is computed along with new plastic strains and stresses.

The open gap modeling considers a thin cylindrical shell loaded by both internal and external pressures. Axisymmetric loading and deformation are assumed. Loading is also restricted to being uniform in the axial direction, and no bending is considered. The geometry and coordinates are shown in Figure 2.10. The displacements of the midplane of the shell are *u* and *w* in the radial and axial directions, respectively.

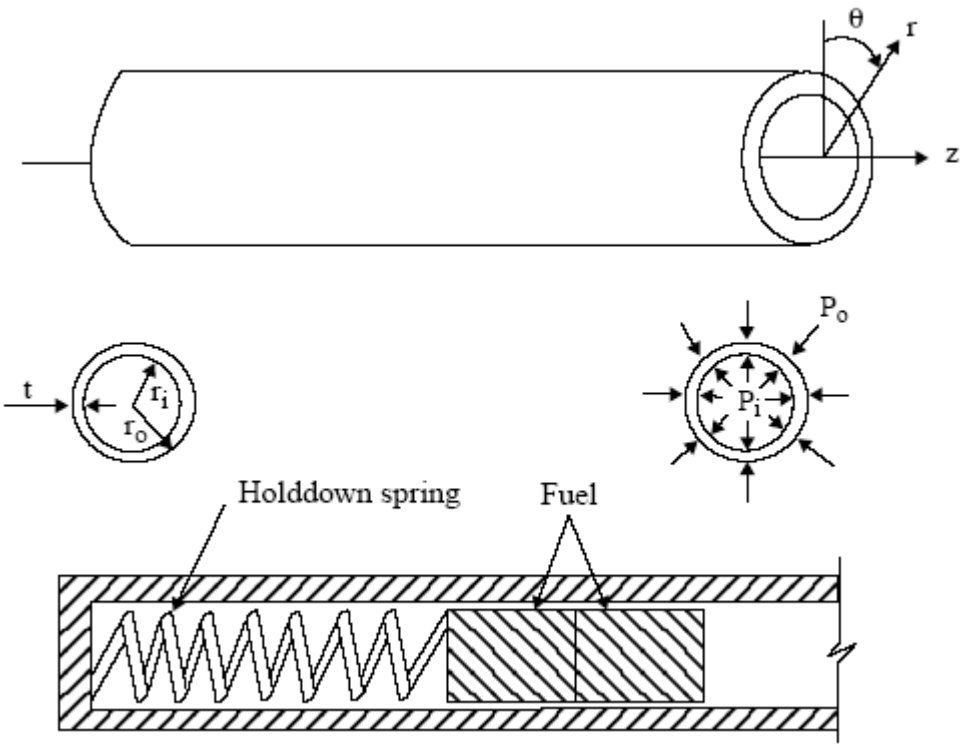

Figure 2.10 Fuel rod geometry and coordinates

For this case, the equilibrium equations are identically satisfied by

$$\sigma_\theta = \frac{r_i P_i - r_o P_o}{t} \tag{2-102}$$

$$\sigma_z = \frac{r_i^2 P_i - r_o^2 P_o}{r_o^2 - r_i^2} \tag{2-103}$$

where

σ_q	=	hoop stress (MPa)
σ_z	=	axial stress (MPa)
r_i	=	inside radius of cladding (m)
r_o	=	outside radius of cladding (m)
P_i	=	fuel rod internal gas pressure (MPa)
P_o	=	coolant pressure (MPa)
t	=	cladding thickness (m)

For membrane shell theory, the strains are related to the midplane displacements by

$$\varepsilon_z = \frac{\partial w}{\partial z} \tag{2-104}$$

$$\varepsilon_\theta = \frac{u}{\bar{r}} \tag{2-105}$$

where $\bar{r}$ is the radius of the midplane. Strain across the thickness of the shell is allowed. In shell theory, since the radial stress can be neglected, and since the hoop stress, σ_q, and axial stress, σ_z, are uniform across the thickness when bending is not considered, the radial strain is due only to the Poisson effect and is uniform across the thickness. (Normally, radial strains are not considered in a shell theory, but plastic radial strains must be included when plastic deformations are considered.)

The stress-strain relations are written in incremental form as

$$\varepsilon_\theta = \frac{1}{E}\{\sigma_\theta - \nu\sigma_z\} + \varepsilon_\theta^P + d\varepsilon_\theta^P + \int_{T_0}^{T} \alpha_\theta dT \tag{2-106}$$

$$\varepsilon_z = \frac{1}{E}\{\sigma_z - \nu\sigma_\theta\} + \varepsilon_z^P + d\varepsilon_z^P + \int_{T_0}^{T} \alpha_z dT \tag{2-107}$$

$$\varepsilon_r = -\frac{\nu}{E}\{\sigma_\theta + \sigma_z\} + \varepsilon_r^P + d\varepsilon_r^P + \int_{T_0}^{T} \alpha_r dT \tag{2-108}$$

where

T_o	=	strain-free reference temperature (K)
α	=	coefficient of thermal expansion
T	=	current average cladding temperature (K)
E	=	modulus of elasticity
ν	=	Poisson's ratio

The terms ε_θ^P, ε_z^P, and ε_r^P are the plastic strains at the end of the last load increment, and $d\varepsilon_\theta^P$, $d\varepsilon_z^P$, and $d\varepsilon_r^P$ are the additional plastic strain increments which occur due to the new load increment.

The magnitude of the additional plastic strain increments is determined by the effective stress and the Prandtl-Reuss flow rule, expressed as

$$\sigma_e = \frac{1}{\sqrt{2}}[(\sigma_\theta - \sigma_z)^2 + (\sigma_z)^2 + (\sigma_\theta)^2]^{\frac{1}{2}} \tag{2-109}$$

$$d\varepsilon_i^p = \frac{3}{2}\frac{d\varepsilon^p}{\sigma_e} S_i \text{ for } i = r, \theta, z \tag{2-110}$$

$$S_i = \sigma_i - \frac{1}{3}(\sigma_\theta + \sigma_z) \text{ for } i = r, \theta, z \tag{2-111}$$

The solution of the open gap case proceeds as follows. At the end of the last load increment the plastic strain components, ε_θ^P, ε_z^P, and ε_r^P are known. Also the total effective plastic strain, ε^P, is known.

The loading is now incremented with the prescribed values of P_i, P_o, and T. The new stresses can be determined from Equations (2-102) and (2-103), and a new value of effective stress is obtained from Equation (2-109).

The increment of effective plastic strain, $d\varepsilon^P$, which results from the current increment of loading, can now be determined from the uniaxial stress-strain curve at the new value of σ_e, as shown in Figure 2.11. (The new elastic loading curve depends on the value of ε^P_{old}.)

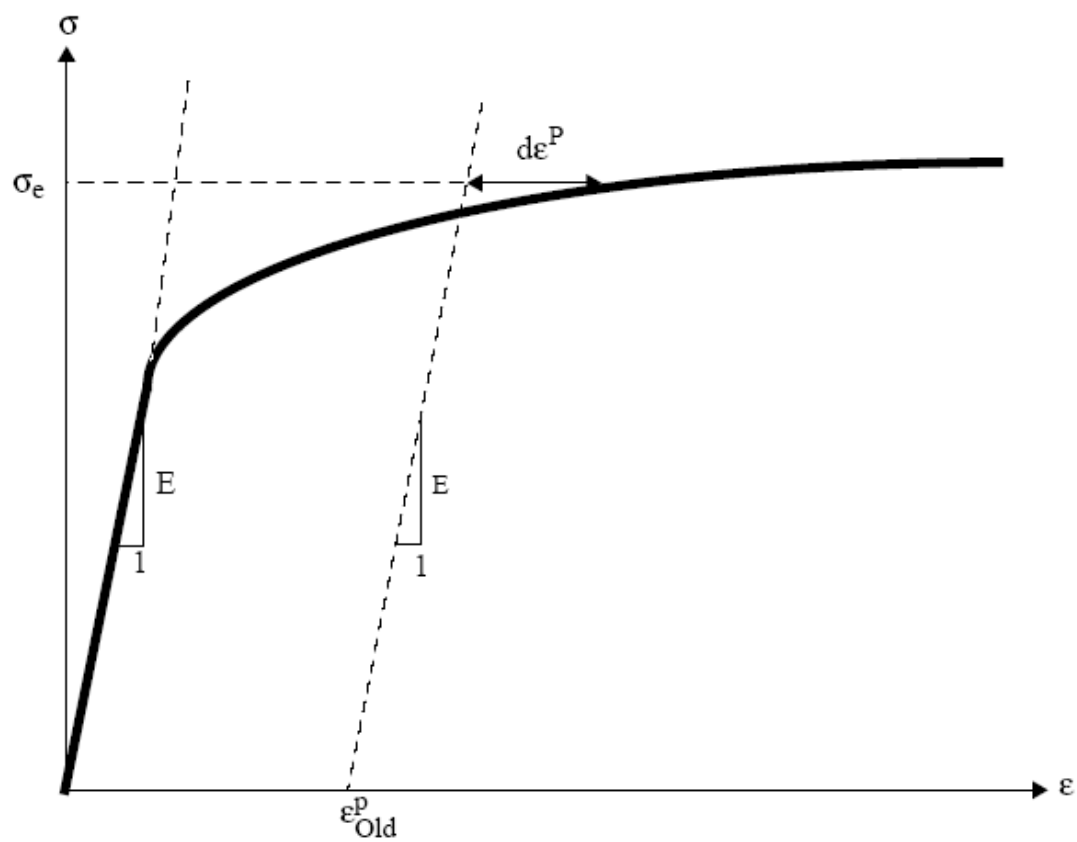

Figure 2.11 Calculation of effective stress σ_e from $d\varepsilon^P$

Once $d\varepsilon^P$ is determined, the individual plastic strain components are found from Equation (2-110), and the total strain components are obtained from Equations (2-106) through (2-108).

The displacement of the inside surface of the shell must be determined so that a new fuel-cladding gap width can be computed. The radial displacement of the inside surface is given by

$$u(r_i) = \bar{r}\varepsilon_\theta - \frac{t}{2}\varepsilon_r \tag{2-112}$$

where the first term is the radial displacement of the midplane [from Equation (2-105)] and ε_r is the uniform strain across the cladding thickness, t.

The cladding thickness is computed by the equation

$$t = (1 + \varepsilon_r)\, t_o \tag{2-113}$$

where

t_o = as-fabricated, unstressed thickness

The final step performed is to add the plastic strain increments to the previous plastic strain values; that is,

$$\begin{aligned}
(\varepsilon_\theta^P)_{new} &= (\varepsilon_\theta^P)_{old} + d\varepsilon_\theta^P \\
(\varepsilon_z^P)_{new} &= (\varepsilon_z^P)_{old} + d\varepsilon_z^P \\
(\varepsilon_r^P)_{new} &= (\varepsilon_r^P)_{old} + d\varepsilon_r^P \\
(\varepsilon^P)_{new} &= (\varepsilon^P)_{old} + d\varepsilon^P
\end{aligned} \tag{2-114}$$

These values are used for the next load increment.

Thus, all the stresses and strains can be computed directly, since in this case the stresses are determinate. In the case of the driven cladding displacement, the stresses depend on the displacement, and such a straightforward solution is not possible.

The closed gap modeling considers the problem of a cylindrical shell for which the radial displacement of the inside surface and axial strain are prescribed. Here the stresses cannot be computed directly since the pressure at the inside surface (the fuel-cladding interfacial pressure) must be determined as part of the solution.

As in the open gap modeling, the displacement at the inside surface is given by

$$u(r_i) = u - \frac{t}{2}\varepsilon_r \tag{2-115}$$

where u is the radial displacement of the midplane. From Equation (2-106), $u = r\varepsilon_\theta$ and

$$u(r_i) = \bar{r}\varepsilon_\theta - \frac{t}{2}\varepsilon_r \tag{2-116}$$

Thus, prescribing the displacement of the inside surface of the shell is equivalent to a constraining relation between ε_θ and ε_i. As before, Hooke's law is taken in the form

$$\varepsilon_\theta = \frac{1}{E}\{\sigma_\theta - \nu\sigma_z\} + \varepsilon_\theta^P + d\varepsilon_\theta^P + \int_{T_0}^{T} \alpha_\theta dT \tag{2-117}$$

$$\varepsilon_z = \frac{1}{E}\{\sigma_z - \nu\sigma_\theta\} + \varepsilon_z^P + d\varepsilon_z^P + \int_{T_0}^{T} \alpha_z dT \tag{2-118}$$

$$\varepsilon_r = -\frac{\nu}{E}\{\sigma_\theta + \sigma_z\} + \varepsilon_r^P + d\varepsilon_r^P + \int_{T_0}^{T} \alpha_r dT \tag{2-119}$$

Use of Equations (2-116) and (2-119) in Equation (2-117) results in a relation between the stresses σ_θ and σ_z, and the prescribed displacement $u(r_i)$:

$$\frac{u(r_i)}{\bar{r}} + \frac{1}{2}\frac{1}{2\bar{r}}\left\{\varepsilon_r^P + d\varepsilon_r^P + \int_{T_0}^{T} \alpha dT\right\} - \left\{\varepsilon_\theta^P + d\varepsilon_\theta^P + \int_{T_0}^{T} \alpha dT\right\} = \frac{1}{E}\left[\left(1 + \frac{\nu t}{2\bar{r}}\right)\sigma_\theta + \nu\left(\frac{t}{2\bar{r}} - 1\right)\sigma_z\right] \tag{2-120}$$

Equations (2-118) and (2-120) are now a pair of simultaneous algebraic equations for the stresses σ_θ and σ_z, which may be written as

$$\begin{bmatrix} A_{11} & A_{12} \\ A_{21} & A_{22} \end{bmatrix}\begin{bmatrix} \sigma_\theta \\ \sigma_z \end{bmatrix} = \begin{bmatrix} B_1 \\ B_2 \end{bmatrix} \tag{2-121}$$

where

$$\begin{aligned}
A_{11} &= 1 + \frac{\nu t}{2\bar{r}} \\
A_{12} &= \nu\left(\frac{t}{2\bar{r}} - 1\right) \\
A_{21} &= -\nu \\
A_{22} &= 1 \\
B_1 &= \left(E\frac{u(r_i)}{\bar{r}} + \frac{Et}{4\bar{r}}\left\{\varepsilon_r^P + d\varepsilon_r^P + \int_{T_0}^{T} \alpha dT\right\}\right) - E\left\{\varepsilon_\theta^P + d\varepsilon_\theta^P + \int_{T_0}^{T} \alpha dT\right\} \\
B_2 &= E\left(\varepsilon_z - E\varepsilon_z^P + d\varepsilon_z^P + \int_{T_0}^{T} \alpha dT\right)
\end{aligned}$$

Then the stresses can be written explicitly as

$$\sigma_\theta = \frac{B_1 A_{22} - B_2 A_{12}}{A_{11}A_{22} - A_{12}A_{21}} \tag{2-122}$$

$$\sigma_z = \frac{B_2 A_{11} - B_1 A_{21}}{A_{11} A_{22} - A_{12} A_{21}} \tag{2-123}$$

These equations relate the stresses to $u(r_i)$ and ε_z, which are prescribed, and to $d\varepsilon_\theta^P$, $d\varepsilon_z^P$, and $d\varepsilon_r^P$, which are to be determined. The remaining equations which must be satisfied are

$$\sigma_e = \frac{1}{\sqrt{2}}[(\sigma_\theta - \sigma_z)^2 + (\sigma_z)^2 + (\sigma_\theta)^2]^{\frac{1}{2}} \tag{2-124}$$

$$d\varepsilon^p = \frac{\sqrt{2}}{3}[(d\varepsilon_r^p - d\varepsilon_\theta^p)^2 + (d\varepsilon_\theta^p - d\varepsilon_z^p)^2 + (d\varepsilon_z^p - d\varepsilon_r^p)^2]^{1/2} \tag{2-125}$$

and the Prandtl-Reuss flow equations [defined in Equation (2-110)]

$$d\varepsilon_\theta^p = \frac{3}{2}\frac{d\varepsilon^p}{\sigma_e}\left[\sigma_\theta - \frac{1}{3}(\sigma_\theta + \sigma_z)\right] \tag{2-126}$$

$$d\varepsilon_z^p = \frac{3}{2}\frac{d\varepsilon^p}{\sigma_e}\left[\sigma_z - \frac{1}{3}(\sigma_\theta + \sigma_z)\right] \tag{2-127}$$

$$d\varepsilon_r^p = -d\varepsilon_\theta^p - d\varepsilon_z^p \tag{2-128}$$

The effective stress, σ_e, and the plastic strain increment, $d\varepsilon^P$, must, of course, be related by the uniaxial stress-strain law. Equations (2-122) through (2-128) must be simultaneously satisfied for each loading increment.

As discussed in Section 2.4.1.1, a straightforward numerical solution to these equations can be obtained using the method of successive elastic solutions. By this method, arbitrary values are initially assumed for the increments of plastic strain, and Equations (2-122) through (2-128) are used to obtain improved estimates of the plastic strain components. The following steps are performed for each increment of load:

1. Values of $d\varepsilon_\theta^P$, $d\varepsilon_z^P$, and $d\varepsilon_r^P$ are assumed. Then, $d\varepsilon^P$ is computed from Equation (2-125) and the effective stress is obtained from the stress-strain curve at the value of $d\varepsilon^P$.

2. From Hooke's law, still using the assumed plastic strain increments and the prescribed values of $u(r_i)$ and ε_z, values for the stresses can be obtained from Equations (2-122) and (2-123).

3. New values for $d\varepsilon_\theta^P$, $d\varepsilon_z^P$, and $d\varepsilon_r^P$ are now computed from the Prandtl-Reuss relations,

$$d\varepsilon_i^p = \frac{3}{2}\frac{d\varepsilon^p}{\sigma_e}\left[\sigma_i - \frac{1}{3}(\sigma_\theta + \sigma_z)\right] \text{ for } i = r, \theta, z \tag{2-129}$$

using σ_e as computed in step 1, and σ_i as computed in step 2.

4. The old and new values of $d\varepsilon_\theta^P$, $d\varepsilon_z^P$, and $d\varepsilon_r^P$ are compared and the process continued until convergence is obtained.

5. Once convergence has been obtained, the fuel-cladding interfacial pressure is computed from the following equation.

$$P_{\text{int}} = \frac{t\sigma_\theta + r_o P_o}{r_i} \tag{2-130}$$

When steps 1 through 5 have been accomplished, the solution is complete, provided that the fuel-cladding interface pressure is not less than the local gas pressure.

However, due to unequal amounts of plastic straining in the hoop and axial directions upon unloading, the fuel-cladding interfacial pressure as obtained in step 5 is often less than the gas pressure even though the fuel-cladding gap has not opened. When this situation occurs, the frictional "locking" (which is assumed to constrain the cladding axial deformation to equal the fuel axial deformation) no longer exists. The axial strain and stress adjust themselves so that the fuel-cladding interfacial pressure equals the gas pressure, at which point the axial strain is again "locked." Thus, upon further unloading, the axial strain and the hoop and axial stresses continually readjust themselves to maintain the fuel-cladding interfacial pressure equal to the gas pressure until the fuel-cladding gap opens. Since the unloading occurs elastically, a solution for this portion of the fuel-cladding interaction problem can be obtained directly as discussed below.

Since the external pressure and the fuel-cladding interfacial pressure are known, the hoop stress is obtained from Equation (2-130) as

$$\sigma_\theta = \frac{r_i P_{\text{int}} - r_o P_o}{t} \tag{2-131}$$

From Equation (2-116), the following expression can be written:

$$\varepsilon_\theta = \frac{u_r^{fuel} - \delta + \frac{t}{2}\varepsilon_r}{\bar{r}} \tag{2-132}$$

Substitution of ε_θ and ε_r, as given by Equations (2-117) and (2-119), into Equation (2-132) results in an explicit equation for σ_z:

$$\nu r_i \sigma_z = (r + \nu\frac{t}{2})\sigma_\theta + rE\left(\int \alpha dT + d\varepsilon_\theta^P\right) - \frac{t}{2}E\left(\int \alpha dT + d\varepsilon_r^P\right) - Eu(r_i) \tag{2-133}$$

in which σ_θ is known from Equation (2-20). With σ_z and σ_θ known, the strains may be computed from Hooke's law, Equation (2-117) through (2-119). This set of equations is automatically invoked whenever P_{int} is computed to be less than the local gas pressure.

As in the open gap modeling, the last step is to set the plastic strain components and total effective strain equal to their new values by adding in the computed increments $d\varepsilon_i^P$ and $d\varepsilon^P$.

The stress-strain modeling is used to relate stress and plastic strain, taking into consideration the direction of loading and the previous plastic deformation. A typical stress-strain curve is shown in Figure 2.12. This curve presents the results of a uniaxial stress-strain experiment and may be interpreted beyond initial yield as the focus of work-hardened yield stresses. The equation of the curve is provided by the updated MATPRO properties at each temperature given in Section 2.4.1.3.

To use this information, the usual idealization of the mechanical behavior of metals is made. Thus, linear elastic behavior is assumed until a sharply defined yield stress is reached, after which plastic (irrecoverable) deformation occurs. Unloading from a stress state beyond the initial yield stress, σ_y^o, is assumed to occur along a straight line having the elastic modulus for its slope. When the (uniaxial) stress is removed completely, a residual plastic strain remains, and this completely determines the subsequent yield stress. That is, when the specimen is loaded again, loading will occur along line BA in Figure 2.12, and no additional deformation will occur until point A is again reached. Point A is the subsequent yield stress. If $\sigma = f(\varepsilon)$ is the equation of the plastic portion of the stress-strain curve (YAC), then for a given value of plastic strain, the subsequent yield stress is found by simultaneously solving the pair of equations.

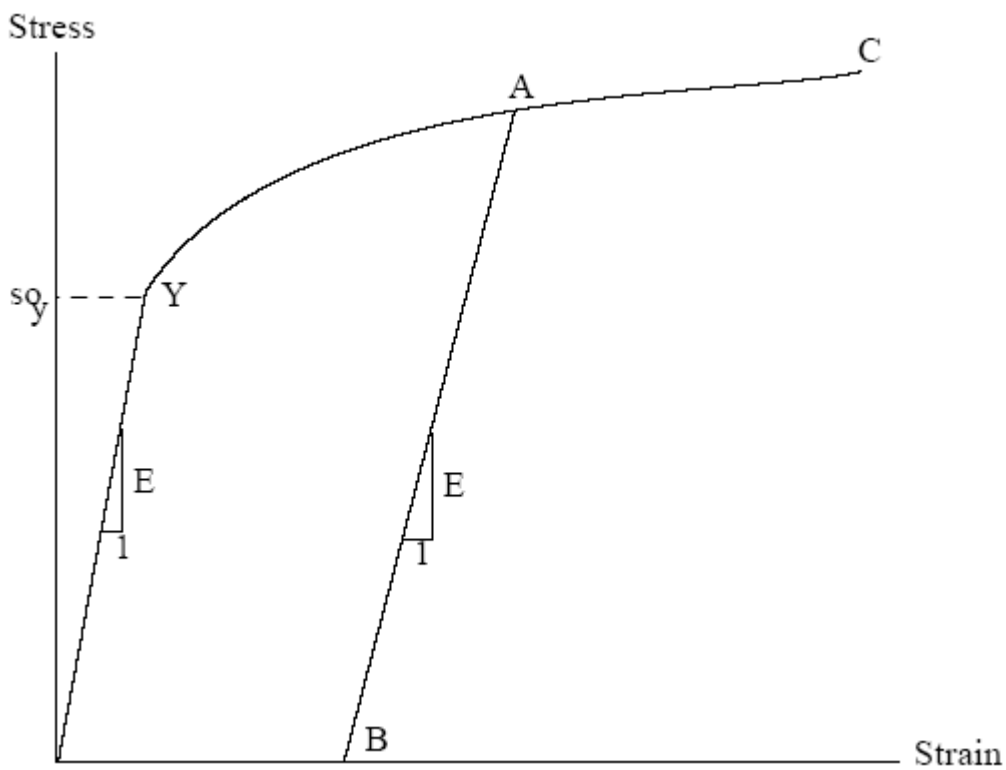

Figure 2.12 Idealized stress-strain behavior

$$\left| \begin{array}{l} \sigma = f(\varepsilon) \\ \sigma = E(\varepsilon - \varepsilon^P) \end{array} \right. \tag{2-134}$$

which may be written as

$$\sigma = f\left(\frac{\sigma}{E} + \varepsilon^P\right).$$

This nonlinear equation may be solved efficiently by using an iteration scheme:

$$\sigma^{m+1} = f\left(\frac{\sigma^m}{E} + \varepsilon^P\right) \quad m = 0, 1, 2, \ldots \tag{2-135}$$

The initial iterate, σ^m, is arbitrary, and without loss of generality, is taken as 34.5 MPa. For any monotonically, increasing stress-plastic strain relation, the iteration scheme in Equation (2-135) will converge uniformly and absolutely.

The computations of the stress-strain modeling are described below. The first computes strain as a function of plastic strain, temperature, and stress. The second computes stress as a function of plastic strain, temperature, and plastic strain increments.

Values of plastic strain, ε^P, temperature, and stress are used as follows:

1. For a given temperature, $\sigma = f(\varepsilon)$ is obtained from the updated MATPRO properties given in Section 2.1.4.3.
2. The yield stress σ_y for given ε^P is obtained from Equation (2-135).
3. For a given value of stress, σ,

$$\text{if } \sigma \leq \sigma_y, \quad \begin{aligned} \varepsilon &= \frac{\sigma}{E} + \varepsilon^P \\ \varepsilon^P_{new} &= \varepsilon^P_{old} \\ \varepsilon &= f(\sigma) \end{aligned} \tag{2-136}$$

$$\text{if } \sigma > \sigma_y, \quad \begin{aligned} \varepsilon^P_{new} &= \varepsilon - \frac{\sigma}{E} \\ d\varepsilon^P &= \varepsilon^P_{new} - \varepsilon^P_{old} \end{aligned} \tag{2-137}$$

where E is computed using the correlation in the material properties handbook (Luscher and Geelhood, 2010).

Values of plastic strain, ε^P, temperature, and plastic strain increment, $d\varepsilon^P$, are used as follows:

1. For a given temperature, $\sigma = f(\varepsilon)$ is obtained from the updated MATPRO properties given in Section 2.1.4.3.
2. The yield stress σ_y for given ε^P is obtained from Equation (2-135).
3. Given $d\varepsilon^P$ (see Figure 2.13).

$$\varepsilon^P_{new} = \varepsilon^P_{old} + d\varepsilon^P \tag{2-138}$$

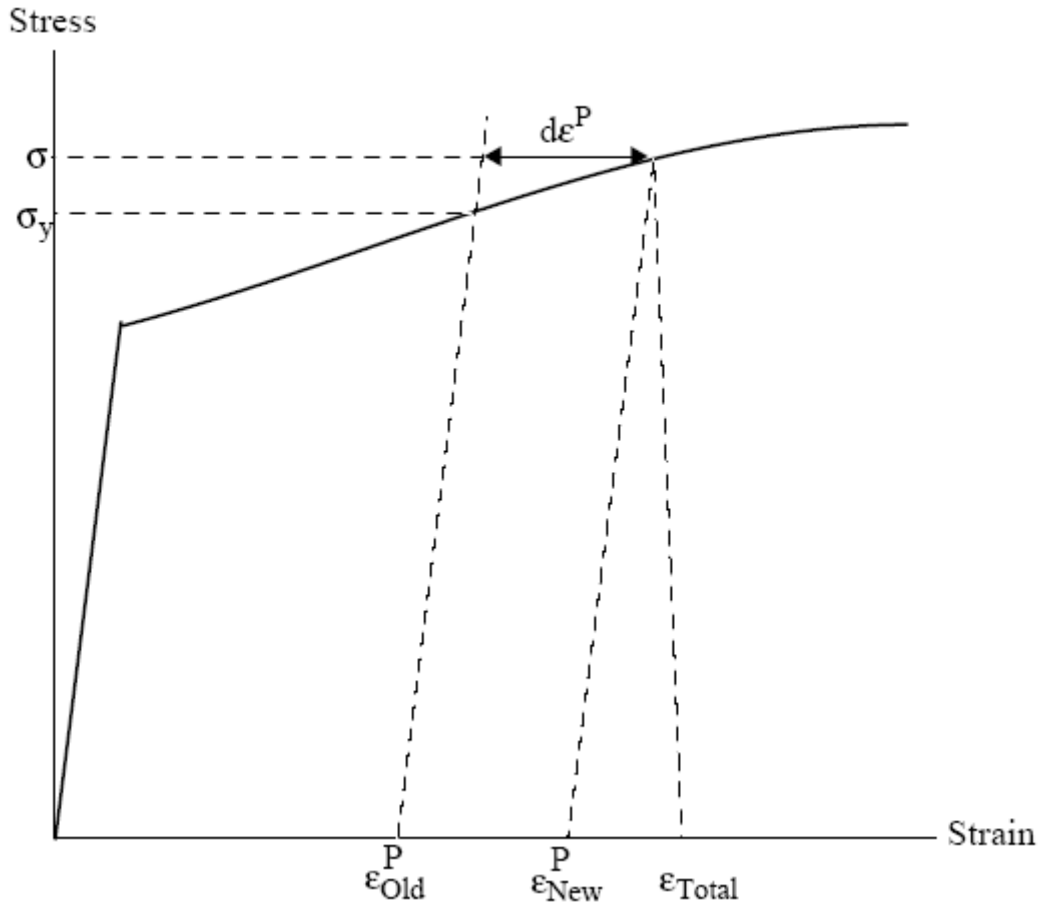

Figure 2.13 Computing stress

Since $d\varepsilon^P > 0$, the new value of stress and strain must lie on the plastic portion of the stress-strain curve $\sigma = f(\varepsilon)$. So, σ and ε are obtained by performing a simultaneous solution, as before.

2.4.1.3 Updated MATPRO Cladding Mechanical Properties Models

The mechanical properties of fuel rod Zircaloy cladding are known to change with irradiation because of damage induced from the fast neutron fluence. The changes are similar to cold-working the material because dislocation tangles are created that tend to both strengthen and harden the cladding while decreasing the ductility. In addition to the fast fluence effects, the presence of excess hydrogen in the Zircaloy, in the form of hydrides, may also affect the mechanical properties.

An analysis of recent data from mechanical testing of irradiated Zircaloy was conducted as part of the development work for FRAPCON-3 and revised equations for use in MATPRO routines were then generated. The revised MATPRO routines have also been incorporated in FRAPTRAN. The following summarizes the revised mechanical property equations.

Three MATPRO models have been modified to account for the high fast neutron fluence levels, temperature, and strain rate. Those models are a) the strength coefficient in CKMN, b) the strain hardening exponent in CKMN, and c) the strain rate exponent in CKMN.

Strength Coefficient, K

The strength coefficient, K, has been modified from MATPRO and is a function of temperature, fast neutron fluence, cold work, and alloy composition. The strength coefficient has not been found to be a function of hydrogen concentration. The fluence dependency, $K(\Phi)$, has been modified from MATPRO to better fit the high burnup data. The models for the strength coefficients of Zircaloy-2 and Zircaloy-4 are given below.

$$K = K(T)\cdot(1 + K(CW) + K(\Phi))/K(Zry)$$

where

K = strength coefficient (Pa)

$$K(T) = 1.17628\times10^{9} + 4.54859\times10^{5}T - 3.28185\times10^{3}T^{2} + 1.72752\cdot T^{3} \qquad T < 750\text{K}$$

$$K(T) = 2.522488\times10^{6}\exp\left(\frac{2.8500027\times10^{6}}{T^{2}}\right) \qquad 750\text{K} < T < 1090\text{K}$$

$$K(T) = 1.841376039\times10^{8} - 1.4345448\times10^{5}T \qquad 1090\text{K} < T < 1255\text{K}$$

$$K(T) = 4.330\times10^{7} - 6.685\times10^{4}T + 3.7579\times10^{1}T^{2} - 7.33\times10^{-3}T^{3} \qquad 1255\text{K} < T < 2100\text{K}$$

$$K(CW) = 0.546\cdot CW$$

$$K(\Phi) = (-0.1464 + 1.464\times10^{-25}\Phi)f(CW,T) \qquad \Phi < 0.1\text{x}10^{25}\ \text{n/m}^2$$

$$K(\Phi) = 2.928\times10^{-26}\Phi \qquad 0.1\text{x}10^{25}\text{n/m}^2 < \Phi < 2\text{x}10^{25}\ \text{n/m}^2$$

$$K(\Phi) = 0.53236 + 2.6618\times10^{-27}\Phi \qquad 2\text{x}10^{25}\ \text{n/m}^2 < \Phi < 12\text{x}10^{25}\ \text{n/m}^2$$

$$f(CW,T) = 2.25\exp(-20\cdot CW)\cdot\min\left[1,\exp\left(\frac{T-550}{10}\right)\right] + 1$$

In the above equations:

$K(Zry)$	=	1 for Zircaloy-4
$K(Zry)$	=	1.305 for Zircaloy-2
T	=	temperature (K)
CW	=	cold work (unitless ratio of areas) (valid from 0 to 0.75)
Φ	=	fast neutron fluence (n/m²) (E > 1MeV)

The effective cold work and fast neutron fluence used to calculate the strength coefficient, K, can be reduced by annealing if the time and/or temperature are high enough. FRAPCON-3 uses the MATPRO model, CANEAL, to calculate the effective cold work and fast neutron fluence at each time step using the following equations.

$$CW_i = CW_{i-1}\exp\left[-1.504(1 + 2.2\times10^{-25}\phi_{i-1})(t)\exp\left(\frac{-2.33\times10^{18}}{T^{6}}\right)\right]$$

$$\phi_i = \frac{10^{20}}{2.49\times10^{-6}(t)\exp\left(\frac{-5.35\times10^{23}}{T^8}\right)+\frac{10^{20}}{\phi_{i-1}}}$$

where

$CW_{i\text{-}1}$, and CW_i	=	the effective cold work for strength coefficient at the start and end of the time step, respectively (unitless ratio of areas)
ϕ_i, and $\phi_{i\text{-}1}$	=	effective fast neutron fluence for strength coefficient at the start and end of the time step, respectively (n/m^2)
t	=	time step size (s)
T	=	cladding temperature (K)

Strain-Hardening Exponent, n

The strain-hardening exponent, *n*, has been modified from MATPRO to better fit the high burnup data and is a function of temperature, fast neutron fluence, and alloy composition. The strain hardening exponent has not been found to be a function of hydrogen concentration. The models for the strain hardening exponents of Zircaloy-2 and Zircaloy-4 are given below.

$$n = n(T)\cdot n(\Phi)/n(Zry)$$

where

n = strain-hardening exponent

$$n(T) = 0.11405 \qquad T < 419.4\text{K}$$

$$n(T) = -9.490\times10^{-2} + 1.165\times10^{-3}T - 1.992\times10^{-6}T^2 + 9.588\times10^{-10}T^3 \qquad 419.4\text{K} < T < 1099.0772\text{K}$$

$$n(T) = -0.22655119 + 2.5\times10^{-4}T \qquad 1099.0772\text{K} < T < 1600\text{K}$$

$$n(T) = 0.17344880 \qquad T > 1600\text{K}$$

$$n(\Phi) = 1.321 + 0.48\times10^{-25}\Phi \qquad \Phi < 0.1\times10^{25}\ \text{n/m}^2$$

$$n(\Phi) = 1.369 + 0.096\times10^{-25}\Phi \qquad 0.1\text{x}10^{25}\ \text{n/m}^2 < \Phi < 2\times10^{25}\ \text{n/m}^2$$

$$n(\Phi) = 1.5435 + 0.008727\times10^{-25}\Phi \qquad 2\text{x}10^{25}\ \text{n/m}^2 < \Phi < 7.5\times10^{25}\ \text{n/m}^2$$

$$n(\Phi) = 1.608953 \qquad \Phi > 7.5\times10^{25}\ \text{n/m}^2$$

In the above equations

$n(Zry)$	=	1 for Zircaloy-4
$n(Zry)$	=	1.6 for Zircaloy-2
T	=	temperature (K)
Φ	=	fast neutron fluence (n/m²) (E > 1MeV)

The effective fast neutron fluence used to calculate the strain-hardening exponent, n, can be reduced by annealing if the time or temperature, or both, are high enough. FRAPCON-3 uses the

MATPRO model, CANEAL, to calculate the fast neutron fluence at each time step using the following equation.

$$\phi_i = \frac{10^{20}}{2.49\times10^{-6}(t)\exp\left(\frac{-5.35\times10^{23}}{T^8}\right)+\frac{10^{20}}{\phi_{i-1}}}$$

where

ϕ_i, and ϕ_{i-1}	=	effective fast neutron fluence for strain hardening exponent at the start and end of the time step, respectively (n/m^2)
t	=	time step size (s)
T	=	cladding temperature (K)

Strain Rate Exponent

The strain rate exponent, m, has been modified from MATPRO to better fit the high burnup data and is given by a function of temperature only as described in the equation below.

$$m = 0.015 \qquad T < 750\text{K}$$

$$m = 7.458\times10^{-4}T - 0.544338 \qquad 750\text{K} < T < 800\text{K}$$

$$m = 3.24124\times10^{-4}T - 0.20701 \qquad T > 800\text{K}$$

where

m	=	strain rate exponent
T	=	temperature (K)

The impact of the strain rate exponent on yield stress is to increase the yield strength with increasing strain rate, but the effect is not large. For example, increasing the strain rate from 1×10^{-4}/s to 1.0/s will increase the yield strength by about 15 percent.

Assembled Model

Tensile strength, yield strength, and strain are calculated using the same relationships in MATPRO's CMLIMT subroutine with slight modifications. The true ultimate strength is calculated using

$$\sigma = K\left(\frac{\dot{\varepsilon}}{10^{-3}}\right)^m \varepsilon_{p+e}^n \tag{2-139}$$

where

σ	=	true ultimate strength (MPa)
K	=	strength coefficient (MPa)
$\dot{\varepsilon}$	=	strain rate (unitless)
m	=	strain rate sensitivity constant from MATPRO (unitless)
ε_{p+e}	=	true strain at maximum load (unitless)
n	=	strain hardening exponent (unitless)

This is a change in the original MATPRO model in that the true strain at maximum load in the original model was set equal to the strain hardening exponent.

The CMLIMT subroutine equations predicting true yield strength and true strain at yield remain unchanged.

This model is applicable over the following ranges with an uncertainty (standard deviation) on yield and tensile strength of approximately 17 percent relative. A plot of predicted vs. measured yield stress is shown in Figure 2.14 Further data comparisons are shown in Geelhood et al. (2008).

cladding temperature:	560 to 700K
oxide corrosion thickness:	0 to 100 µm
excess hydrogen level:	0 to 650 ppm
strain rate:	10^{-4} to 10^{-5} s^{-1}
fast neutron fluence:	0 to 12×10^{25} n/m^2
Zircaloy:	cold work and stress relieved

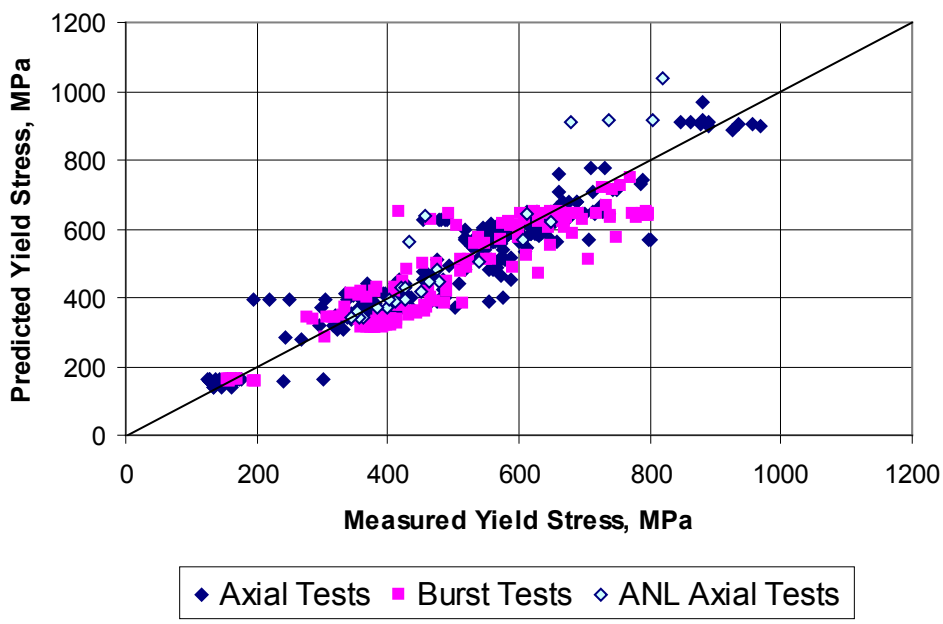

Figure 2.14 Predicted vs. measured yield stress from the PNNL database (293K≤T≤755K), $0\leq\Phi\leq14\text{x}10^{25}$ n/m^2, $0\leq H_{ex}\leq850$ ppm

2.4.1.3.1 Rigid Pellet Fuel Deformation in FRACAS-I

This section describes the analytical models used to compute fuel deformation in FRACAS-I. Models are available to calculate length change and fuel radial displacement. Relocation is also considered in FRACAS-I and is also discussed in this section. The effect of relocation is included in the thermal response; however, no hard contact between the fuel and cladding (and therefore no mechanical interaction) is allowed until the other fuel expansion components (swelling and thermal expansion) recover 50 percent of the original relocated pellet radius. Therefore, the rigid pellet for mechanical analyses, and that also controls contact conductance, includes 50 percent of the original relocated pellet radius as well as the other pellet expansion components.

The assumptions made with respect to fuel deformation in FRACAS-I are that no pellet deformation is induced by fuel-cladding contact stress or thermal stress and that free-ring thermal expansion applies. Each individual fuel ring is assumed to expand without restraint from any other ring, and the total expansion is the sum of the individual expansions.

2.4.1.3.2 Radial Deformation

Radial deformation of the pellet due to thermal expansion, irradiation swelling, and densification is calculated with a free-ring expansion model. The governing equation for this model is

$$R_H = \sum_{i=1}^{N} \Delta r_i [1 + \alpha_{T_i} (T_i - T_{ref}) + \varepsilon_i^s + \varepsilon_i^d \tag{2-140}$$

where

R_H	=	hot-pellet radius (m)
α_{T_i}	=	coefficient of thermal expansion of the i-th radial temperature (1/K)
T_i	=	average temperature of i-th radial ring (K)
T_{ref}	=	reference temperature (K)
Δr_i	=	width of i-th radial ring (m)
N	=	number of annular rings
ε_i^s	=	swelling strain (positive)
ε_d^s	=	densification strain (negative)

The fuel densification and swelling models are briefly discussed. The densification asymptotically approaches the (input) ultimate density change, typically over a local (node-average) burnup of approximately 5 GWd/MTU. Fuel swelling is considered only as the athermal swelling associated with solid fission product accumulation. It is linear with local (node-average) burnup, and starts following a burnup of 6 GWd/MTU (delayed for swelling into as-fabricated porosity). It then accumulates per time step at a rate equal to 0.062 volume percent per GWd/MTU up to 80 GWd/MTU and 0.086 volume percent per GWd/MTU beyond 80 GWd/MTU (Luscher and Geelhood, 2010).

2.4.1.3.3 Axial Deformation

Axial deformation of the total fuel stack takes into account the thermal, densification, and swelling strains at each axial node. The calculation proceeds differently for flat-ended versus dished-pellets as described below.

For flat-ended pellets, the volume-averaged ring axial deformation is calculated for each axial node, and these are summed to find the total stack deformation assuming isotropic behavior. The ring deformations account for thermal, densification, and swelling strains specific to each ring.

For dished pellets, the axial deformation of the "maximum ring" (the ring with the maximum deformed length) per node is found, and these "maximum ring" deformations are summed to find the total deformation. Typically, the "maximum ring" is the innermost ring on the dish shoulder because the deformation of the rings within the dish does not fill the dish volume, as illustrated in Figure 2.15.

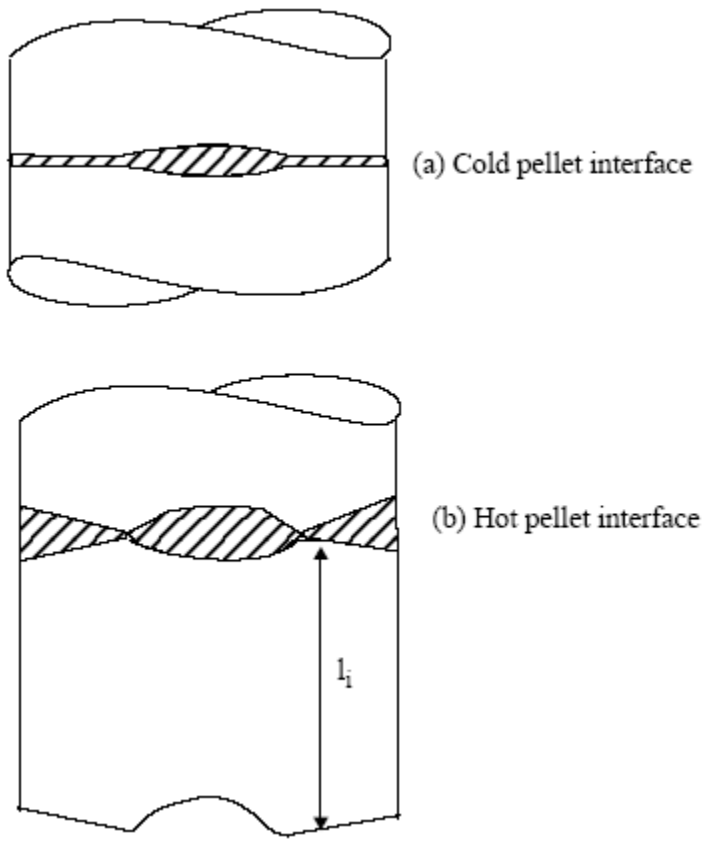

Figure 2.15 Interpellet void volume

2.4.1.3.4 Fuel Relocation

Fuel pellet center temperatures measured at beginning of life (BOL) in instrumented test rods have repeatedly been found to be lower than values predicted by thermal performance computer programs when the predicted fuel-cladding gap in operation is calculated based only on fuel and cladding thermal expansion (Lanning 1982). It has long been concluded, based on microscopic

examination of fuel cross sections (Galbraith, 1973; Cunningham and Beyer, 1984), that fuel pellet cracking promotes an outward relocation of the pellet fragments that causes additional gap closure. This process begins at BOL and quickly reaches equilibrium. Oguma (1983) characterized this approach to equilibrium based on his analysis of BOL test rod elongation data from Halden instrumented test assemblies.

The fuel pellet cracking that promotes relocation is predominantly radial; however, some circumferential components to these crack patterns exist, and these components could alter the fuel thermal conductivity. Thus, cracking and relocation will to some degree increase the thermal resistance in the pellet while reducing the thermal resistance of the pellet-cladding gap by reducing its effective size. The relocation model implicitly includes any crack effects on heat transfer because the model is based on fuel centerline temperature data.

The best estimate pellet relocation model developed for GT2R2 (Cunningham and Beyer, 1984), has been altered for use in FRAPCON in conjunction with the FRACAS-I mechanical model. The original GT2R2 relocation model was altered to provide a best estimate prediction of fuel temperatures for FRAPCON-3. This GT2R2 model is a function of LHGR and burnup that is similar to Oguma's model, but less complex in form. The gap closure due to relocation as a fraction of the as-fabricated pellet-cladding gap is given by

$$\begin{aligned} \Delta G/G &= 30 + 10\,FBU \text{ for } LHGR < 20 \text{ kW/m} \\ &= 28 + PFACTOR + (12 + PFACTOR)\,FBU \text{ for } LHGR < 40 \text{ kW/m} \\ &= 32 + 18\,FBU \text{ for } LHGR > 40 \text{ kW/m} \end{aligned} \tag{2-141}$$

where

FBU	=	*BURNUP*/5, for *BURNUP* < 5 GWd/MTU
	=	1.0 for *BURNUP* > 5 GWd/MTU
PFACTOR	=	(*LHGR* - 20)5/20
BURNUP	=	fuel nodal burnup (GWd/MTU)
LHGR	=	nodal LHGR (kW/m)

A plot of this model (subroutine GTRLOC) as a function of burnup and LHGR is shown in Figure 2.16.

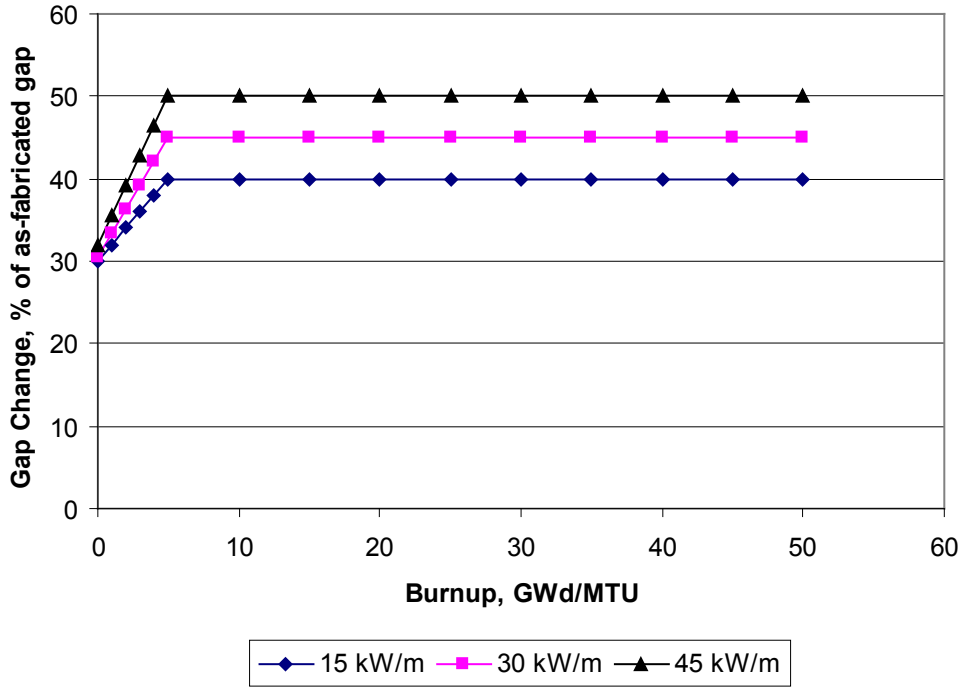

Figure 2.16 Power and burnup dependence of the FRAPCON-3 relocation model

The fuel-cladding gap size used in the thermal and internal pressure calculations includes the fuel relocation, while the fuel-cladding gap size used in the mechanical calculations allows for 50 percent of the relocation to be recovered before cladding stress/strain is driven by the fuel.

2.5 Fission Gas Release and Fuel Rod Internal Gas Pressure Response

After the fuel rod temperature and deformation calculations have been completed, the pressure of the gas in the fuel rod is computed. To calculate the gas pressure, the temperature and volume of the gas are required. The thermal models discussed in Section 2.3 provide the temperature of the gas in the fuel rod plenum, fuel-cladding gap, and fuel voids. The deformation models discussed in Section 2.4 provide information for computing the volume of the fuel rod plenum, fuel-cladding gap, and fuel voids.

The fuel rod internal gas pressure model is based on the following assumptions:

1. Perfect gas law holds (PV = NRT).
2. Gas pressure is constant throughout the fuel rod.
3. Gas in the fuel cracks is at the average fuel temperature.

2.5.1 Fuel Rod Internal Gas Pressure

Fuel rod internal gas pressure is calculated from the application of the perfect gas law to a multiple volume region. The volumes accounted for in FRAPCON-3 include the hot plenum volume, gap, annulus, crack, dish, porosity, roughness, and pellet-pellet interface volumes specific to each node. Thus, the equation for rod internal pressure is

$$P = \frac{MR}{\frac{V_P}{T_P} + \sum_{n=1}^{N}\left[\frac{V_g}{T_g} + \frac{V_{ch}}{T_{ch}} + \frac{V_{cr}}{T_{cr}} + \frac{V_{dsh}}{T_{dsh}} + \frac{V_{por}}{T_{por}} + \frac{V_{rf}}{T_{rf}} + \frac{V_i}{T_i}\right]} \tag{2-142}$$

where the volumes, V (m^3), and the temperatures, T (K), and

P	=	rod internal pressure (Pa)
M	=	total moles of gas
R	=	universal gas constant, 8.34 J/mole-K
N	=	number of axial nodes into which fuel rod is divided for numerical solution
n	=	axial node number
V_p, T_p	=	plenum volume and temperature
V_g, T_g	=	nodal gap volumes and temperatures
V_{ch}, T_{ch}	=	nodal central hole volumes and temperatures
V_{cr}, T_{cr}	=	nodal crack volumes and temperatures
V_{dsh}, T_{dsh}	=	nodal dish volumes and temperatures
V_{por}, T_{por}	=	nodal open-porosity volumes and temperatures
V_{rf}, T_{rf}	=	nodal roughness volumes and temperatures
V_i, T_i	=	nodal interface volumes and temperatures

Note that the temperatures assigned to the various volumes are as follows:

- The plenum temperature is dependent on the upper cladding temperature and the fuel temperature, as described in Section 2.3.6.
- The gap temperature is the average of the cladding inner and the fuel outer temperatures.
- The annulus temperature is the nodal fuel center temperature.
- The crack temperature is the average between pellet surface temperature and temperature at the restructured fuel radius.
- The open porosity temperature is the pellet volume average temperature.
- The dish temperature is the pellet volume average temperature.
- The roughness temperature is the gap temperature.
- The interface temperature is the average between the volume average temperature and the pellet surface temperature.

Note that in the FRAPCON-3 time step output, a table appears that presents the fractions of total volume represented by the plenum, gap, cracks, dishes, annulus, open porosity, and roughness, and the rod-averaged temperatures associated with these various volume-fractions. These are not the node-specific values that appear in the above equation, but are the results of the sum of each axial node for each volume type.

The gas pressure calculation, therefore, requires information on the gas inventory, void volumes, and the void temperatures, which is provided by the following supportive models.

2.5.2 Fission Gas Production

Given production rates for the major diffusing gases, the burnup-dependent total fission gas generated at axial elevation z is calculated as

$$GPT(z) = \frac{BU(z)VF(z)}{100A_v}(PR_{krypton} + PR_{helium} + PR_{xenon}) \tag{2-143}$$

where

$GPT(z)$	=	total fission gas produced at z (mole)
$BU(z)$	=	burnup at z (fission/cm^3)
$VF(z)$	=	fuel volume (cm^3)
A_v	=	Avogadro's number
PR	=	fission gas production rate (atoms/100 fissions) for krypton, xenon, and helium

All the fission gas produced, however, is not released. A portion is trapped in the fuel and a portion is released to the fuel-cladding gap volume. Only the released portion is used to calculate the rod internal gas pressure. The gas release fraction is calculated as discussed in the following sections.

2.5.3 Fuel Rod Gas Release

Gas release models in FRAPCON-3 account for not only fission gas release (krypton, xenon, and helium) but also nitrogen release. The nitrogen is released from the fuel lattice, where it is trapped during the fuel fabrication process. Fission gas release in FRAPCON-3 includes three model options: ANS-5.4 (Rausch and Panisko, 1979); the modified Forsberg and Massih model (Forsberg and Massih, 1985), modified at PNNL; and the FRAPFGR model developed at PNNL. All three of these release models are based on earlier formulations for diffusion from a sphere by Booth (1957) and are discussed below.

The user can select the Massih model, the ANS-5.4 model, or the FRAPFGR model. The Massih model is recommended by PNNL and is set as the default model. The ANS-5.4 model is useful for calculating the release of short-lived radioactive gas nuclides. The FRAPFGR model is useful for initializing the transient gas release model in FRAPTRAN 1.4. However, neither the ANS-5.4 model nor the FRAPFGR model predicts stable fission gas release as well as the Massih model does. For this reason, PNNL recommends the Massih model for best-estimate calculation of stable fission gas release.

2.5.3.1 ANS-5.4 Gas Release Model

The ANS-5.4 fractional fission gas release is calculated as a function of time and radial fuel temperature and axial burnup. The fuel is divided into radial and axial nodes according to the proposed American Nuclear Society (ANS) standard. A user requirement is that the time step sizes be such that the burnup increments do not exceed 2 GWd/MTU.

The modeling is divided into two main sections, one for release of stable isotopes and the other for release of short-lived isotopes. There are high- and low-temperature models for both the stable and radioactive fission products. The release is calculated using both the high-temperature and the low-temperature models, and the larger release value is used. Time steps should not exceed 50 days.

The ANS-5.4 fission gas release model (ANS, 1982) is incorporated as specified by the standard and will not be described in this document. A revised ANS-5.4 fission gas release model has been proposed but has not been approved as a standard at this time. The 1982 model is not

currently an approved standard and provides a very conservative prediction of release in the FRAPCON-3.4 code, while the revised model provides a less conservative prediction even at the 95/95 upper bound.

2.5.3.2 Modified Forsberg-Massih Model

The original Forsberg-Massih model begins with a solution of the gas diffusion equation for constant production and properties in a spherical grain:

$$\frac{dC}{dt} = D(t)\Delta_r C(r,t) + \beta(t) \tag{2-144}$$

where

C = gas concentration
β = gas production
Δ_r = $\frac{d^2}{dr^2} + \frac{2}{r}\left(\frac{d}{dr}\right)$
D = diffusion constant
t = time

with boundary conditions

$C(r,0)$ = 0
$C(a,t)$ = 0

Forsberg and Massih attempt to solve the equation for the case where there is re-solution of gas on the grain surface, which changes the outer boundary condition to

$$C(a,t) = \frac{b(t)\lambda N(t)}{2D} \tag{2-145}$$

where

N = surface gas concentration
λ = resolution layer depth
a = hypothetical grain radius
b = resolution rate

They make use of a four-term approximation to the integration kernel, K, where

$$\int_0^a 4\pi r^2 C(r,t)dr = \int_0^\tau K(\tau - \tau_0)\beta_e(\tau_0)d\tau_0 \tag{2-146}$$

and

$$\beta_e = \frac{\beta}{D} \tag{2-147}$$

$$\tau = Dt \tag{2-148}$$

and

$$K = \frac{8a^3}{\pi} \sum_{n=1}^{\infty} \frac{\exp\left(\frac{-n^2\pi^2\tau}{a^2}\right)}{n^2} \tag{2-149}$$

2.5.3.2.1 Low-Temperature Fission Gas Release Model at High Burnup

The modified Forsberg-Massih model is used to calculate fission gas release unless the low-temperature fission gas release model predicts a higher value for fission gas release. The low-temperature fission gas release model is defined as

$$F = 7 \times 10^{-5} BU + C \tag{2-150}$$

where

F	=	fission gas release fraction
BU	=	local burnup in GWd/MTU
C	=	0; for $BU \leq 40$ GWd/MTU
	=	$0.01(BU\text{-}40)/10$; for burnup > 40 GWd/MTU and $F \leq 0.05$

2.5.3.2.2 Grain Boundary Accumulation and Re-Solution

The final solution for a given time step, without re-solution and with constant production rate during the step, can be written as

$$\Delta G_n = f_n G_n(\tau_1) + A_n \int_{\tau_1}^{\tau_2} \exp\left[\frac{-B_n}{a^2}(\tau_2 - \tau_0)\right] q(\tau_0) d\tau_0 \tag{2-151}$$

$$\Delta G = \sum_{n=1}^{4} \Delta G_n \tag{2-152}$$

ΔG = change in gas concentration in fuel grain

$$\Delta G_B = \sum f_n G_n(\tau_1) + A_n \int_{\tau_1}^{\tau_2} funct(\tau_2 - \tau_0) q(\tau_0) d\tau_0 \tag{2-153}$$

ΔG_B = change in gas concentration on grain boundaries

$$f_n = \exp\left(\frac{(-B_n)(\tau_2 - \tau_0)}{a^2}\right) - 1 \tag{2-154}$$

f_n = fission gas production fraction remaining in the grain from the previous time step

where q is determined from

$$a^2 q\left[-\sum_{n=1}^{4}\left(\frac{f_n A_n}{B_n}\right) + funct(\Delta\tau)\right] = \beta\Delta t \tag{2-155}$$

where

$$funct\,(\Delta\tau) = \int_{\tau_1}^{\tau_2} funct(\tau_2 - \tau_0)\,d\tau$$

$$funct\,(\Delta\tau) = \frac{6}{\sqrt{\pi}}\left[\frac{\tau_2 - \tau_0}{a^2}\right]^{1/2} - 3\left[\frac{\tau_2 - \tau_0}{a^2}\right] \quad \text{if } \tau < 0.1$$

$$funct\,(\Delta\tau) = 1 - \frac{6}{\pi^2}\exp\left[-\pi^2\frac{\tau_2 - \tau_0}{a^2}\right] \quad \text{if } t > 0.1$$

A_n and B_n are constants given by Massih.

$$K_2 = \frac{a}{3} - \frac{K}{4\pi a^2}$$

$$K_3 = \frac{3}{a}K_2$$

$$1 + K_3 = \sum_{n=1}^{4} A_n \exp\left(-\frac{B_n\tau}{a^2}\right), \text{ n = 1, 2, 3, 4}$$

In modifying the original model, we have chosen to introduce re-solution by defining the partition of the gas arriving at the boundary each time step as follows:

$$\Delta \text{ Re-solved Gas} = \frac{F}{1+F}\Delta G_B \tag{2-156}$$

$$\Delta G_B = \frac{\Delta G_B}{1+F} \tag{2-157}$$

where

F	=	$FITMULT$[1.84 x 10^{-14} x GRN/(3 x D)]
GRN	=	grain radius (m)
D	=	diffusion constant (m^2/s)
$FITMULT$	=	an empirical multiplier on the term in brackets that is the original Massih equation for the resolution rate ($FITMULT$ = 300)

It should be noted that, although F is unitless in Massih's derivation, it does not represent the fraction of retained gas.

2.5.3.2.3 Diffusion Constant

The diffusion constant in the original Forsberg-Massih model is defined over three temperature ranges, as follows:

1. $D = 1.09 \times 10^{-17} \exp(-6614/T)$, $T > 1650$K
2. $D = 2.14 \times 10^{-13} \exp(-22884/T)$, $1381 < T < 1650$K
3. $D = 1.51 \times 10^{-17} \exp(-9508/T)$, $T < 1381$K

D = diffusion constant (m^2/s)

In the FRAPCON-3 subroutine, MASSIH, only the mid-range diffusion constant (number 2 above), is generally used, and the activation energy term (Q/R) is 22884 * 1.15. If the modified constant from MASSIH is less than the low-range Massih diffusion constant (number 3 above), the latter is used. The high-temperature diffusion constant (number 1 above) is not used.

A burnup enhancement factor multiplies the mid-range diffusion constant (number 2 above) and has the form $100^{\frac{BURNUP-21}{40}}$, where $BURNUP$ = burnup in GWd/MTU with a maximum value of 20000 for this enhancement factor. A factor of 12 is applied to the burnup-enhanced diffusion constant as a final step.

2.5.3.2.4 Gas Release

The gas is accumulated at the grain boundary until a saturation concentration is achieved, at which time the grain boundary gas is released. The saturation area density of gas is given by

$$N_S = \left[\frac{4rF(\theta)V_c}{3K_B T \sin^2(\theta)}\right]\left(\frac{2\gamma}{r} + P_{ext}\right) \tag{2-158}$$

where

N_s	=	saturation concentration, atoms/m^2
θ	=	dihedral half-angle = 50°
K_B	=	Boltzman constant
γ	=	surface tension = 0.6 (J/m^2)
V_c	=	critical area coverage fraction = 0.25
r	=	bubble radius = 0.5 microns
$F(\theta)$	=	$1 - 1.5\cos(\theta) + 0.5\cos^3(\theta)$
P_{ext}	=	external pressure on bubbles = gas pressure (Pa)

The final modification to the original model was to release both the grain boundary and the re-solved gas whenever the saturation condition is achieved and the grain boundary gas is released.

To summarize, optimized parameters have been applied based on comparisons to selected steady-state and transient data:

The activation energy (Q/R) = 1.15*22884. = 29060 (high temperature diffusion).
The resolution parameter = 300 x 1.84E-14 = 1.47E-12.
Burnup enhancement factor on diffusion constant = 100(BURNUP-21)/40
Multiplier on the diffusion constant = 12.0 (applied after all other modifications).

2.5.3.3 FRAPFGR Model

The FRAPFGR model has recently been developed at PNNL to initialize the transient release model in FRAPTRAN that is used to calculate fission gas release during fast transients such as a reactivity initiated accident. Because of this, it is important that the FRAPFGR model predict not only the steady state gas release, but also the amount of gas that remains within the grains and the amount of gas that is currently residing on the grain boundaries for each axial and radial node. The grain boundary gas is released during a fast transient due to cracking along the grain boundaries. To do this, gas release data as well as electron probe microanalysis (EPMA) and X-ray fluorescence (XRF) data have been used to validate that the model can accurately predict these parameters.

The basic layout of the FRAPFGR model is similar to the modified Massih model with the following differences.

2.5.3.3.1 Grain Growth Model

The FRAPFGR model accepts an input grain size that can be specified in the input. The default value for this is 10 micrometers (μm) using the mean linear intercept (MLI) method. The subcode uses a grain growth model proposed by Khoruzhii et al. (1999) given by

$$\frac{da}{dt} = K\left(\frac{1}{a} - \frac{1}{a_{\max}} - \frac{1}{a_{ir}}\right) \tag{2-159}$$

where

$\frac{da}{dt}$ = grain radius growth rate (μm/hour)

$$K = 5.24 \times 10^{7} \exp\left(\frac{-32100}{T}\right)$$

T = temperature (K)
a = grain size (μm)

$$a_{\max} = 2.23 \times 10^{3} \exp\left(\frac{-7620}{T}\right)$$

$$a_{ir} = \left[\frac{50}{\dot{F}} \cdot \frac{1400}{T}\right] \cdot 326.5 \exp\left(\frac{-5620}{T}\right)$$

$\dot{F}$ = fission rate, MW/tU

Equation (2-159) is solved by dividing the current time step into 100 steps and solving assuming constant rates within each sub-step.

2.5.3.3.2 High Burnup Rim Thickness and Porosity

The high burnup rim that is observed in the outer edge of high burnup pellets can be characterized in terms of sub-micron grains and high porosity. These two items are modeled in the FRAPFGR model. The size of the high burnup rim has been measured by optical microscopy (Manzel and Walker, 2002) and is modeled using the equation

$$t_{rim} = 1.439 \times 10^{-6} BU^{4.427} \tag{2-160}$$

where

t_{rim} = thickness of high burnup rim (μm)
BU = pellet average burnup (GWd/MTU)

Figure 2.17 shows how the high burnup structure is modeled in FRAPFGR. The calculated value of t_{tim} sets a thickness on the pellet surface that is entirely restructured grains. The grain size (MLI) for these grains is set at 0.15μm. The next region, which has a width also set by t_{rim}, is composed of a mixture of restructured grains and non-restructured grains. The fraction of restructured grains decreases linearly to zero across this thickness of this region. If the temperature in a given axial node is greater than 1000°C, then no restructured grains are assumed to form.

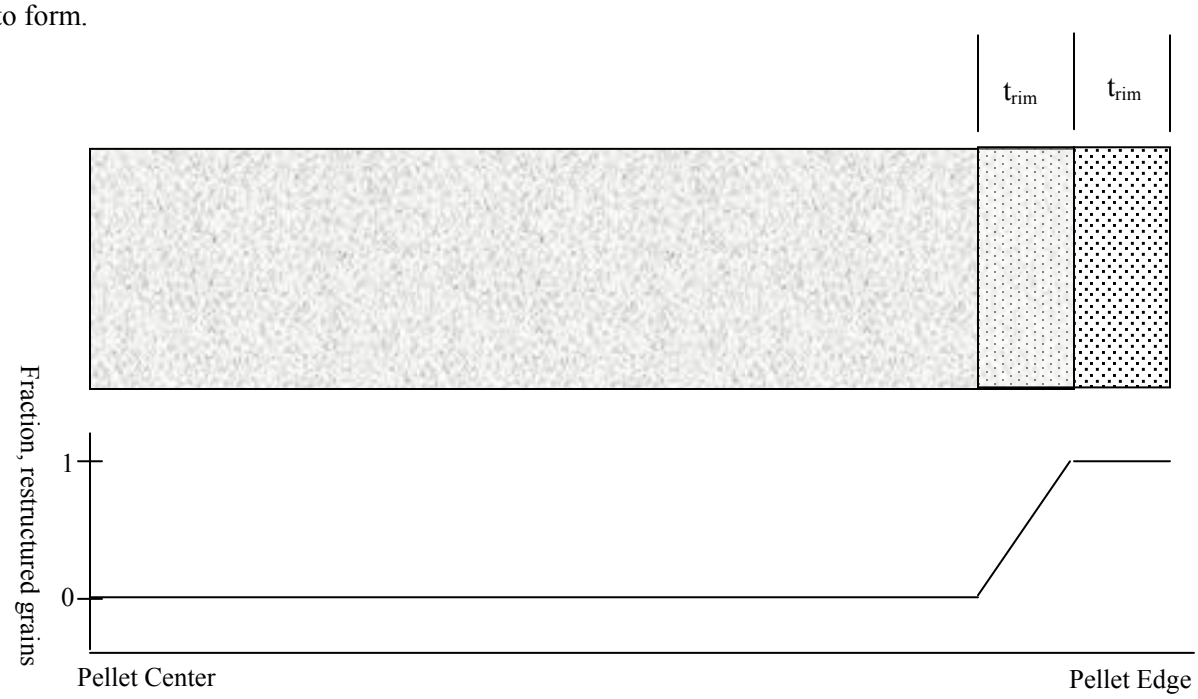

Figure 2.17 Modeling the pellet high burnup rim structure in FRAPFGR

In addition to the restructured grains, there is also a porosity increase within the high burnup rim. The porosity is modeled based on a fit to observations on high burnup fuel (Spino et al., 1996; Une et al., 2001; and Manzel and Walker, 2000). This model is given by

$$P = 11.283\ln(BU_{local}) - 45.621 \qquad \text{if } BU_{local} > 60 \text{ GWd/MTU} \tag{2-161}$$
$$P = 0 \qquad \text{if } BU_{local} < 60 \text{ GWd/MTU}$$

where

P = porosity increase in high burnup rim structure (fraction theoretical density)
BU_{local} = local radial node burnup, GWd/MTU

This porosity is subtracted off the input theoretical density, which is used to calculate the production in each radial node. Therefore, as the porosity in the rim increases, the power production in the outer radial nodes is slightly decreased due to increase porosity.

2.5.3.3.3 Diffusion Constant

The diffusion constant used in FRAPFGR is given by

$$\begin{aligned}
D(T) &= 1.15\times10^{-23} && T < 675\text{K} \\
D(T) &= 1.51\times10^{-17}\exp(-9508/T) && 675\text{K} < T < 1381\text{K} \\
D(T) &= 2.14\times10^{-13}\exp(-22884/T) && 1381\text{K} < T < 1650\text{K} \\
D(T) &= 7.14433\times10^{-10}\exp(-34879/T) && 1650\text{K} < T < 1850\text{K} \\
D(T) &= 4.63\times10^{-18} && T > 1850\text{K}
\end{aligned} \tag{2-162}$$

where

D = diffusion constant (m²/s)
T = temperature (K)

The diffusion constant is modified for the effects of burnup using the formula in Equation (2-163).

For non-restructured grains

$$D(T,Bu) = D(T)\left(10^{\frac{\max(Bu-21,0)}{40}} + 10\cdot\frac{\min(Bu,12)}{12}\right) \tag{2-163}$$

up to a maximum adjustment of 49.81

For restructure grains, there is no burnup adjustment.

where

$D(T,Bu)$ = diffusion constant adjusted for burnup (m^2/s)
$D(T)$ = temperature dependent diffusion constant given by Equation (2-162) (m^2/s)
Bu = local radial node burnup (GWd/MTU)

The diffusion constant is also modified for the effects of low power using an error function

$$D(T, Bu, Pow) = \frac{D(T, Bu)}{2.5 - 1.5erf(Pow - 3)} \tag{2-164}$$

where

$D(T, Bu, Pow)$	=	diffusion constant adjusted for burnup and power (m^2/s)
$D(T, Bu)$	=	diffusion constant adjusted for burnup given by Equation (2-163) (m^2/s)
Pow	=	local radial node power (kW/ft)

2.5.3.3.4 Gas Release

Gas release calculations are performed separately for restructured grains and non-restructured grains. For those nodes that contain both restructured and non-restructured grains, the releases from each are combined based on the relative amount of each type of grain.

For the restructured grains, it is assumed that, because the grains are so small, all the gas produced in the grain will diffuse out to the grain boundary. Therefore, the only gas that will remain in these grains at the end of the time step is the gas that is re-solved back into the grains.

The gas re-solved back into the grain is given by the resolution factor from Massih (Forsberg and Massih, 1985). The gas that is in the grain for a given time step, *i*, is given by

$$GG_i = GB_{i-1} \frac{f}{1+f} \tag{2-165}$$

where

GG	=	gas in grains ($moles/m^3$)
GB	=	gas on grain boundaries ($moles/m^3$)

$$f = \frac{1.84 \times 10^{-14} a}{3D} \tag{2-166}$$

where

a	=	grain radius (0.075×10^{-6} m for restructured grains)
D	=	diffusion constant (m^2/s)

For the non-restructured grains, the same formulas as those in MASSIH are used to calculate diffusion from the grains except that the release is reduced to account for resolution during the calculation of release. The following terms are changed as follows.

From Equation (2-153), the following term is changed:

$$\sum f_n G_n(\tau_1) \rightarrow \frac{\sum f_n G_n(\tau_1)}{resolterm} \tag{2-167}$$

From Equation (2-155), the following term is changed:

$$\left[-\sum_{n=1}^{4}\left(\frac{f_n A_n}{B_n}\right)+funct(\Delta\tau)\right]\rightarrow\frac{\left[-\sum_{n=1}^{4}\left(\frac{f_n A_n}{B_n}\right)+funct(\Delta\tau)\right]}{resolterm} \tag{2-168}$$

where

$resolterm = \max(1, 0.14009\exp(0.00282T)\ \ T < 1528.77\text{K}$
$resolterm = \max(1, 22.976 - 0.0082T\ \ T > 1528.77\text{K}$
T = temperature (K)

In order for gas to be released from the grain boundaries, the saturation concentration must be reached. The saturation concentration is given by

$$gs = \frac{3N_s}{2a} \tag{2-169}$$

where

gs	=	grain boundary saturation concentration (moles/m^3)
N_s	=	saturation area density given in Equation (2-146) (moles/m^2)
a	=	grain radius (m)

When the grain boundary gas concentration for a given radial node exceeds the saturation value for the first time, all the gas on the grain boundary except 65 percent of the saturation value is released. From then on for that radial node, any gas above 65 percent of the saturation values is released.

As discussed, for radial nodes that contain some restructured grains and some non-restructured grains, the released gas is calculated as

$$\Delta rel_{tot} = \Delta rel_1(restructure^2) + \Delta rel_2(1 - restructure^2) \tag{2-170}$$

where

Δrel_{tot}	=	total release from a radial node (moles/m^3)
Δrel_1	=	release from restructured grains in a radial node (moles/m^3)
Δrel_2	=	release from non- restructured grains in a radial node (moles/m^3)
restructure	=	fraction of restructured grains in radial node

As with the MASSIH model, an athermal release term of 1 percent for every 10 GWd/MTU beyond 40 GWd/MTU is added on if the predicted release is less than 5 percent to account for the observed gas release from rods with very low power at high burnup.

2.5.4 Nitrogen Release

The release of nitrogen initially present in fuel material from fabrication occurs as a result of a diffusion transport mechanism. The release of nitrogen affects the rod internal pressure and the gas conductivity. The model proposed by Booth (1957) is used, given the following assumptions:

1. The initial concentration of diffusing substance, C, is uniform throughout a sphere of radius, a.
2. Transport of material does not occur from the external phase (gaseous nitrogen) back into the initial carrier medium.

The governing equation is

$$r\frac{\partial C}{\partial t} = D\left(\frac{\partial^2}{\partial r^2}(C \cdot r)\right) \tag{2-171}$$

where

r	=	radial location (m)
C	=	concentration of diffusing substance
t	=	time (s)
D	=	diffusion coefficient (m^2/s)

with

C	=	0.0, when $r = a$
C	=	C, when $t = 0$

By applying a series solution method, the fractional release of the diffusing substance (nitrogen) can be approximated based on the value of B:

$$B = \pi^2 \frac{D_{N_2}}{a^2} t \tag{2-172}$$

where

$\frac{D_{N_2}}{a^2}$	=	temperature-dependent diffusion coefficient for nitrogen divided by the effective diffusion radius squared (s^{-1})
t	=	time from the start of diffusion (s)

Then, when $B > 1$, the fraction of nitrogen released as of time, t, equals

$$F_{N_2} = 1 - \frac{6}{\pi^2}\exp(-B) \tag{2-173}$$

and, when $B < 1$,

$$F_{N_2} = 6\left[\frac{D_{N_2}}{a^2} t / \pi\right]^{0.5} - 3\frac{D_{N_2}}{a^2} t \tag{2-174}$$

From the experimental data of Ferrari (1963, 1964)

$$\frac{D_{N_2}}{a^2} = 1.73 \exp\left(\frac{33400}{1.9869T}\right) \tag{2-175}$$

where

T = temperature (K)

2.5.5 Helium Production and Release

Helium is produced at different rates in UO_2 and MOX. The release of helium affects the rod internal pressure and the gas conductivity.

For UO_2, helium production is given by

$$He_{prod} = 1.297 \times 10^{-18} Q \cdot t \cdot SA \cdot gasprod \tag{2-176}$$

where

He_{prod}	=	helium produced for a given axial node (moles)
Q	=	surface heat flux (W/m^2)
t	=	time (s)
SA	=	axial node surface area (m^2)
$gasprod$	=	number of fission gas atoms produced per 100 fissions (default value = 31)

For MOX, a formula has been developed as a function of Pu concentration and burnup:

$$He_{prod} = (A_1 Pu + A_2)(BU)^2 + (B_1 Pu + B_2)(BU) \tag{2-177}$$

where

He_{prod}	=	helium produced for a given axial node (moles)
BU	=	node burnup (GWd/MTU)

Table 2.4 shows the fitting parameters that should be used for reactor-grade plutonium and weapons-grade plutonium.

Table 2.4 Fitting parameters for helium production in MOX

	Reactor-Grade Plutonium	Weapons-Grade Plutonium
A_1	1.5350×10^{-4}	-2.4360×10^{-4}
A_2	2.1490×10^{-3}	3.6059×10^{-3}
B_1	-2.9080×10^{-3}	3.3790×10^{-3}
B_2	9.7223×10^{-2}	5.3658×10^{-2}

The above equations calculate the amount of helium produced as a function of time. In order to calculate the helium released to the void volume, an approach similar to the approach for nitrogen release is used. By applying a series solution method, the fractional release of the diffusing substance (helium) can be approximated based on the value of B:

$$B = \pi^2 \frac{D_{He}}{a^2} t \tag{2-178}$$

where

$\frac{D_{He}}{a^2}$ = temperature dependent diffusion coefficient for helium divided by the effective diffusion radius squared (s^{-1})

t = time from the start of diffusion (s)

If $t \leq 1/(\pi^2 D_{He}/a^2)$ then the fraction of helium released, F_{He}, as of time, t, equals

$$F_{He} = 4\left[\frac{D_{He} t}{a^2 \pi}\right]^{0.5} - \frac{3 D_{He} t}{2a^2} \tag{2-179}$$

If this fraction is greater than 0.57, then, when $B < 1$, the fraction of helium released as of time, t, equals

$$F_{He} = 1 + \frac{(0.607927 \exp(-B) - 0.653644)}{B} \tag{2-180}$$

and, when $B > 1$,

$$F_{He} = 1 \tag{2-181}$$

$$\frac{D_{He}}{a^2} = 0.452847 \times 10^{-10} \text{ if } T \leq 873 \text{ K} \tag{2-182}$$

$$\frac{D_{He}}{a^2} = 0.28 \times 10^{-5} \exp\left(\frac{4 \times 10^4}{1.986}\left(\frac{1}{1673} - \frac{1}{T}\right)\right) \text{ if } T > 873 \text{ K} \tag{2-183}$$

Some fuel designs use a thin layer of ZrB_2 applied to the surface of the pellets to act as an integral fuel burnable absorber (IFBA). The use of such coatings produces a large amount of helium.

The following empirical correlation was fit to results from Monte Carlo N-Particle (MCNP), a neutron transport code, for helium production from IFBA liners.

$$He_{prod} = -(A_1 IFBA + A_2)(B10)^2 + (B_1 IFBA + B_2)(B10) \tag{2-184}$$

where

He_{prod}	=	helium production (atoms He/cm³-s)
$IFBA$	=	percent of fuel rods in a core containing IFBA liners (percent) (valid only between 10 and 50 percent)
$B10$	=	boron-10 enrichment (percent) (valid from 0 to 90 percent)
A_1	=	6.23309×10^{-9}
A_2	=	7.02006×10^{-7}
B_1	=	-1.35675×10^{-7}
B_2	=	3.1506×10^{-4}

It can be seen from Equation (2-184) that the helium production rate is a function of the number of IFBA rods in a core and the boron-10 enrichment. Helium is produced as the boron-10 burns out until there is no more boron-10 in the liners. The rate of boron-10 depletion is equal to the helium production rate. The depletion of boron-10 is calculated in the code and the boron-10 enrichment, $B10$ in Equation (2-184), at the end of the time step is used to calculate the helium production for the next time step.

It is assumed in the code that all helium produced in the ZrB_2 coatings is released directly to the rod-free volume.

2.5.6 Fuel Rod Void Volumes

Void volumes computed by FRAPCON-3 include the pellet dishing, the fuel-cladding gap, the crack, the plenum, the open porosity, and the roughness volume. These are calculated as indicated below.

2.5.6.1 Pellet Dish Volume

The volume between pellets is calculated and included as part of the overall volume in the internal gas pressure model. The interpellet volume is calculated at each time step based on hot-pellet geometries. Figure 2.15 shows 1) a cold-pellet interface configuration for the case where the pellets are dished and 2) an exaggerated hot-pellet interface configuration. The void volume available for internal fill gas is defined by the cross-hatched areas (*a* and *b* in the figure). The dish volume is that portion of the hot interpellet volume that is within the dishes, excluding the volume of any central hole.

2.5.6.2 Interface Volume

The pellet-pellet interface volume is calculated as the difference between the hot interpellet volume and the dish volume.

2.5.6.3 Fuel-Cladding Gap Volume

The fuel-cladding gap volume is calculated by considering the area between two concentric cylinders. The outer cylinder is assumed to have a diameter equal to the diameter of the cladding inside surface based on plastic deformation. The inside cylinder is assumed to have a diameter equal to the diameter of the relocated fuel pellets.

2.5.6.4 Fuel Crack Volume

As the fuel expands, extensive cracking occurs due to the high thermally induced stresses, resulting in a relocated fuel surface. The crack volume is computed as

$$V_c = V_g - V_{eg} - V_{TX} \tag{2-185}$$

where

V_c = fuel crack volume per unit length (m^2)
V_{eg} = fuel volume per unit length defined by expanded radial nodes, including the thermal expansion, swelling, and densification (m^2)
V_{TX} = the computed fuel-cladding gap volume per unit length based on the relocated fuel surface (m^2)
V_g = the volume per unit length within the thermally expanded cladding (m^2)

2.5.6.5 Plenum Volume

The plenum volume is calculated from geometry considerations of the thermally expanded cladding and the thermal expansion, densification, and swelling of the fuel. The volume of the hold-down spring is considered.

2.5.6.6 Open Porosity Volume

A portion of the initial fabrication porosity is open to free gas flow, which is given by the expressions

$$V_{por} = 0.0 \text{ when } G_{den} \geq 94.0 \tag{2-186}$$

$$V_{por} = 1.97 \times 10^{-8} (94.0 - G_{den}) \text{ when } 91.25 < G_{den} < 94.0 \tag{2-187}$$

$$\begin{aligned} V_{por} &= 2.77 \times 10^{-4} - 3.818 G_{den} \\ &- 1.43 \times 10^{-8} G_{den}^2 + 2.497 \times 10^{-10} G_{den}^3 \end{aligned} \quad \text{when } G_{den} < 91.25 \tag{2-188}$$

where

V_{por} = porosity volume per unit length (m^2)
G_{den} = DEN - 1.25
DEN = fuel density (percent of theoretical density)

It should be noted that most commercially fabricated fuel today has little open porosity.

2.5.6.7 Roughness Volume

The roughness of the surface of the fuel and cladding results in a small void volume accounted for by

$$V_{rough} = \frac{5.27 \times 10^{-5} \pi D_P}{V_f} \tag{2-189}$$

where

V_{rough} = roughness volume per unit length (m^2)
D_P = initial pellet diameter (m)
V_f = geometric fuel volume per unit length (m^2)

The gas pressure response resulting from the above models feeds back into the mechanical and temperature response models in the iteration scheme.

2.5.6.8 Central Hole Volume

The central hole volume is calculated by considering the area of the central hole (if present), the length of the axial node, and the length of the central hole.

2.6 Waterside Corrosion and Hydrogen Pickup

The cladding waterside corrosion and hydrogen pickup models have been altered from those in FRAPCON-2, as described below.

2.6.1 PWR and BWR Waterside Corrosion Models

For Zircaloy-4 under pressurized-water reactor (PWR) conditions, a cubic rate law for corrosion-layer thickness as a function of time is applied until a transition thickness of 2.0 microns is attained (Garzarolli et al., 1982):

$$\frac{d(s^3)}{dt} = \frac{A}{s^2} \exp\left\{\frac{-Q_1}{RT_1}\right\} \tag{2-190}$$

In FRAPCON-3, this equation is integrated without regard to the feedback between oxide layer thickness and oxide metal interface temperature to obtain

$$s_{i+1} = \left(3A \exp\left\{\frac{-Q_1}{RT_1}\right\}(t_{i+1} - t_1) + s_i^3\right)^{\frac{1}{3}} \tag{2-191}$$

where

i, i+1 = refers to (ends of) previous and current time step
s = oxide thickness (m)

A	=	6.3×10^9 (m^3/day)
Q_1	=	32289 (cal/mol)
R	=	1.98 (cal/mol-K)
T_1	=	metal-oxide interface temperature (K)
t	=	time (days)

After the transition thickness is attained, a flux-dependent linear rate law is applied, with the rate constant being an Arrhenius function of oxide-metal interface temperature:

$$\frac{ds}{dt} = \left\{C_0 + U(M\Phi)^P\right\}\exp\left(\frac{-Q_2}{RT_1}\right) \tag{2-192}$$

Because there is significant feedback between oxide-layer thickness and oxide-metal interface temperature, the oxide thickness is converted to weight gain, and the approximate integral solution from Garzarolli et al. (1982) is used. This solution has the form

$$\Delta w_{i+1} = \Delta w_i + \frac{RT_o^2\lambda}{\gamma Q_2 q''}\ln\left[1 - \frac{\gamma Q_2 q''}{RT_o^2\lambda}k_0 \exp\left(\frac{-Q_2}{RT_o}\right)\exp\left(\frac{\gamma Q_2 q''\Delta w_i}{RT_o^2\lambda}\right)(t_{i+1} - t_i)\right]^{-1} \tag{2-193}$$

Weight gain can be converted to thickness using the following formula:

$$s = \frac{\Delta w \gamma}{100} \tag{2-194}$$

where

i, i+1	=	refers to (ends of) previous and current time step
s	=	oxide thickness (m)
Δw	=	weight gain (g/cm^2)
R	=	1.98 (cal/mol-K)
T_o	=	oxide-to-water interface temperature (K)
λ	=	oxide thermal conductivity (W/cm-K)
γ	=	0.6789 (cm^3/g)
Q_2	=	27354 (cal/mol)
q''	=	heat flux (W/cm^2)
k_0	=	$11863 + 3.5 \times 10^4 (1.91 \times 10^{-15}\Phi)^{0.24}$ (g/(cm^2-day))
Φ	=	fast neutron flux (E>1 MeV) (n/cm^2/s)
t	=	time (days)

For M5 under PWR conditions, the same equations are used with the following changes.

- Q_1 = 27446 (cal/mol)
- Q_2 = 29816 (cal/mol)
- Transition thickness at 7 μm

For ZIRLO under PWR conditions, the same equations are used with the following changes.

- Q_2 = 27080 (cal/mol)
- Above the transition thickness if the oxide thickness is less than 80 μm then use 2*Δw_i in the second term of Equation (2-193) and then divide that term by 2 as shown below.

$$\Delta w_{i+1} = \Delta w_i + \frac{1}{2}\frac{RT_o^2\lambda}{\gamma Q_2 q''}\ln\left[1 - \frac{\gamma Q_2 q''}{RT_o^2\lambda}k_0 \exp\left(\frac{-Q_2}{RT_o}\right)\exp\left(\frac{\gamma Q_2 q'' 2\Delta w_i}{RT_o^2\lambda}\right)(t_{i+1} - t_i)\right]^{-1} \quad (2\text{-}195)$$

For Zircaloy-2 under boiling-water reactor (BWR) conditions, a flux-dependent linear rate law is applied, with the rate constant being an Arrhenius function of oxide-metal interface temperature:

$$\frac{ds}{dt} = K\exp\left(\frac{-Q}{RT_1}\right)\left[1 + Cq''\exp\left(\frac{Q}{RT_1}\right)\right] \quad (2\text{-}196)$$

Because there is significant feedback between oxide-layer thickness and oxide-metal interface temperature, the oxide thickness is converted to weight gain, and the approximate integral solution from Garzarolli et al. (1982) is used. This solution has the form

$$\Delta w_{i+1} = \Delta w_i + \frac{RT_o^2\lambda}{\gamma Q q''}\ln\left[1 - \frac{\gamma Q q''}{RT_o^2\lambda}k\exp\left(\frac{-Q}{RT_o}\right)\exp\left(\frac{\gamma Q q''\Delta w_i}{RT_o^2\lambda}\right)(t_{i+1} - t_i)\right]^{-1} + Ck(t_{i+1} - t_i)q'' \quad (2\text{-}197)$$

Weight gain can be converted to thickness using the following formula:

$$s = \frac{\Delta w \gamma}{100} \quad (2\text{-}198)$$

where

i, i+1	=	refers to (ends of) previous and current time step
s	=	oxide thickness (m)
Δw	=	weight gain (g/cm^2)
R	=	1.98 (cal/mol-K)
T_o	=	oxide-to-water interface temperature (K)
λ	=	oxide thermal conductivity (W/cm-K)
γ	=	0.6789 (cm^3/g)
Q	=	27350 (cal/mol)
q''	=	heat flux (W/cm^2)
k	=	11800 (g/(cm^2-day))
Φ	=	fast neutron flux (E>1 MeV) (n/cm^2/s)
C	=	2.5x10^{-16} (m^2/W)
t	=	time (days)

To achieve numerical stability, the rate equation is integrated across each time step and applied to calculated corrosion layer increments per time step, which are accumulated to calculate cumulative layer thickness as a function of axial position (axial node) along the rod.

2.6.2 Hydrogen Pickup Fraction

The fraction of the hydrogen liberated by the metal-water corrosion reaction that is absorbed locally by the cladding is called the pickup fraction. For PWR conditions, a constant hydrogen pickup fraction has been found to be applicable. For Zircaloy-4, a pickup fraction of 0.15 is used. For M5, a pickup fraction of 0.10 is used. For ZIRLO, a pickup fraction of 0.125 is used (Geelhood and Beyer, 2008).

For BWR conditions, a constant hydrogen pickup fraction does not fit the observed hydrogen concentration data. Therefore, FRAPCON-3 uses a burnup-dependent hydrogen concentration model (Geelhood and Beyer, 2008). For Zircaloy-2 prior to 1998 (when the vendors did not have tight control over concentration and second-phase precipitate particle size), the following equations are used

$$H_{conc} = 47.8\exp\left(\frac{-1.3}{1+BU}\right) + 0.316BU \quad \text{if } BU < 50 \text{ GWd/MTU} \tag{2-199}$$

$$H_{conc} = 28.9 + \exp\left(0.177(BU - 20)\right) \text{ if } BU > 50 \text{ GWd/MTU} \tag{2-200}$$

For modern Zircaloy-2 since 1998 (when the vendors have had tight control over concentration and second phase precipitate particle size), the following equation is used

$$H_{conc} = 22.8 + \exp\left(0.177(BU - 20)\right) \tag{2-201}$$

where

H_{conc} = hydrogen concentration (ppm)
BU = local burnup (GWd/MTU)

3.0 General Code Description

3.1 Code Structure and Solution Routine

FRAPCON-3 is a large and complex code that contains over 200 subroutines. This section discusses the code structure, solution scheme, and the major subroutines involved in the solution scheme.

3.1.1 Code Structure

The FRAPCON-3 subroutines have been grouped in packages, not all of which need to be compiled for every run. These packages are listed in Table 3.1. Note that every execution requires the FRPCON package and the MATPRO package; the former contains the driver routine, the setup routines, and the thermal models. Using only these two packages restricts one to the FRACAS-I mechanical modeling option.

Table 3.1 Major FRAPCON-3 packages

Package	Description
FRPCON	The main section of the code, including all of the thermal modes; also includes the FRACAS-I mechanics model
FRACAS-I	Contains the subroutines comprising the FRACAS-I mechanics model
MATPRO	The MATPRO material properties package

3.1.2 Solution Scheme

Figure 3.1 shows a flowchart of FRAPCON-3 beginning with case setup, following through the convergence loops, and ending with output. Each major section of this sequence will be discussed, together with the subroutines involved. To aid this discussion, Figure 3.2 presents an abbreviated outline of the main subprogram, FRPCON, arranged in the same order as the flowchart. Major subroutines appear in the figure as do the major Fortran loops.

The first portion of the flowchart has to do with case setup and initialization. This includes reading the input data, the dynamic dimensioning procedure, initializing variables, and an initial problem description output. The subroutines listed in Table 3.2 are involved in the setup and initialization.

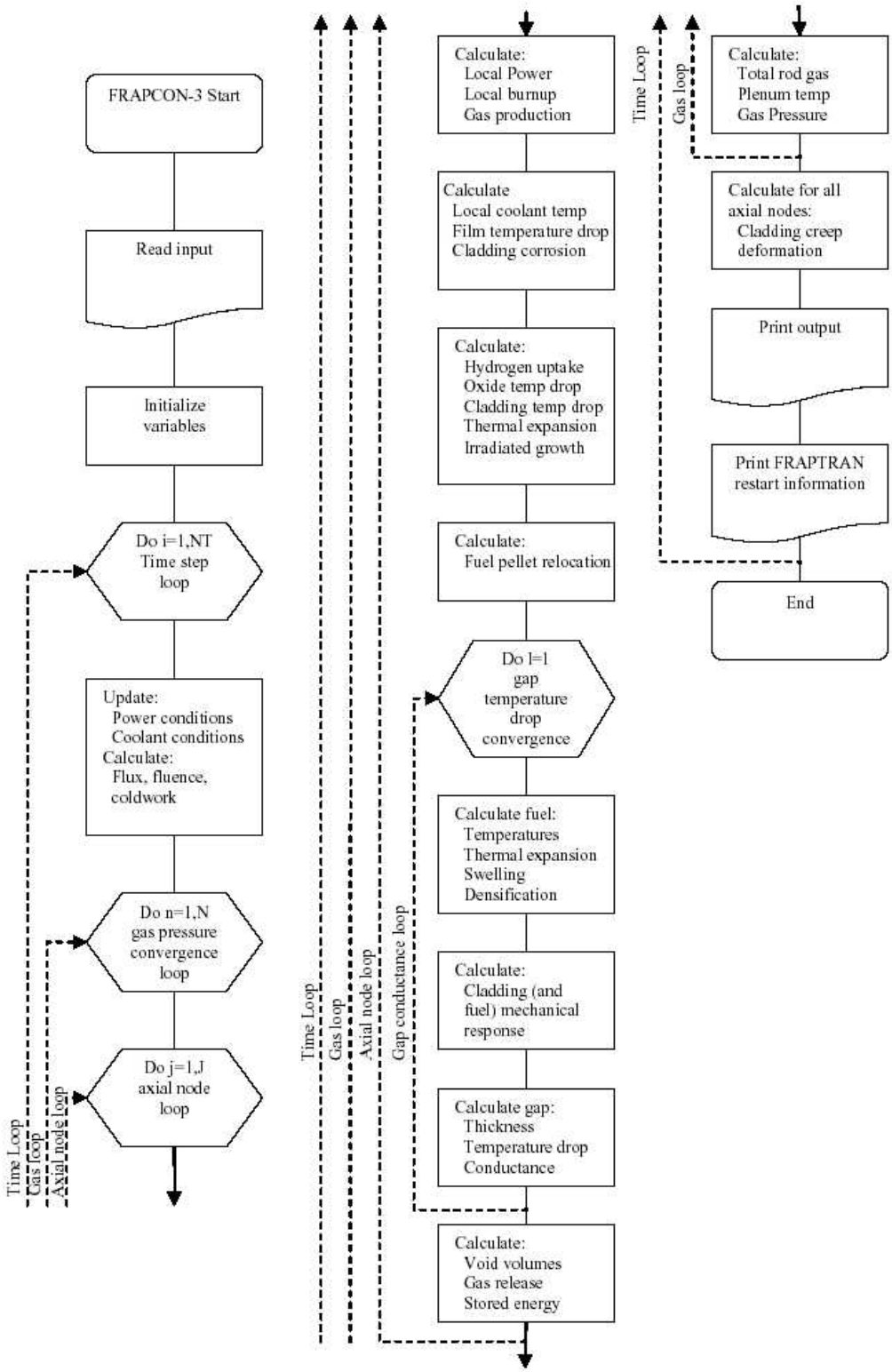

Figure 3.1 FRAPCON-3 flowchart

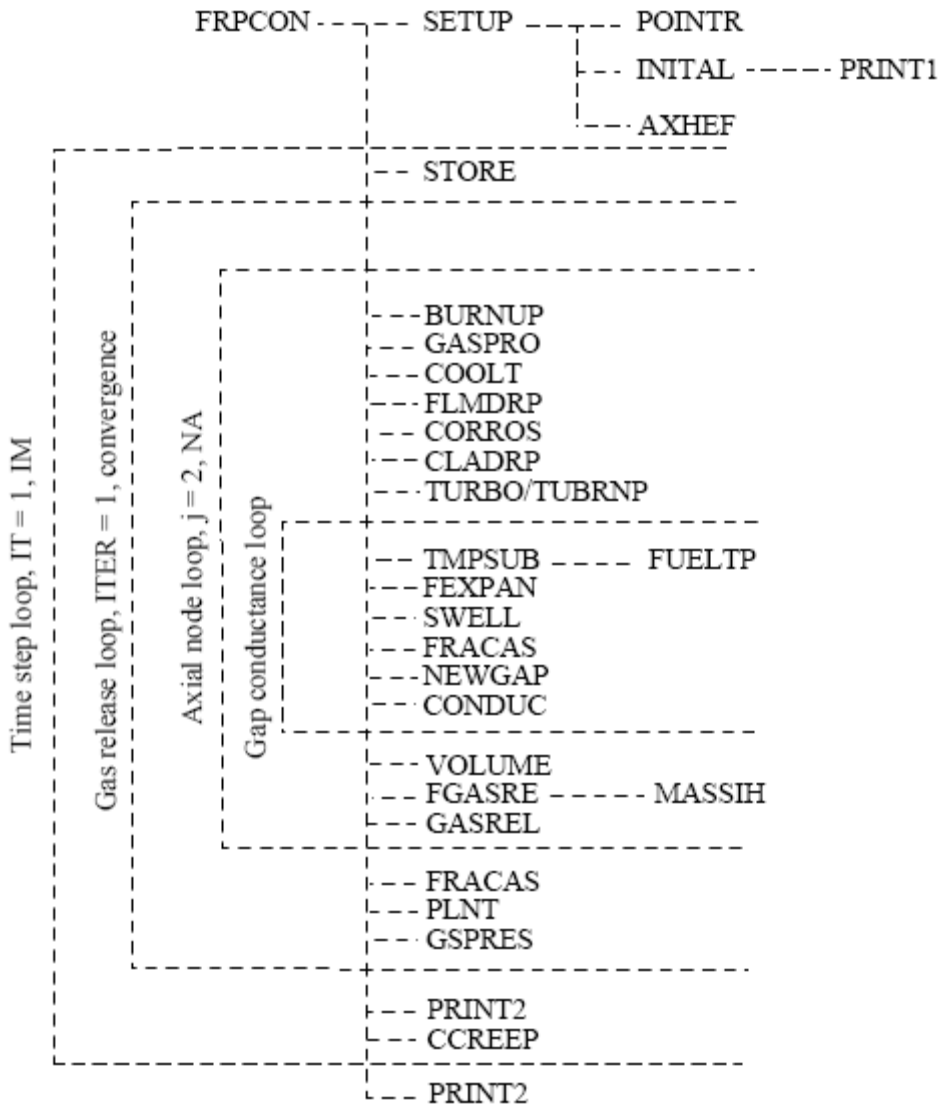

Figure 3.2 Calling sequence for FRAPCON-3 subroutines

Table 3.2 Initialization subroutines

Subroutine	Description
SETUP	Reads the data input pertaining to the problem size requirements.
POINTR	Performs the dynamic dimensioning procedure.
INITIAL	Reads the remaining problem description input and initializes the variables.
PRINT1	Generates the output, reflecting the initial conditions and specifications of the fuel rod, and lists the proposed power history.
AXHEF	Calculates the axial power profile as it affects the axial regions of the fuel rod and also any varying axial power profile changes.

Next, the code enters the first of four major loops in the Fortran coding, the time-step loop. The time-step loop encompasses virtually all of the remainder of the FRAPCON-3 code. In each

execution of the time-step loop, the code solves for the thermal and mechanical equilibrium of the fuel rod at a new point along the rod power versus time history input by the user. Those subroutines, which are executed only once per time step, are listed in Table 3.3.

Table 3.3 Subroutines in the time-step loop

Subroutine	Description
STORE	Stores variable values as necessary to account for history dependency.
PRINT2	Generates output for the code that presents converged values for all of the axial nodes for both thermal and mechanical solutions.
CCREEP	The cladding creep portion of the FRACAS-I mechanics model (the subroutine calls FCMI, which in turn calls CLADF that calls CREPR where the creep rate model is located).

Three additional loops exist in the code. The next loop encountered within the time-step loop is the gas-release loop. This loop is cycled until the value for calculated rod internal gas pressure (dependent on temperature, volume, and fission gas release) converges. Subroutines called from within this loop are listed in Table 3.4.

Table 3.4 Subroutines in the gas-release loop

Subroutine	Description
FRACAS	The FRACAS-I fuel-cladding mechanical response model is controlled by this subroutine. This loop calculates the time-independent permanent deformation.
PLNT	Calculates the current plenum gas temperature and volume.
GSPRES	Calculates the rod internal gas pressure.

The next inner loop in the coding is the axial-node loop. For every pass through the gas-release loop, the axial-node loop sequences through each of the axial regions defined by the input. The subroutines controlled by this loop are listed in Table 3.5.

Table 3.5 Subroutines in the axial-node loop

Subroutine	Description
BURNUP	Calculates the local fuel burnup.
GASPRO	Calculates the fission gas production.
COOLT	Calculates the coolant temperature.
FLMDRP	Calculates the temperature drop from the cladding surface to the coolant.
CORROS	Calculates the corrosion on the cladding surface.
CLADRP	Calculates the temperature drop from the cladding inside surface to the cladding outside surface.
TUBRNP	Calculates the radial power and burnup distribution.

The innermost loop is the gap conductance loop. This loop iterates on each axial node until thermal equilibrium in the radial direction is achieved. Thermal equilibrium is signified by a converged value for the calculated temperature drop from the fuel outer surface to the cladding inner surface. The subroutines listed in Table 3.6 comprise the gap conductance loop.

Table 3.6 Subroutines in the gap conductance loop

Subroutine	Description
TMPSUM	Calculates the radial temperature distribution through the fuel.
FUELTP	Solves the equations for the radial heat balance.
FEXPAN	Fuel thermal expansion routine.
SWELL	Calculates fuel swelling and fuel densification.
FRACAS	This subroutine calculates the new position of the cladding due to deflection caused by internal gas pressure changes.
NEWGAP	Calculates the new fuel-cladding gap size (used with the FRACAS mechanics model only).
CONDUC	Calculates new values for the gap conductance and the fuel-cladding gap temperature drop.

At the completion of all the time steps, and before returning to the driver package, a final call to PRINT2 is made. This call prints a summary table for the entire power history of the rod.

3.2 Code Results

FRAPCON-3 generates fuel rod response information as a function of fuel rod fabrication information, boundary conditions, and power history. This information is provided to the user as printed output and as plots (optional). The capability also exists to supply this information for steady-state initialization of the FRAPTRAN computer code. The information provided to the transient fuel rod analysis code consists of permanent burnup effects, such as cladding creepdown, fuel swelling, fuel densification, normalized radial power and burnup profiles, and fission gas inventory. This section presents the important response parameters, the plotting package, and information on the FRAPCON link with FRAPTRAN.

3.2.1 Fuel Rod Response

FRAPCON-3 provides the calculated fuel rod thermal, mechanical, and pressure response data. The results are presented in three forms: an axial-region printout, a power-time step printout, and a summary-page printout.

The axial-region printout presents local information on power, time, time step, and burnup. Also presented are rod radial-temperature distribution, coolant temperature, cladding stresses and strains (both recoverable and permanent), gap conductance, fuel-cladding interfacial pressure, and coolant film heat-transfer information for each axial node.

The power-time step printout presents rod burnup, void volumes and associated temperatures, mole fractions of constituent gases and release fractions, total moles of rod gas, and rod gas pressure. Also, this printout presents stresses, strains, temperatures, and stored energy for each axial node.

The summary page printout presents time-dependent information about the hot axial node. This includes temperatures of the cladding, fuel-cladding gap, and fuel; fuel-cladding interfacial pressure; cladding stress and strain; fuel outside diameter; gap conductance and gas pressure; Zircaloy oxide thickness; and hydrogen uptake.

3.2.2 Plot Package

The input instructions, Appendix A, identify the option to specify a file (FILE66) for graphics data output. This file is designed to be read by a PNNL-developed routine that works with Excel software. The file name needs to be specified in the input file as FILE66. When using the Excel input generator, this is done automatically. The Excel plot routine will be provided along with the FRAPCON-3 code to users. The user instructions for the Excel plot routine are shown in Appendix C.

3.2.3 FRAPTRAN Initialization

FRAPCON-3 contains subroutine RESTFS, which, when the flag NTAPE is set to 1, stores sets of history-dependent information for each power-time step. This information is stored on unit TAPE1 and is for FRAPTRAN initialization. This gives the user the ability to model the fuel rod initial conditions following steady-state operation accumulating significant burnup before a transient excursion.

3.3 Features of FRAPCON-3

FRAPCON-3 has been designed with special features to aid the user. These features include options for the code solution, an Excel input file generator, and options for uncertainty analysis.

3.3.1 Code Solution

FRAPCON-3 has been dynamically dimensioned so that a minimum of core storage is required for any given fuel modeling process. Parameters that are a function of the problem size are dimensioned to the exact size required by the axial and radial nodalization and the number of power-time steps. The user can set the core size based on the number of axial and radial nodes and the number of time steps.

3.3.2 Excel Input Generator

The input to FRAPCON-3.4 is a text file with variables described in Appendix A input through namelist format. It has been found that the manual creation of such an input file can be a time consuming process, can be subject to errors (particularly unit errors), and can be difficult for a new user to learn how to set up.

To assist with all these issues, an Excel Input Generator has been created. In this file, users fill in the requested information with different units available in dropdown boxes. The Excel Input Generator then creates the text file with the required units that FRAPCON-3.4 reads as input. The Excel Input Generator is available for download on the FRAPCON-3/FRAPTRAN Code Users' Group webpage. The instructions for using the Excel Input Generator are shown in Appendix A.

3.3.3 Uncertainty Analysis

One use fuel performance codes is running bounding design calculations. To do this, the models in the fuel performance code and the fuel rod design inputs must be biased up or down based on their uncertainty levels. Since FRAPCON-3 is a best-estimate fuel performance code, it had not previously been possible to perform these studies on the effect of model uncertainties without changing the code. To facilitate these studies, standard deviations for the models in FRAPCON-3.4 that are known to most impact the outputs of regulatory interest have been calculated based on the available data. These standard deviations have been hardwired into the code, and new input variables have been added that allow the user to select the level of uncertainty to apply (e.g., $+1\sigma$ or -1.6σ).

The FRAPCON-3.4 models selected to allow for a bounding design calculation were those expected to have a significant impact on outputs of regulatory interest such as rod internal pressure, fuel centerline temperature, and cladding strain. A sample sensitivity study was performed for a typical PWR and BWR rod (Geelhood et al., 2009) and based on the results of this study; eight models were identified as necessary in a bounding design calculation in FRAPCON-3.4. The eight models selected are

- fuel thermal conductivity
- fuel thermal expansion
- fission gas release
- fuel swelling
- irradiation creep
- cladding thermal expansion
- cladding corrosion
- cladding hydrogen pickup

These models may be biased through the use of the appropriate input variables in Appendix A.

4.0 References

American Nuclear Society (ANS). 1982. "Method for Calculating the Fractional Release of Volatile Fission Products from Oxide Fuel," *ANS5.4 of the Standards Committee of the American Nuclear Society,* ANSI/ANS-5.4-1982.

Berna, G.A., C.E. Beyer, K.L. Davis, and D.D. Lanning. 1997. *FRAPCON-3: A Computer Code for the Calculation of Steady-State, Thermal-Mechanical Behavior of Oxide Fuel Rods for High Burnup*, NUREG/CR-6534, Vol. 2, PNNL-11513, Vol. 2, Pacific Northwest National Laboratory, Richland, WA.

Beyer, C. E., C. R. Hann, D. D. Lanning, F. E. Panisko, and L. J. Parchen. 1975. *GAPCONTHERMAL-2: A Computer Program for Calculating the Thermal Behavior of an Oxide Fuel Rod,* BNWL-1898, Battelle Northwest Laboratory, Richland, WA.

Bohn, M. P. 1977. *FRACAS: A Subcode for the Analysis of Fuel Pellet-Cladding Mechanical Interaction,* TREE-NUREG-1028, EG&E Idaho, Inc., Idaho National Engineering Laboratory, Idaho Falls, ID.

Booth, A. H. 1957. *A Method of Calculating Fission Gas Diffusion from UO_2 Fuel and Its Application to the X-2 Loop Test,* AECL-496, CRDC-721, Atomic Energy of Canada, Ltd., Chalk River Project, Chalk River, Ontario.

Cunningham, M. E., and C. E. Beyer. 1984. *GT2R2: An Updated Version of GAPCONTHERMAL-2,* NUREG/CR-3907, PNL-5178, Pacific Northwest Laboratory, Richland, WA.

Dittus, F., and L. M. K. Boelter. 1930. "Heat Transfer in Automobile Radiators of the Tubular Type," *University of California Publications in Engineering,* 2(13):443–461.

Ferrari, H. M. 1963. "Nitrogen Release from UO_2 Pellets at Elevated Temperatures," *Nuclear Science and Engineering,* 17(4):503–512.

Ferrari, H. M. 1964. "Diffusion of Nitrogen in Uranium Dioxide," *Journal of Nuclear Materials,* 12(2):142–144.

Forsberg, K., and A. R. Massih. 1985. "Diffusion Theory of Fission Gas Migration in Irradiated Nuclear Fuel UO_2," *Journal of Nuclear Materials,* 135:140–148.

Franklin, D.G., G.E. Lucas, and A.L. Bement. 1983. *Creep of Zirconium Alloys in Nuclear Reactors*, ASTM STP 815, American Society for Testing and Materials, West Conshohocken, PA.

Galbraith, K. P. 1973. *Pellet-Cladding Gap Closure from Pellet Cracking Data and Analysis*, XN-73-17, Siemens Power Corporation (Formerly Exxon Nuclear), Richland, WA.

Garzarolli, F., W. Jung, H Shoenfeld, A.M. Garde, G.W. Parray, and P.G. Smerd. 1982. *Review of PWR Fuel Rod Waterside Corrosion Behavior*, EPRI NP-2789, Project 1250 Final Report, Electric Power Research Institute, Palo Alto, CA.

Garnier, J. E. and S. Begej. 1979. *Ex-Reactor Determination of Thermal Gap and Contact Conductance Between Uranium Dioxide: Zircaloy-4 Interfaces; Stage I: Low Gas Pressure,* NUREG/CR-0330, PNL-2696, Pacific Northwest Laboratory, Richland, WA.

Geelhood, K.J., and C.E. Beyer. 2008. "Corrosion and Hydrogen Pickup Modeling in Zirconium Based Alloys," *Proceedings of the 2008 Water Reactor Fuel Performance Meeting*, October 19–23, 2008, Seoul, Korea.

Geelhood, K.J., C.E. Beyer, and W.G. Luscher. 2008. *PNNL Stress/Strain Correlation for Zircaloy*, PNNL-17700, Pacific Northwest National Laboratory, Richland, WA.

Geelhood, K.J., W.G. Luscher, C.E. Beyer, D.J. Senor, M.E. Cunningham, D.D. Lanning, and H.E. Adkins. 2009. *Predictive Bias and Sensitivity in NRC Fuel Performance Codes*, NUREG/CR-7001, PNNL-17644, Pacific Northwest National Laboratory, Richland, WA.

Geelhood, K.J., W.G. Luscher, and C.E. Beyer. 2010a. *FRAPCON-3.4 Integral Assessment*, NUREG/CR-7022, Vol. 2, PNNL-19418, Pacific Northwest National Laboratory, Richland WA.

Geelhood, K.J., W.G. Luscher, C.E. Beyer, and J.M. Cuta. 2010b. *FRAPTRAN 1.4: A Computer Code for the Transient Analysis of Oxide Fuel Rods*, NUREG/CR-7023 ,Vol. 1, PNNL-19400, Vol. 1, Pacific Northwest National Laboratory, Richland, WA.

Gilbon, D., A. Soniak, S. Doriot, and J.P. Mardon. 2000. "Irradiation Creep and Growth Behavior, and Microstructural Evolution of Advanced Zr-Base Alloys," *Zirconium in the Nuclear Industry: Twelfth International Symposium*, *ASTM-STP-1354*, Ed. GP Sabol and GD Moan, American Society of Testing and Materials, West Conshohocken, PA, pp. 51–73.

Hagrman, D.L., G.A. Reymann, and G.E. Mason. 1981. *A Handbook of Materials Properties for Use in the Analysis of Light Water Reactor Fuel Rod Behavior. MATPRO Version 11 (Revision 2)*. NUREG/CR-0479 (TREE-1280), prepared by EG&G Idaho, Inc., Idaho Falls, Idaho for the U.S. Nuclear Regulatory Commission, Washington, D.C.

Jens, W.H., and P.A. Lottes. 1951. *Analysis of Heat Transfer, Burnout, Pressure Drop, and Density Data for High-Pressure Water,* ANL-4627, Argonne National Laboratory, Argonne, IL.

Khorushii, O.V., S.Yu. Kourtchatov, and V.V. Likhanskii. 1999. "New model of equiaxed grain growth in irradiated UO_2," *Journal of Nuclear Materials*, 265:112–116.

Knuutila, A. 2006. *Improvements on FRAPCON-3/FRAPTRAN Mechanical Modeling*, VTT-R-11337-06. VTT, Finland.

Kreith, F. 1964. *Principles of Heat Transfer*, 8th Edition, Scranton: International Book Company.

Lanning, D.D. 1982. "The Possible Impact of Fuel Pellet Cracking on Inferred Gap Conductance and Stored Energy," *Nuclear Technology*, 56:565–574.

Lassman, K., C. O'Carrol, J. VanderLaar, and C.T. Walker. 1994. "The Radial Distribution of Plutonium in High Burnup UO_2 Fuels," *Journal of Nuclear Materials,* 28:223–231.

Lassman, K., C.T. Walker, and J. van de Laar. 1998. "Extension of the TRANSURANUS Burnup Model to Heavy Water Reactor Conditions," *Journal of Nuclear Materials*, 255:222–233.

Limbäck, M., and T. Andersson. 1996. "A Model for Analysis of the Effect of Final Annealing on the In- and Out-of-Reactor Creep Behavior of Zircaloy Cladding," *Zirconium in the Nuclear Industry: Eleventh International Symposium*, ASTM STP 1295, E.R. Bradley and G.P. Sabol, Eds., American Society for Testing and Materials, West Conshohocken, PA, pp. 448–468.

Lucuta, P.G., H.S. Matzke, and I.J. Hastings. 1996. "A Pragmatic Approach to Modeling Thermal Conductivity of Irradiated UO_2 Fuel: Review and Recommendations," *Journal of Nuclear Materials*, 232:166–180.

Luscher, W.G., and K.J. Geelhood. 2010. *Material Property Correlations: Comparisons between FRAPCON-3.4, FRAPTRAN 1.4, and MATPRO*, NUREG/CR-7024, PNNL-19417, Pacific Northwest National Laboratory, Richland, WA.

Manzel, R., and C.T. Walker. 2000. "High Burnup Fuel Microstructure and Its Effect on Fuel Rod Performance," *LWR Fuel Performance Meeting*, Park City, UT.

Manzel, R., and C.T. Walker. 2002. "EPMA and SEM of fuel samples from PWR rods with an average burn-up of around 100 MWd/kgHM", *Journal of Nuclear Materials*, 301:170–182.

Matsuo, Y. 1987. "Thermal Creep of Zircaloy-4 Cladding under Internal Pressure," *Journal of Nuclear Science and Technology,* 24(2):111–119.

McAdams, W.H. 1954. *Heat Transmission*, 34th Edition, New York: McGraw-Hill Book Company, Inc.

Mendelson, A. 1968. *Plasticity: Theory and Applications*, New York: The MacMillan Company.

Oguma, M. 1983. "Cracking and Relocation Behavior of Nuclear Fuel Pellets During Rise to Power," *Nucl. Eng. Design,* 76:35–45.

Ohira, K., and N. Itagaki. 1997. "Thermal Conductivity Measurements of High Burnup UO_2 Pellets and Benchmark Calculation of Fuel Center Temperature," *Proceedings of the ANS International Topical Meeting on LWR Fuel Performance*, pp. 541–549. March 2–6, 1997, Portland, OR.

Rapier, A.C., T.M. Jones, and J.E. McIntosh. 1963. "The Thermal Conductance of Uranium Dioxide/Stainless Steel Interfaces," *International Journal of Heat Mass Transfer,* 6:397–416.

Rausch, W.N., and F E. Panisko. 1979. *ANS54: A Computer Subroutine for Predicting Fission Gas Release,* NUREG/CR-1213, PNL-3077, Pacific Northwest Laboratory, Richland, WA.

Ross, A.M., and R.L. Stoute. 1962. *Heat Transfer Coefficients Between UO_2 and Zircaloy-2,* CRFD-1075, AECL-1552, Atomic Energy of Canada, Limited.

Sabol, G.P., Comstock, R.J., Weiner, R.A., Larouere, P., and Stanutz, R.N. 1994. "In-Reactor Corrosion Performance of ZIRLO™ and Zircaloy-4," *Zirconium in the Nuclear Industry: Tenth*

International Symposium, ASTM STP 1245, A.M. Garde and E.R. Bradley, Eds. American Society for Testing and Materials, Philadelphia, PA, pp. 724–744.

Shestopalov, A., K. Lioutov, L. Yegorova, G. Abyshov, and K. Mikitiouk. 1999. *Modification of USNRC's FRAP-T6 Fuel Rod Transient Code for High Burnup VVER Fuel*, NUREG/IA-0164, U.S. Nuclear Regulatory Commission, Washington, D.C.

Soniak, A., N. L'Hullier, J-P. Mardon, V. Rebeyrolle, P. Boffioux, and C. Bernaudat. 2002. "Irradiation Creep Behavior of Zr-Base Alloys," *Zirconium in the Nuclear Industry: Thirteenth International Symposium*, ASTM STP 1423, G.D. Moan and P. Rudling, Eds. ASTM International, West Conshohocken, PA, pp.837–862.

Sontheimer, F., and K.L. Nissen. 1994. "Evaluation of the Stress Reversal Creep Experiment IFA-585 in the HBWR and the Lift-Off Experiment ROPE-1 in the R2 Studsvik using the Siemens/KWU Clad Creep Model," *Enlarged HPG Meeting on High Burn-up Fuel Performance, Safety and Reliability and Degradation of In-Core Materials and Water Chemistry Effect and Man-Machine Systems Research*, HPR-345/28.

Spino, J., K. Vennix, and M. Coquerelle. 1996. "Detailed characterization of the rim microstructure on PWR fuels in the burn-up range 40-67 GWd/tM," *Journal of Nuclear Materials*, 231:179–190.

Todreas, N., and G. Jacobs. 1973. "Thermal Contact Conductance of Reactor Fuel Elements," *Nuclear Science and Engineering,* 50:283.

Une, K., K. Nogita, T. Shiratori, and K. Hayashi. 2001. "Rim structure formation of isothermally irradiated UO_2 fuel discs," *Journal of Nuclear Materials*, 288:20–28.

Appendix A

Input Instructions for the FRAPCON-3 Code

Appendix A Input Instructions for the FRAPCON-3 Code

Input Structure

The NAMELIST input is divided into four sections: case control integers (in $FRPCN); case design and operation descriptors (real and integer variables) located in ($FRPCON); evaluation model options (in $EMFPCN); and plutonium isotopic distributions (in $FRPMOX). The variables in the first group must be separated by commas and placed between the statement $FRPCN and $END. Similarly, the variables in the second, third, and fourth groups must be placed between $FRPCON and $END, between $EMFPCN and $END, and between $FRPMOX and $END, respectively.

Before the NAMELIST input, the following lines must be included in the input file:

FILE05='nullfile', STATUS='UNKNOWN', FORM='FORMATTED',
CARRIAGE CONTROL='NONE'

This line sets up a file called "nullfile" which is needed by FRAPCON-3.3.

FILE06='file.out', STATUS='UNKNOWN', CARRIAGE CONTROL='LIST'

This line specifies the name of the output file. In this case the output file would be called "file.out."

FILE66='file.plot', STATUS='UNKNOWN', FORM='FORMATTED',
CARRIAGE CONTROL='LIST'

This line is needed if a plot output file is being created. (see definition of variable NPLOT) In this case the plot file would be called "file.plot."

The above three lines should not exceed 72 spaces, and if they do, continue on the next line with no continuation symbols needed.

/**********

The line seen above, which is preceded by the character "/", tells the code that the lines specifying files are complete.

The line immediately after this line is reserved for the case description that will be displayed in the page headers in the output. Up to 72 characters can be inserted here to describe the case.

After this line the NAMELIST input can be entered. In the above section any line with a "*" in column 1 is considered a comment and will not be read by the code. An example case input is given in Section 2 below.

The following tables describe the input variables to FRAPCON3.4. Unless otherwise noted in the Limitations/Default value column, the variables should be placed in the $frpcon data input block.

Input Variables Specifying Rod Design

Rod Size

Variable Name (type)	Description	Units British/SI	Limitations/Default Value
dco (R)	Cladding outer diameter	inches / meters	Required Input
thkcld (R)	Cladding wall thickness	inches / meters	Required Input
thkgap (R)	Pellet-cladding as-fabricated radial gap thickness	inches / meters	Required Input
totl (R)	The total (active) fuel column length	feet / meters	Required Input
cpl (R)	Cold plenum length	inches / meters	Required Input

(R) = real, (I) = integer

Spring Dimensions

Variable Name (type)	Description	Units British/SI	Limitations/Default Value
dspg (R)	Outer diameter of plenum spring	inches / meters	Required Input (*dgpg* should be less than the clad inner diameter)
dspgw (R)	Diameter of the plenum spring wire	inches / meters	Required Input
vs (R)	Number of turns in the plenum spring	Dimensionless	Required Input

(R) = real, (I) = integer

Input Variables Specifying Pellet Fabrication

Pellet Shape

Variable Name (type)	Description	Units British/SI	Limitations/Default Value
hplt (R)	Height (length) of each pellet	inches / meters	Required Input
rc (R)	The inner pellet radius	inches / meters	Default = 0.0
hdish (R)	Height (depth) of pellet dish, assumed to be a spherical indentation	inches / meters	Default = 0.0
dishsd (R)	Pellet end-dish shoulder width (outer radius of fuel pellet minus radius of dish)	inches / meters	Default = 0.0

(R) = real, (I) = integer

Pellet Isotopics

Variable Name (type)	Description	Units British/SI	Limitations/Default Value
enrch (R)	Fuel pellet U-235 enrichment	Atom % U-235 in total U	Required Input
imox (I)	Index for modeling MOX: 0 = UO_2 fuel >0 = mixed oxide fuel 1 = use Duriez/Ronchi/NFI Mod thermal conductivity correlation 2 = use Halden thermal conductivity correlation (if *imox*>0, must include *comp* and namelist $FRPMOX)	Dimensionless	Default = 0
comp (R)	Weight percent of plutonia in fuel (Must specify if *imox*>0)	Weight percent	Default = 0.0
moxtype (I)	Type of Pu used in MOX moxtype = 1 reactor grade moxtype = 2 weapons grade	Dimensionless	Default = 1 (namelist frpmox)
enrpu39 (R)	Fuel pellet Pu-239 content	Atom % Pu-239 in total Pu	Default = 0.0 (namelist frpmox)
enrpu40 (R)	Fuel pellet Pu-240 content	Atom % Pu-240 in total Pu	Default = 0.0 (namelist frpmox)

Variable Name (type)	Description	Units British/SI	Limitations/Default Value
enrpu41 (R)	Fuel pellet Pu-241 content	Atom % Pu-241 in total Pu	Default = 0.0 (namelist frpmox)
enrpu42 (R)	Fuel pellet Pu-242 content	Atom % Pu-242 in total Pu	Default = 0.0 (namelist frpmox)
fotmtl (R)	Oxygen-to-metal atomic ratio in the oxide fuel pellet	Dimensionless	Default = 2.0 (If MOX fuel is selected, *fotmtl* should be less than 2.0.)
gadoln (R)	Weight fraction of gadolinia in urania-gadolinia fuel pellets	Dimensionless	Default = 0.0
ifba (R)	Percent of IFBA rods in the core	%	Default = 0.0
b10 (R)	Boron-10 enrichment in ZrB_2	Atom %	Default = 0.0
zrb2thick (R)	ZrB_2 layer thickness on pellets	inches, meters	Default = 0.0
zrb2den (R)	Percent theoretical density of ZrB_2 TD=6.08 g/cm³	% theoretical density	Default = 90.0
ppmh2o (R)	Parts per million by weight of moisture in the as-fabricated pellets	ppm	Default = 0.0
ppmn2 (R)	Parts per million by weight of nitrogen in the as-fabricated pellets	ppm	Default = 0.0

(R) = real, (I) = integer

Pellet Fabrication

Variable Name (type)	Description	Units British/SI	Limitations/Default Value
den (R)	As-fabricated apparent fuel density	% of theoretical density	Required Input (Theoretical density taken as 10.96 g/cm^3)
deng (R)	Open porosity fraction for pellets	% of theoretical density	Default = 0.0
roughf (R)	The fuel pellet surface arithmetic mean roughness, peak-to-average	inches / meters	Required Input

Variable Name (type)	Description	Units British/SI	Limitations/Default Value
rsntr (R)	The increase in pellet density expected during in-reactor operation (determined from a standard re-sintering test per NUREG-0085 and Regulatory Guide 1.126)	kg/m^3	Required Input
tsint (R)	Temperature at which pellets were sintered	°F / K	Default = 2911° F

(R) = real, (I) = integer

Input Variables Specifying Cladding Fabrication

Variable Name (type)	Description	Units British/SI	Limitations/Default Value
icm (I)	Cladding Type Indicator: 2 = Zircaloy 2 4 = Zircaloy 4 5 = M5 6 = ZIRLO™	Dimensionless	Required Input
zr2vinage (I)	Flag to select Zircaloy-2 vintage zr2vintage= 0 older Zircaloy-2 prior to 1998 zr2vintage=1 newer Zircaloy-2 since 1998	Dimensionless	Default = 1
cldwks (R)	Cold-work of the cladding (fractional reduction in cross-section area due to processing). PNNL recommends 0.5 for stress relief annealed cladding and 0.0 for fully re-crystallized cladding.	Dimensionless	Default = 0.2
roughc (R)	The cladding surface arithmetic mean roughness, peak-to-average	inches / meters	Required Input
catexf (R)	Cladding texture factor; defined as the fraction of cladding cells with basal poles parallel to the longitudinal axis of the cladding tube	Dimensionless	Default = 0.05
chorg (R)	As-fabricated hydrogen in cladding	ppm wt.	Default = 10.0

(R) = real, (I) = integer

Input Variables Specifying Rod Fill Conditions

Variable Name (type)	Description	Units British/SI	Limitations/Default Value
fgpav (R)	Initial fill gas pressure (taken to be at room temperature)	psia / Pa	Required Input
idxgas (I)	Initial fill gas type indictator: 1 = helium 2 = air 3 = nitrogen 4 = fission gas 5 = argon 6 = user-specified mix, using the *amfxx* variables *amfair*, etc.	Dimensionless	Default = 1
amfair (R)	Mole fraction of air; use only if *idxgas* = 6.	Mole Fraction	Default = 0.0
amfarg (R)	Mole fraction of argon; use only if *idxgas* = 6.	Mole Fraction	Default = 0.0
amffg (R)	Mole fraction of fission gas; use only if *idxgas* = 6 and if *amfxe* and *amfkry* = 0.0.	Mole Fraction	Default = 0.0
amfhe (R)	Mole fraction of helium; use only *idxgas* = 6.	Mole Fraction	Default = 0.0 (note default on *idxgas* = 1 initializes pure He)
amfh2 (R)	Mole fraction of hydrogen; use only if *idxgas* = 6.	Mole Fraction	Default = 0.0
amfh2o (R)	Mole fraction of water vapor; use only if *idxgas* = 6.	Mole Fraction	Default = 0.0
amfkry (R)	Mole fraction of krypton; use only if *idxgas* = 6.	Mole Fraction	Default = 0.0
amfn2 (R)	Mole fraction of nitrogen; use only if *idxgas* = 6.	Mole Fraction	Default = 0.0
amfxe (R)	Mole fraction of xenon; use only if *idxgas* = 6.	Mole Fraction	Default = 0.0

(R) = real, (I) = integer

Input Variables Specifying Reactor Conditions

Variable Name (type)	Description	Units British/SI	Limitations/Default Value
iplant (I)	Signal for which type of reactor: -2 = PWR -3 = BWR -4 = HBWR	Dimensionless	Default = -2
nsp (I)	Signal for time-dependent input arrays for *p2*, *tw*, and *go*: If *nsp* = 0, single values for these three variables will be used for all time steps. If *nsp* = 1, a value for each variable for each time step must be input.	Dimensionless	Required Input
p2(IT) (R)	Coolant system pressure. Must be input for each time step if *nsp* = 1.	psia / Pa	Required Input
tw(IT) (R)	Coolant inlet temperature. Enter a value for every time step if *nsp* =1.	°F / K	Required Input
go(IT) (R)	Mass flux of coolant around fuel rod. Input a value for each time step if *nsp* = 1. Note that *go* input may have to be adjusted to yield both desired coolant and desired cladding surface temperatures. Concurrent adjustment of *pitch* may also be required.	lb/hr-ft^2 / kg/s-m^2	Required Input
pitch (R)	Center-to-center distance between rods in a square array	inches / meters	Required Input (Must be greater than *dco*)

Variable Name (type)	Description	Units British/SI	Limitations/Default Value
icor (I)	Index for Crud Model: *icor* = 0 or 1 yields constant crud thickness; 0.0 mil crud as default; input *crdt* as constant thickness. Maximum temperature rise permitted across this layer is 20 ºF. *icor* = 2 yields time-dependent crud; growth rate is *crdtr*, starting from zero crud layer. There is no limit to the temperature rise across the crud when *icor*=2. The conductivity of the layer is 0.5 Btu/hr/ft-EF.	Dimensionless	Default = 0
crdt (R)	Initial thickness of crud layer on cladding outside surface	mils/meters	Default = 0.0
crdtr (R)	Rate of crud accumulation (used if *icor* = 2)	mils/hr / meters/s	Default = 0.0
crudmult(J-1) (R)	Axial array of multipliers on crud thickness or crud growth rate	Dimensionless	Default = 1.0
flux(J) (R)	Conversion between fuel specific power (W/g) and fast neutron flux ($n/m^2/s$, E>1MeV). Input as an axial array; the second value of the array corresponds to the first axial node, the *na*+1 value corresponds to the top axial node.	neutrons per square meter per second per W/g of fuel	Default = 0.221×10^{17} (Maximum of 20 values)

(R) = real, (I) = integer
IT = Time Step Index
J = 1 + Axial Node Index

Input Variables Specifying Power History

Variable Name (type)	Description	Units British/SI	Limitations/Default Value
im (I)	Number of time steps	Dimensionless	Greater than 1, less than 400 Required Input (namelist frpcn)
ProblemTime(IT) (R)	Cumulative time at the end of each time step. Note: Time steps greater than 50 days are not recommended. If steady-state operation is being modeled, use time steps greater than 1 day. Time steps less than 1 day should only be used when modeling a fast power ramp.	days	Required Input Limit 400 steps
qmpy(IT) (R)	The linear heat generation rate at each time step. This equals the rod-average value if *iq* = 0 and the peak value if *iq* = 1. Note: Changes in local LHGR of greater than 1.5 kw/ft per time step are not recommended. Size *qmpy* accordingly.	kW/ft / kW/m	Required Input Limit 400 steps

(R) = real, (I) = integer
IT = Time Step Index

Input Variables Specifying Axial Power Profile

Variable Name (type)	Description	Units British/SI	Limitations/Default Value
iq (I)	Indicator for axial power shape: 0 = User-input power shapes, with *qmpy* = rod-average powers and power shapes defined by *qf*,*x*, and *fa* = 1.0. 1 = Chopped-cosine shape, with *fa* = Peak-to-average ratio and *qmpy* = peak power (use na=odd in order to have an axial node corresponding to the input peak power).	Dimensionless	Required Input
x(N) (R)	The elevations in each *qf*, *x* array defining a power shape. Note the first value should be 0.0 and the last value must = *totl*.	feet / meters	Required Input if *iq*=0 Maximum number of *qf*, *x* pairs is 40.
qf(N) (R)	The ratio of the linear power at the *x*(N) elevation to the axially-averaged value for the M-th power shape. The number of QF, X pairs for the Mth power shape is defined by *jn*(M). The code will automatically normalize to an average value of 1.0.	Dimensionless	Required Input if *iq* = 0 Maximum number of *qf*, *x* pairs is 40.
jn(M) (I)	The number of *qf*, *x* value pairs for each axial power shape; required input if *iq* = 0. Input in the same sequence as the *qf* and *x* arrays.	Dimensionless	Required Input if *iq*=0 Maximum number of shapes is 20. Maximum number of *qf*, *x* pairs is 40.
jst(IT) (I)	The sequential number of the power shape to be used for each time step. One value of *jst* is required per time step if *iq* = 0.	Dimensionless	Required Input if *iq*=0 Maximum number of power shapes is 20. Maximum time steps is 400.
fa (R)	Peak-to-average power ratio for cosine-type axial power distribution (= 1.0, unless *iq* = 1; see description of *iq*).	Dimensionless	Required Input

(R) = real, (I) = integer
N = Axial Node Index for Input Power Profile
M = Power Shape Number
IT = Time Step Index

Input Variables Specifying Axial Temperature Distribution (Optional)

Variable Name (type)	Description	Units British/SI	Limitations/Default Value
ifixedtsurf (I)	Indicator for using axial temperature distribution 0 = Cladding temperature will be calculated based on input power and coolant conditions. 1 = Cladding temperature will be specified by the user for certain time steps. Each time step where the temperature will be set by the user, the input variable, *go*, should be set equal to 0.0.	Dimensionless	Default Value = 0
xt(N) (R)	The elevations in each *cladt*, *xt* array defining a cladding temperature profile. Note the first value should be 0.0 and the last value must = *totl*. Begin the input elevations for the second temperature profile at xt(n+1) where n is the number of values in the first profile.	feet / meters	Default Value = 0.0
cladt(N) (R)	The cladding surface temperature *xt*(N) elevation for the M-th temperature profile. The number of *cladt*, *xt* pairs for the Mth power shape is defined by *jnsurftemp*(M).	Dimensionless	Default Value =0.0 Maximum number of *cladt*, *xt* pairs is 40.
jnsurftemp(M) (I)	The number of *cladt*, *xt* value pairs for each axial temperature distribution; Input in the same sequence as the *cladt* and *xt* arrays.	Dimensionless	Default Value = 0 Maximum number of shapes is 20. Maximum number of *cladt*, *xt* pairs is 40.
jstsurftemp(IT) (I)	The sequential number of the temperature profile to be used for each time step. One value of *jstsurftemp* is required per time step if *ifixedtsurf* = 1.	Dimensionless	Default Value = 0 Maximum number of shapes = 20. Maximum time steps is 400.

(R) = real, (I) = integer
N = Axial Node Index for Input Surface Temperature Profile
M = Surface Temperature Profile Number
IT = Time Step Index

Input Variables Specifying Code Operation

Variable Name (type)	Description	Units British/SI	Limitations/Default Value
nr (I)	Number of radial boundaries in the pellet (for temperature calculations and temperature distribution output). These are spaced by the code with greater fraction in the outer region to optimize definition of the heat generation radial distribution.	Dimensionless	Greater than 1, less than 25; suggested minimum number is 17. Default = 17 (namelist frpcn)
ngasr (I)	Number of equal-volume radial rings in the pellet for gas release calculations	Dimensionless	Greater than 6, less than 50; suggested number is 45. Default = 45 (namelist frpcn)
ngasmod (I)	Flag to select fission gas release model ngasmod=1 selects ANS5.4 model ngasmod=2 selects Massih model ngasmod=3 selects FRAPFGR model	Dimensionless	Default = 2
na (I)	Number of equal-length axial regions along the rod, for which calculations are performed and output	Dimensionless	Greater than 1, less than 18 Default = 9 (namelist frpcn)
nunits (I)	Signal for units system to be used for input and output: 1 = British units 0 = SI units Note that input of *nunits* >10 will activate "debug" output, which is significant in volume.	Dimensionless	Default = 1
crephr (R)	Subdivision for internal creep steps (should be set to a minimum of 10 creep steps per time step for smallest step)	hours	Default = 10.0
sgapf (R)	Number of fission gas atoms formed per 100 fissions	Dimensionless	Default = 31.0

slim (R)	Limit on swelling	Volume fraction	Default = 0.05
qend (R)	Fraction of end-node heat that transfers to the plenum gas	Dimensionless	Default = 0.3
igas (I)	Time step to begin calculation of fission gas release. For all time steps prior to *igas*, the calculated gas release will not be included in the gas in the rod void volume. (Note: this option only is available when using the Massih fission gas release model.)	Dimensionless	Default = 0
mechan (I)	Option to select mechanical model mechan=1 selects FEA model mechan=2 selects FRACAS-I model	Dimensionless	Default = 2 (namelist frpcn)
nce (I)	Number of radial elements in the cladding for FEA model	Dimensionless	Default = 5 (namelist frpcn)
frcoef (R)	Coulomb friction coefficient between the cladding and the fuel pellet	Dimensionless	Default = 0.015
igascal (I)	Internal pressure calculation for FEA model igascal=1 normal pressure calculation igascal=0 use prescribed pressure set by p1	Dimensionless	Default = 1
p1(IT) (I)	Rod internal pressure for each time step for FEA model. Needed only if igascal = 0.	psi / Pa	Default = 0

(R) = real, (I) = integer
IT = Time Step Index

Model Uncertainty Variables for Sensitivity Analysis

Variable Name (type)	Description	Units British/SI	Limitations/Default Value
sigftc (I)	Bias on fuel thermal conductivity model. sigftc = 1 biases model up 1σ, sigftc = -1.5 biases model down 1.5σ.	Dimensionless	Default = 0
sigftex (I)	Bias on fuel thermal expansion model. sigftex = 1 biases model up 1σ, sigftex = -1.5 biases model down 1.5σ.	Dimensionless	Default = 0
sigfgr (I)	Bias on fission gas release model. sigfgr=1 biases model up 1σ, sigfgr = -1.5 biases model down 1.5σ.	Dimensionless	Default = 0
sigswell (I)	Bias on fuel swelling model. sigswell=1 biases model up 1σ, sigswell = -1.5 biases model down 1.5σ.	Dimensionless	Default = 0
sigcreep (I)	Bias on cladding creep model. sigcreep=1 biases model up 1σ, sigcreep=-1.5 biases model down 1.5σ.	Dimensionless	Default = 0
siggro (I)	Bias on cladding axial growth model. siggro=1 biases model up 1σ, siggro=-1.5 biases model down 1.5σ.	Dimensionless	Default = 0
sigcor (I)	Bias on cladding corrosion model. sigcor=1 biases model up 1σ, sigcor=-1.5 biases model down 1.5σ.	Dimensionless	Default = 0
sigh2 (I)	Bias on cladding hydrogen pickup model. sigh2=1 biases model up 1σ, sigh2=-1.5 biases model down 1.5σ.	Dimensionless	Default = 0

(R) = real, (I) = integer

Model Selection Variables not Recommended by PNNL

Variable Name (type)	Description	Units British/SI	Limitations/Default Value
imswch (I)	Signal for EM models: =1 All EM models = 0 No EM models = -1 Selected EM models, input signals in $EMFPCN	Dimensionless	Default = 0
impowr (R)	EM Power requirement index; = 0, not assumed to be required	Dimensionless	Default = 0 (namelist emfpcn)
imfuel (R)	Switch on dimensional changes: = 0, BE changes, =1, EM changes	Dimensionless	Default = 0 (namelist emfpcn)
imdens (R)	Switch on densification model	Dimensionless	Default = 0 (namelist emfpcn)
imrelo (R)	Switch on fuel relocation model	Dimensionless	Default = 0 (namelist emfpcn)
imclad (R)	Switch on cladding deformation; = 1, no permanent deformation	Dimensionless	Default = 0 (namelist emfpcn)
imgapc (R)	switch on gap conductance calculation	Dimensionless	Default = 0 (namelist emfpcn)
imenrg (R)	Switch on stored energy reference temperature: = 0 reference = 298 K = 1, reference = 273 K	Dimensionless	Default = 0 (namelist emfpcn)

(R) = real, (I) = integer

Input Variables Specifying Code Output

Variable Name (type)	Description	Units British/SI	Limitations/Default Value
jdlpr (I)	Output print control for each time step: 0 = All axial nodes 1 = peak-power axial node -1 = axial summary for NO printout each step, see *nopt*	Dimensionless	Default = 1 Note: The code sets *jdlpr* to 0 (full output) when *ntape* is greater than 0, to assure full axial array of permanent radial deformations is passed to FRAPTRAN.
nopt (I)	Control on printout = 0, printout each time step, controlled by *jdlpr* =1, Case input and summary sheet only	Dimensionless	Default = 0
nplot (I)	Control on output of plot file for excel plotting routine = 0, No output plot file will be created. =1, Plot output file will be created (File 66). Note: The name of the plot file should be specified in the input file below where the name of the ordinary output (File 06) is specified.	Dimensionless	Default = 0
ntape (I)	Signal for creating a start tape for FRAPTRAN, from subroutine RESTFS. If *ntape* > 0, RESTFS is called and a tape (file 22="restart") is incrementally written each time step.	Dimensionless	Default = 0.
nread (I)	Signal to start up from a restart tape (File 13). The value of *nread* is the time step to start from. Note: User must switch the restart-write tape file number from 12 to 13 to make it a restart-read tape. Note that the restart tape does not currently contain complete restart information for the fission gas release models.	Dimensionless	Default = 0

Variable Name (type)	Description	Units British/SI	Limitations/Default Value
nrestr (I)	Signal for writing a restart tape for FRAPCON-3. If *nrestr* not equal to 0, subroutine TAPEGEN generates a restart tape (file 12) at each time step. Note that the restart tape does not currently contain complete restart information for the fission gas release models.	Dimensionless	Default = 0

(R) = real, (I) = integer

Example Case with MOX Fuel

```
*********************************************************************
*        frapcon3, steady-state fuel rod analysis code
*
*-------------------------------------------------------------------
*
*
*
*         CASE DESCRIPTION: MOX example rod
*
*
*
*UNIT     FILE DESCRIPTION
*
*----     ------------------------------------------------Output:
*
*         Output :
*
*    6        STANDARD PRINTER OUTPUT
*
*
*
*         Scratch:
*
*    5        SCRATCH INPUT FILE FROM ECH01
*
*
*
*  Input:   FRAPCON3 INPUT FILE (UNIT 55)
*
*
*
*********************************************************************
* GOESINS:
FILE05='nullfile', STATUS='UNKNOWN', FORM='FORMATTED',
         CARRIAGE CONTROL='NONE'
*
* GOESOUTS:
FILE06='MOXexample.out',    STATUS='UNKNOWN', CARRIAGE CONTROL='LIST'
FILE66='MOXexample.plot', STATUS='UNKNOWN', FORM='FORMATTED',
        CARRIAGE CONTROL='LIST'
/*******************************************************************
         MOX Example Rod
 $frpcn
 im=50, na=4,
 ngasr = 45,
 $end
 $frpcon
 cpl = 2., crdt = 0.0, thkcld = 0.0224, thkgap = 0.0033,
 dco = 0.374, pitch = 0.5,nplot=1,
 rc = 0.0453, fotmtl = 1.997,dishsd=0.06488,
 den = 94.43, dspg = 0.3,fa = 1.,
 dspgw = 0.03, enrch = 0.229, fgpav = 382, hdish = 0.011,
 hplt = 0.5, icm = 4, imox = 1, comp = 5.945,
 idxgas = 1, iplant =-2, iq = 0, jdlpr = 0,
```

```
jn = 5,5,
totl = 1.31, roughc = 3.94e-5, roughf = 7.9e-5, vs = 10.0,
nunits = 1, rsntr = 52., nsp = 1,
p2(1) = 44*2250., p2(45) = 6*2352,
tw(1) = 44*570, tw(45) = 6*590
go(1) = 50*2.0e6,
jst = 44*1, 6*2
qf(1) = 1.0, 1.0, 1.0, 1.0, 1.0
x(1) = 0.0, 0.3275, 0.6650, 0.9925, 1.31
qf(6) = 0.9, 1.0, 1.1, 1.0, 0.9
x(6) = 0.0, 0.3275, 0.6650, 0.9925, 1.31
ProblemTime=
0.1, 0.2, 0.3, 0.4, 0.5,
0.6, 30., 60., 90., 120.,
150., 180., 210., 240., 270.,
300., 331., 360., 390., 420.,
450., 480., 510., 540., 570.,
600., 625., 650., 700., 750.,
800., 850., 900., 945., 990.,
1000., 1050., 1100., 1150., 1200.,
1250., 1300., 1350., 1400
1401., 1402., 1403., 1404., 1405.,
1406.
qmpy =
1,2,3,4,5,
6., 6.7, 6.7, 6.7, 6.7,
5*6.7
6.7, 6.7, 7.0, 7.0, 7.0,
5*7.0,
7.0, 7.0, 7.0, 5.8, 5.8,
5*5.8,
5*4.11,
4.11, 4.11, 4.11, 4.11,
4.0, 3.5, 3.0,
2.5, 2.0, 1.5
slim = .05,
$end
$frpmox
enrpu39 = 65.83, enrpu40 = 23.45, enrpu41 = 7.39,
enrpu42 = 3.33
$end
```

Input Variables Arranged Alphabetically and by Input Block

$frpcn input block

Variable Name	Page Number
im	A-12
mechan	A-18
na	A-17
nce	A-18
ngasr	A-17
nr	A-17

$frpmox input block

Variable Name	Page Number
enrpu39	A-5
enrpu40	A-6
enrpu41	A-6
enrpu42	A-6
moxtype	A-5

$emfpcn input block

Variable Name	Page Number
imclad	A-20
imdens	A-20
imenrg	A-20
imfuel	A-20
imgapc	A-20
impowr	A-20
imrelo	A-20

$frpcon input block

Variable Name	Page Number	Variable Name	Page Number
amfair	A-9	imox	A-5
amfarg	A-9	imswch	A-20
amffg	A-9	iplant	A-10
amfh2	A-9	iq	A-13
amfh2o	A-9	jdlpr	A-21
amfhe	A-9	jn	A-13
amfkry	A-9	jnsurftemp	A-15
amfn2	A-9	jst	A-14
amfxe	A-9	jstsurftemp	A-16
b10	A-6	ngasmod	A-17
catexf	A-8	nopt	A-21
chorg	A-8	nplot	A-21
cladt	A-15	nread	A-22
cldwks	A-8	nrestr	A-22
comp	A-5	nsp	A-10
cpl	A-4	ntape	A-21
crdt	A-11	nunits	A-17
crdtr	A-11	p1	A-19
crephr	A-18	p2	A-10
crudmult	A-11	pitch	A-10
dco	A-4	ppmh2o	A-6
den	A-6	ppmn2	A-6
deng	A-7	ProblemTime	A-12
dishd	A-5	qend	A-18
dspg	A-4	qf	A-13
dspgw	A-4	qmpy	A-12
enrch	A-5	rc	A-5
fa	A-14	roughc	A-8
fgpav	A-9	roughf	A-7
flux	A-11	rsntr	A-7
fotmtl	A-6	sigcreep	A-19
frcoef	A-18	sigcor	A-19
gadoln	A-6	sigfgr	A-19
go	A-10	sigftc	A-19
hdish	A-5	sigftex	A-19
hplt	A-5	siggro	A-19
icm	A-8	sigh2	A-20
icor	A-11	sigswell	A-19
idxgas	A-9	sgapf	A-18
ifba	A-6	slim	A-18
ifixedtsurf	A-15	thkcld	A-4
igas	A-18	thkgap	A-4
igascal	A-18	totl	A-4
tsint	A-7	xt	A-15
tw	A-10	zr2vintage	A-8
vs	A-4	zrb2den	A-6
x	A-13	zrb2thick	A-6

FRAPCON-3 Auto Input Instructions

1. Open the file FRAPCON3_4_Auto_input.xls.
2. In the pop-up box click to enable macros.
3. If you would like to save the excel file, click file/save as to save as a different name.
4. In the "Input" worksheet, fill out all the values in red and blue for the specific case you are creating.
    a. Values shown in red are required input.
    b. Values shown in blue are not required and are often left as the default value shown.
    c. Units shown in red or blue can be changed using the drop down boxes.

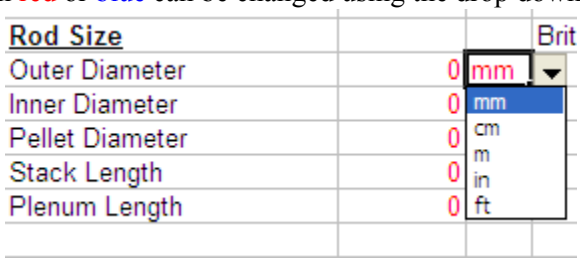

5. In the "Power History" worksheet, fill out the columns of Time or Burnup, Power, and power shape number to be used for each time step.

Time/Burnup

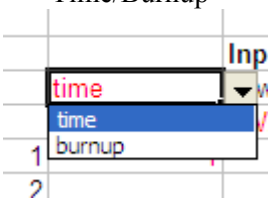

Power

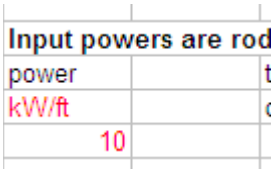

Axial Power Shape Number

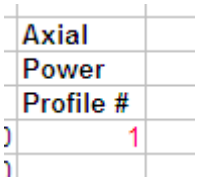

6. In the "Axial Power Profiles" worksheet, fill out the number of shapes to use for the run and the axial profile vs. elevation for each shape. The input shape will automatically be normalized to an average value of 1.0 in FRAPCON-3.
7. In the "Coolant Conditions" worksheet, select constant or time dependent coolant conditions, and fill out the appropriate table.
8. In the "FRAPCON-3 Input" worksheet, click on the button "Add time dependant variables." The FRAPCON-3 input file will be created in that Excel sheet.
9. Click on the button "Create Input File" to create a file in the directory and file name specified in the "Input Worksheet."

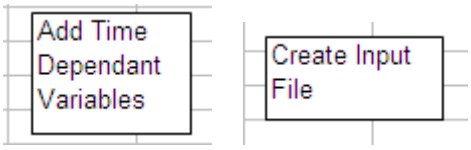

Appendix B

List of Subroutines in FRAPCON-3

Appendix B List of Subroutines in FRAPCON-3

The list of subroutines in FRAPCON-3 is given in Table B-1 and Table B-2, with a brief description of each subroutine. Table B-1 lists those subroutines from the MATPRO library. All of the MATPRO subroutines are distributed with FRAPCON-3.4, but not all of them are used as noted in the table. The evaluation models (EM) in this table refer to evaluation models that are included, but not recommended by PNNL. Table B-2 lists all the remaining subroutines (not found in MATPRO) in FRAPCON-3. Table B-3 lists those subroutines in the MECH library used for the finite element analysis mechanical package.

Table B-1 MATPRO subroutines in FRAPCON-3

Subroutine name	Model	Comments
CAGROW	Cladding axial growth	Models for PWR Zircaloy-4, M5 and ZIRLO and BWR Zircaloy-2
CANEAL	Calculates general annealing of cladding coldwork as a function of temperature and fluence	Called from top of FRPCON, (before gas iteration loop) once per time step—uses the axial average current flux
CANISO	Calculates coefficients of anisotropy to be used in stress-strain relationships for the cladding	Not used. No call.
CBRTTL	Calculates cladding embrittlement due to oxygen absorption	Not used. No call.
CCLAPS	Calculates a cladding collapse pressure	Not used. No call.
CCP	Cladding specific heat at constant pressure	Not used. No call.
CCRPR	Cladding creep strain rate	Not used. Replaced by CREPR.
CELAST	Cladding elastic compliance constants, based on orientation parameters	Not used. No call.
CELMOD	Cladding Young's modulus	Same correlation used for Zircaloy-2, Zircaloy-4, M5 and ZIRLO
CESIOD	Calculates cesium and iodine isotopes available in the gap	Not used. No call.
CFATIG	Fatigue constants and exponent for low and high cycle fatigue failure	Not used. No call.
CHITOX	Calculates Zr oxide and "xi" layer thickness – this is for high temperature oxidation only.	Not used. No call.

Subroutine name	Model	Comments
CHSCP	Addition of specific heat from dissolution of hydrides	Not used. No call.
CHUPTK	Cladding hydrogen uptake	Models for PWR Zircaloy-4, M5 and ZIRLO and BWR Zircaloy-2
CKMN	Strength coefficient and exponent	Updated properties based on PNNL database of Zircaloy mechanical properties
CMHARD	Cladding Meyer hardness as a function of temperature	Same correlation used for Zircaloy-2, Zircaloy-4, M5 and ZIRLO
CMLIMT	Calculates limit points of mechanical deformation	Not used. No call.
COBILD	High-temperature oxidation—layer thickness	Not used. No call.
CORROS	Cladding waterside corrosion	Models for PWR Zircaloy-4, M5 and ZIRLO and BWR Zircaloy-2
CSHEAR	Calculates shear modulus of cladding based on type and conditions	Same correlation used for Zircaloy-2, Zircaloy-4, M5 and ZIRLO
CSIGMA	True stress as a function of true strain	Not used. No call.
CSRUPT	Fraction increase in cladding diameter upon rupture	Not used. No call.
CSTRAN	True strain as a function of true stress	Not used. No call.
CSTRES	Effective stress as a function of true strain	Not used. No call.
CSTRNI	True strain as a function of initial true strain and local current stresses	Not used. No call.
CTHCON	Cladding thermal conductivity	Same correlation used for Zircaloy-2, Zircaloy-4, M5 and ZIRLO
CTHEXP	Cladding axial and diametral thermal expansion	Same correlation used for Zircaloy-2, Zircaloy-4, M5 and ZIRLO
CTXTUR	Calculates texture orientation parameters from basal pole figure data	Not used. No call.
EMCCP	EM model for cladding specific heat	Not used. No call.
EMCLEM	EM version of cladding elastic modulus	Not used. No call.
EMCPIR	EM version of cladding Poisson's ratio	Not used. No call.
EMCTON	EM version of cladding thermal conductivity	Not used. No call.

Subroutine name	Model	Comments
EMCTXP	EM version of cladding thermal expansion	Not used. No call.
EMFCP	EM version of fuel heat capacity	Not used. No call.
EMFEOD	EM version of fuel elastic modulus	Not used. No call.
EMFESS	EM version of fuel emissivity	Not used. No call.
EMFPIR	EM version of fuel Poisson's ratio	Not used. No call.
EMFTON	EM version of fuel thermal conductivity	Not used. No call.
EMFTXP	EM version of fuel thermal expansion	Not used. No call.
EMGTON	EM version of gas thermal conductivity	Not used. No call.
EMSTRN	EM version of cladding strain to rupture	Not used. No call.
FCP	Fuel specific heat	Include effects of plutonia and effect of gadolinia added
FCREEP	Fuel creep strain	Not used. No call.
FELMOD	Fuel elastic modulus	Not used. No call.
FEMISS	Fuel emissivity	
FFRACS	Fuel fracture stress	Not used. No call.
FGASRL	Fission gas release	Not used. Replaced by MASSIH, ANS54, and FRAPFGR.
FHOTPS	Fuel hot pressing	Not used. No call.
FPOIR	Fuel Poisson's ratio	Not used. No call.
FRESTR	Fuel restructuring	
FSWELL	Fuel swelling	Includes solid swelling only
FTHCON	Fuel thermal conductivity	Include effects of plutonia and effect of gadolinia added
FTHEXP	Fuel thermal expansion	
FUDENS	Fuel densification	
FVAPRS	Fuel vapor pressure	Not used. No call.
GTHCON	Gas thermal conductivity	
GVISCO	Gas viscosity	
PHYPRP	Contains UO_2 and $(U,Pu)O_2$ and Zircaloy melting points and heat of fusion and the zirconium and Zircaloy alpha and beta phase transition temperatures	
PROPID	Identifies material property module	
ZOEMIS	Zircaloy oxide emissivity	
ZOTCON	Zircaloy oxide layer thermal conductivity	Called from FRPCON

Table B-2 FRAPCON-3 subroutines in FRAP directory

Subroutine name	Description of subroutine or function
ANS54	Calculates fission gas release using ANS5.4 standard.
AXHEF	Calculates axial power shape factors.
BES2	Bessel functions used by TUBRNP.
BES	Not used.
BURNUP	Calculates burnup for node j.
CCREEP	Coordinates the cladding creep strep. Calls FCMI, which calls CLADF, which calls CREPR.
CEXPAN	Calls CTHEXP—the cladding thermal expansion function.
CHECK	Checks the input values and writes error messages
CLADF	Calculates cladding deformation of the free-standing cladding, including creep. Calls CTHEXP, STRAIN, and CREPR.
CLADRP	Calculates cladding ΔT; calls CTHCON (cladding thermal conductivity function).
CLDGRO	Calculates cladding incremental axial growth; calls CAGROW.
CLOCKX	Changes time to hh:mm:ss.
CONDUC	Calls GAPRS. Outputs gap conductance and gap temperature drop.
CONEU	Converts units.
COOLT	Calculates bulk coolant temperature and saturation temperature.
COUPLE	Outputs interfacial pressure. Class STRAIN, STRESS, and CREEP.
CRAP	Function that calculates effective stress as a function of creep rate strain.
CREEP	Finds correct value of stress for given creep increment.
CREPR	Calculates transverse cladding creep strain rate.
DRIVER	Calls IOFILES, ECHO1, and FRPCON.
ECHO1	Writes the input echo into the output file.
EDATE	Returns date as dd-mm-yy.
EFFCON	Computes the factor to be applied to the fuel conductivity to account for the effects of cracking for FRACAS-II only.
EMDNSF	Function to calculate fuel densification (EM option).
EMRLOC	Function to calculate relocation (EM option)
EMSSF2	Calculates emissivity factor for fuel-cladding gap. Calls ZOEMIS.
ENERGY	Calculates fuel stored energy at volumetric average temperature.
ERFAPPROX	Approximates values for the error function.
ERFD	Error function (called by ANS54 only).
FCMI	Does elasto-plastic analysis. Calls CLADF, GAPCLS, COUPLE.
FENTHL	Function to calculate enthalpy of fuel relative to absolute zero.
FEXPAN	Calculates thermal expansion of the fuel. Class FTHEXP.
FGASRE	Calculates gas release. Calls MASSIH, ANS54, or FRAPFGR.
FLMDRP	Calculates temperature drop across the film and the crud.
FORMFA	Function to calculate fuel ring averaged from factor or burnup.

Subroutine name	Description of subroutine or function
FRACAS	Calculates fuel and cladding mechanical states. Calls MEMSET, FCMI, and FCMI2.
FRAFORT	Contains subroutines and functions for calculation of stress and strain.
FRAPFGR	New fission gas release model.
FRPCON	Calls all major subcodes: SETUP, TEPEGN, CANEAL, STORE, BURNUP, BURBO, PHYPRO, GASPRO, COOLT, FLMDRP, CORROS, CHUPTK,CMLIMIT, CLADRP, FLUXD, CEXPAN, CLDGRO, MEMSET, TMPSUB, FEXPAN, SWELL, FRACAS, NEWGAP, CONDUC, VOLUME, GFASRE, ENERGY, TOTGAS PLNT, GSPRES, GASPLT, CCREEP, LPRT, PRINT2 PLTOUT, and RESTFS.
FUELTP	Calculates steady-state fuel temperature, Calls FTHCON, and EFFCON.
GAPCLS	Finds the point of pellet-cladding gap closure for mechanical analysis if close to closure for a given time step and axial node.
GAPRS	Computes gas conductance. Calls EMSSF2, FTHCON, CHTCON, and GTHCON.
GAPT	Function to calculate gap thickness. Calls CLADF.
GASPLT	Outputs radioactive gas release predicted by ANS54.
GASPRO	Computes the fission gas and helium production.
GDRADPOWHWR	Calculates radial power profile for UO_2-Gd_2O_3 fuel under heavy water reactor conditions.
GDRADPOWLWR	Calculates radial power profile for UO_2-Gd_2O_3 fuel under light water reactor conditions.
GRAFINI	Sets up variables for Excel plot routine.
GRAFOUT	Outputs values to file for Excel plot routine.
GRAINGRO	Calculates fuel grain growth for FRAPFGR.
GSPRES	Calculates rod internal gas pressure.
GTRLOC	Computes the radial outward relocation of the fuel pellet.
INITIAL	Initializes the program. Calls NEMSET, LACINPU, CHECK, TUBRIN, and PRINT1.
IOFILES	Reads input file. Calls EDATE and CLOCKX.
LACINP	Sets up lace option input.
LPRT	Stores average stresses and strains for use in summary printout.
MASSIH	Fission gas release model based on Forsberg-Massih model.
MEMSET	Fills pointer arrays (real variables).
NEMSET	Fills pointer arrays (integer variables).
NEWGAP	Calculates new estimate of gap temperature drop.
PGHEAD	Prints out program version identification at the top of every page. Calls PROPID and EDATE.
PLNT	Calculates plenum temperature and hot plenum volume. Calls CTHEXP and CTHCON and uses the fuel axial expansion from volume.
POINTR	Sets up index pointers. Calls NEWMSET, FR2PTR, and SETPNL.
POLATE	Interpolation routine.
PRINT1	Writes case setup output. Calls PGHEAD.

Subroutine name	Description of subroutine or function
PRINT2	Writes time-step and summary output. Calls PGHEAD.
PWRDEP	Not used.
REPACK	Not used.
RESTFS	Writes output for FRAPTRAN initialization.
SETPNT	Assigns correct point location ID.
SETUP	Reads and processes input and sets up pointers. Calls MEMSET, NEMSET, POINTER, INITIAL, and AXHEF.
SIMQ	Solves simultaneous linear equations.
STORE	Stores converged values of parameters.
STRAIN	Calculates uniaxial strain. Calls CSTRES and CSTRAN.
STRESS	Calculates stress. Calls CSTRES.
SWELL	Calculates fuel ring swelling and densification displacement. Calls FSWELL.
TAPEGN	Used if FRAPCON is reading or writing to a tape.
TERP	Function that interpolates to find values.
TMPSUB	Calculates fuel temperature distribution. Calls FUELTP.
TOTGAS	Calculates cumulative fission gas release, helium and nitrogen for entire rod.
TUBRNP	Calculates Pu buildup and radial power profiles as a function of burnup.
TURBIN	Calculates initial concentrations of $^{235, 238}$U and $^{239, 240, 241, \text{and}}$ ^{242}Pu. Calls TUBRNP.
TURBO	Calculates radial form factor used to calculation power and burnup. Calls TUBRNP.
VOLUME	Calculates rod internal void volume.

Table B-3 FRAPCON-3 subroutines in MECH directory used for the FEA option

Subroutine name	Description of subroutine or function
CLADDING	Cladding material properties
COMMON_PARAMETER	Stores common variables
COMPUTE_STATIC	Static FEA with Newton-Raphson iteration method
CONT1D	1D contact element
CONT2D	2D contact element
CONT3D	3D contact element
CREATE_COUPLED	Add DOF to the coupled set or create a new coupled set if it doesn't exist yet
CREATE_DISPL	Create forced DOF values for a coupled set
CREATE_GASCAV	Create or update gas cavity data
CREATE_NODE	Create node
CREPR2	Calculate cladding creep rate
DATA_GRID	Handle input data that is given in different mesh than what the finite element model uses
DEFAULT_VALUES	Set variables to their default values
DEL_NODE	Remove node entry from the database
EXH2C	Return excess H2 concentration at axial node ia
FILEO	Opening the input and output files
FORCED_DISPL	Modify force residual vector and stiffness matrix to take into account forced displacements

Subroutine name	Description of subroutine or function
FRAPCON_VARIABLES	FRAPCON specific variables
GASAV1D	1 1/2-dimensional axisymmetric gas cavity
GASAV2D	Axisymmetric 2D gas cavity
GASAV3D	3D gas cavity
GASAV_PRESSURE	Calculate pressures at gas cavities
GEOMETRY	Geometric and meshing entities
HEX8	Hexahedral 8-node brick element with mean dilation procedure 2x2x2 quadrature for the deviatoric part and mean dilation procedure for the dilational part
INIT	Initialize parameters and variables with default values
INIT_DISPL	Initialize displacements from the explicit values
INPUT_READ_ERROR	Report line number and stop program
LINESEARCH	Line search
LOAD_STEP	Calculate load and temperature increments
M5_CLADDING	M5 cladding material properties
MATERIALS	Material parameters
MATH	General purpose mathematical functions and subroutines
MECH	Driver subroutine for the finite element model of FRAPCON-3
MESH_FUEL_ROD	Create element mesh for a fuel rod and mark nodes and elements to correct groups
NLFEMP_DEALLOCATE	Deallocate all finite element variables
NLFEMP_STOP	Stop the calculation
NUCLEAR_FUEL	UO_2 fuel material properties
NUMBER_DOFS	Set status and number of all DOFs
PRESSURE1D	Axisymmetric pressure boundary element for SOLID1D element Nodes 1, 2, and 3 must be connected to the same solid element
PRESSURE2D	Axisymmetric pressure boundary element Nodes 1 and 2 must be connected to the same solid element
PRESSURE3D	3D pressure boundary element
QUAD4	Axisymmetric mean dilation Q4 element
READ_INPUT_LINE	Read next uncommented nonempty line from input line
READ_OUTPUT	Read restart file for the FE model from output unit
RUPTURE	Check for rupture of gas cavity
SOLID1D	1 1/2-dimensional axisymmetric SOLID1D element
SPARCE_DIRECT	Sparse matrix calculations for symmetric positive definite sparse matrix that has been stored in the row major storage format
SPARCE_MATRIX	Matrix calculations for symmetric or non symmetric sparse matrices with a symmetric non zero structure
SPRING	Spring: 2-noded two or three dimensional linear spring element (takes into account geometric nonlinearities)
TEMP_STORAGE	Store temperatures for output
TIME_STEP	Calculate load and temperature increments
UPDATE	Update explicit values
UPDATE_DATABASE	Create element database
UPDATE_DISPL	Update displacements after line search
WRITE_OUTPUT	Write restart/output file for the FE model to unit “out_unit”

Appendix C

Instruction for using Excel Plot Routine for FRAPCON-3

Appendix C Instruction for using Excel Plot Routine for FRAPCON-3

FRAPCON can create a separate plot file that can be read by an Excel plotting routine .

In the FRAPCON input file, add the variable nplot=1 under $frpcon.

```
  mechan = 2, ngasr = 45,
 $end
 $frpcon
   cpl = 4.0145, crdt = 1., crdtr = 0.0, thkcld=0.0243,
   dco = 0.4220, pitch = 0.505,
   den = 94.77, dishsd = 0.0504, thkgap=0.00375, dspg = 0.370,
   dspgw = 0.055, enrch = 6.42, fgpav = 200.01, hdish = 0.0135,
   hplt = 0.60, icm = 4, nplot = 1,
   icor = 0, idxgas = 1, iplant = -2, iq = 0, jdlpr = 0,fa = 1.0,
   jn = 15,15,15,15,15,15,15,15
   totl = 3.2, roughc = 1.97e-5, roughf = 2.36e-5, vs = 8.0,
   nunits = 1, rsntr = 101.9,
   flux(1) = 10*0.21e17, p2(1) = 2199.0, tw(1) = 491, go(1) = 2.1e6,
```

In the FRAPCON input file, add the plot file output name (unit=66) after the frapcon file output name (unit=6).

```
*****************************************************************************
* GOESINS:
FILE05='nullfile', STATUS='UNKNOWN', FORM='FORMATTED',
         CARRIAGE CONTROL='NONE'
*
* GOESOUTS:
FILE06='24I6.out',    STATUS='UNKNOWN', CARRIAGE CONTROL='LIST'
FILE66='stripf.br3', STATUS='UNKNOWN', FORM='FORMATTED',
        CARRIAGE CONTROL='LIST'
/*****************************************************************************
         Westinghouse BR-3 Rod 24I6
 $frpcn
   im=54, na=9, nr=17,
   mechan = 2, ngasr = 45,
 $end
 $frpcon
```

Run FRAPCON with the modified input file.

Open the Excel file Aplotter.xls. It must be located in the same folder as the plotting output file.

The warning seen below will appear. Click "Enable Macros" to enable the plotting macros.

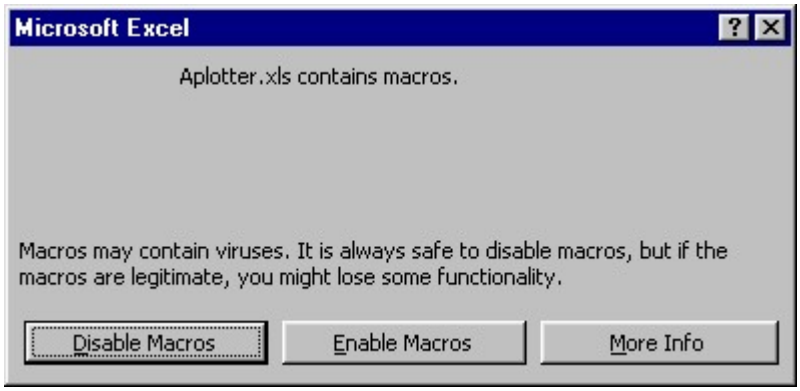

Type the name of the plot output file in cell D1 as indicated.

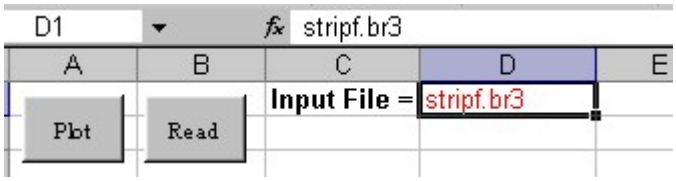

Press Enter and then click “Read.”

The values available for plotting will appear in the boxes below.

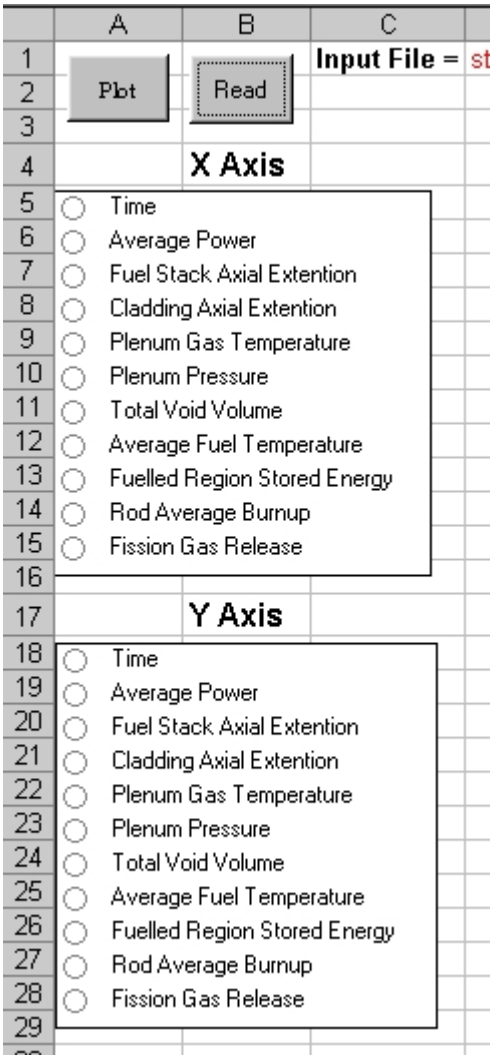

Select values to plot on the x and y axes and click “Plot.”

The values will be plotted in the chart on the left.

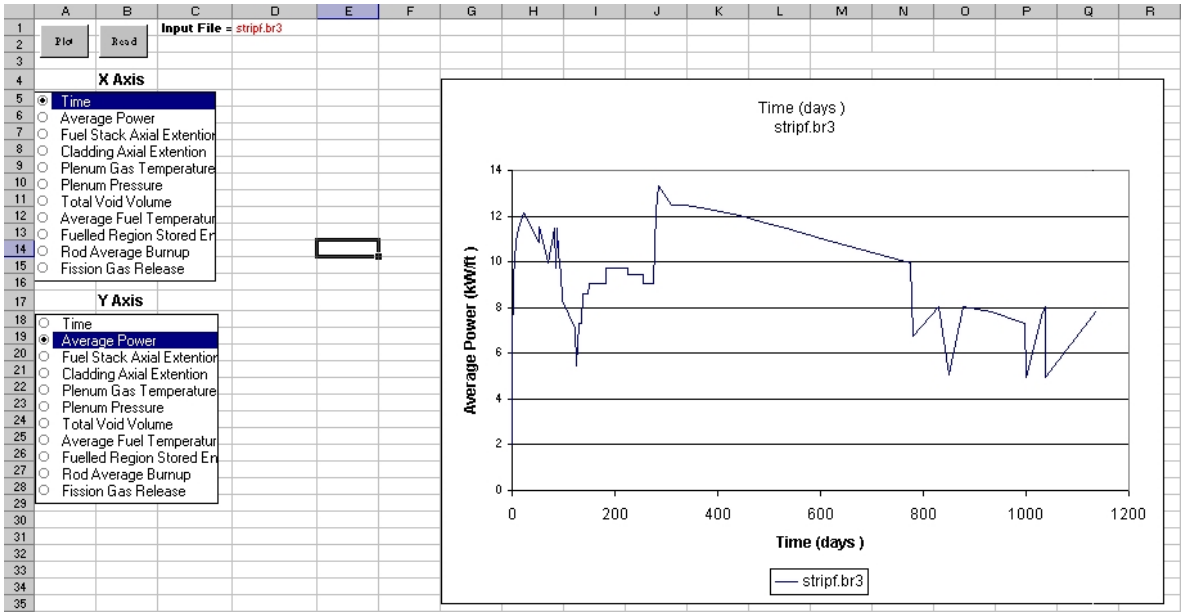

The tabs at the bottom of the sheet apply to other data that can be plotted.

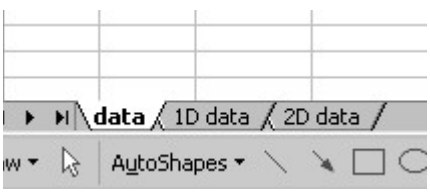

Click on them to go to the different data.

The tab, “1D data,” contains data for each axial node plotted as a function of time.

Select the value to be plotted.

Click “Plot” to plot this value for each axial node.

Click “Time An” to see an animation of the data with respect to time.

Click “Axial An” to see an animation of the data with respect to axial node.

Click "Chart Background" to toggle the background color from white to gray.

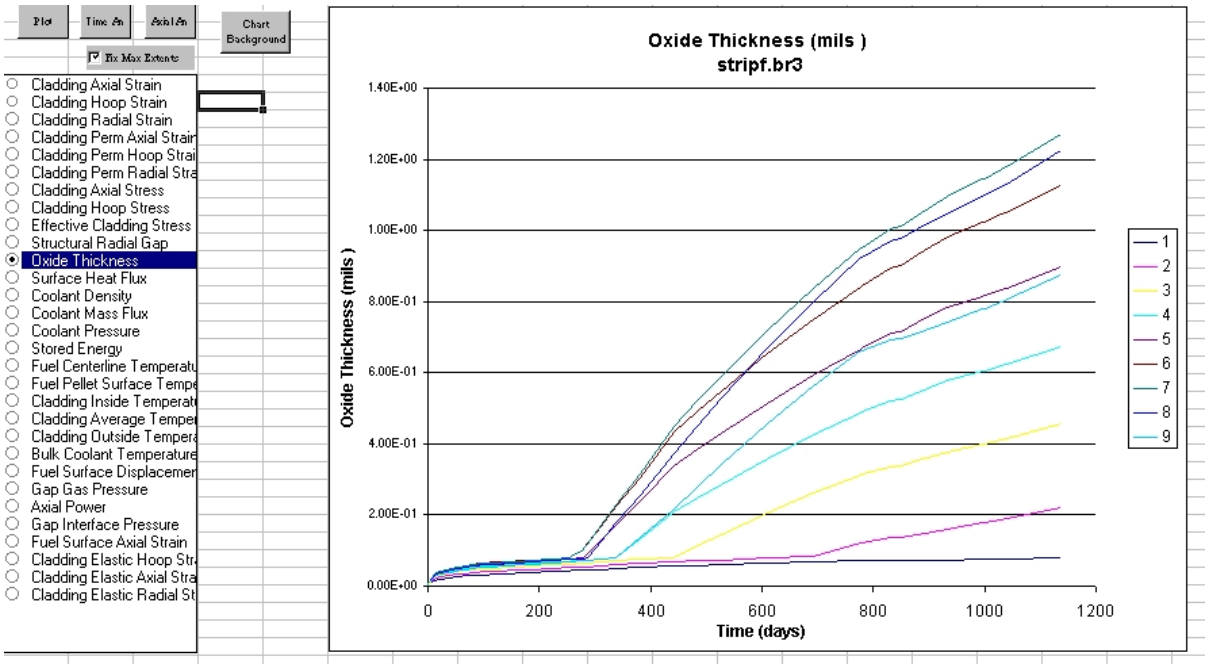

The tab, “2D data,” contains 3-D plots that can be animated.

Select the value to be plotted.

The animation speed can be changed with the slider bar.

Click “Animate” to start the animation.

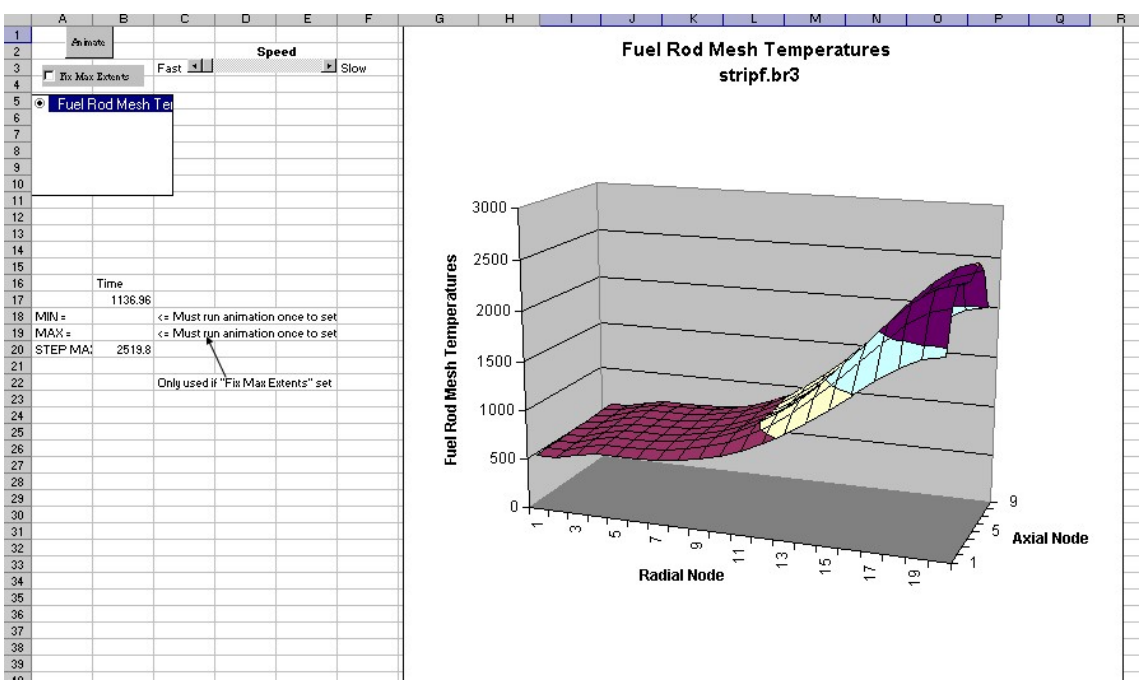

When you are finished, close the Excel file without saving or if you want to save some graphs, use the "save as" function to avoid overwriting the initial plot file.

NRC FORM 335
(9-2004)
NRCMD 3.7

U.S. NUCLEAR REGULATORY COMMISSION

BIBLIOGRAPHIC DATA SHEET

(See instructions on the reverse)

1. REPORT NUMBER
(Assigned by NRC, Add Vol., Supp., Rev., and Addendum Numbers, if any.)

NUREG/CR-7022, Vol. 1

2. TITLE AND SUBTITLE

FRAPCON-3.4: A Computer Code for the Calculation of Steady-State, Thermal-Mechanical Behavior of Oxide Fuel Rods for High Burnup

3. DATE REPORT PUBLISHED

MONTH	YEAR
March	2011

4. FIN OR GRANT NUMBER

NRC Job Code N6609

5. AUTHOR(S)

K. J. Geelhood, W.G. Luscher, C.E. Beyer

6. TYPE OF REPORT

Technical

7. PERIOD COVERED *(Inclusive Dates)*

8. PERFORMING ORGANIZATION - NAME AND ADDRESS *(If NRC, provide Division, Office or Region, U.S. Nuclear Regulatory Commission, and mailing address; if contractor, provide name and mailing address.)*

P.O. Box 999
Pacific Northwest National Laboratory
Richland, WA 99352

9. SPONSORING ORGANIZATION - NAME AND ADDRESS *(If NRC, type "Same as above"; if contractor, provide NRC Division, Office or Region, U.S. Nuclear Regulatory Commission, and mailing address.)*

Division of Systems Analysis
Office of Nuclear Regulatory Reserach
U.S. Nuclear Regulatory Commission
Washington DC 20555-0001

10. SUPPLEMENTARY NOTES

M.E. Flanagan, NRC Project Manager

11. ABSTRACT *(200 words or less)*

FRAPCON-3 is a Fortran 90 computer code that calculates the steady-state response of light-water reactor fuel rods during long-term burnup. The code calculates the temperature, pressure, and deformation of a fuel rod as functions of time-dependent fuel rod power and coolant boundary conditions. The phenomena modeled by the code include 1) heat conduction through the fuel and cladding to the coolant; 2) cladding elastic and plastic deformation; 3) fuel-cladding mechanical interaction; 4) fission gas release from the fuel and rod internal pressure; and 5) cladding oxidation. The code contains necessary material properties, water properties, and heat-transfer correlations. FRAPCON-3 is programmed for use on Windows-based computers, but the source code may be compiled on any computer with a Fortran 90 compiler.

The FRAPCON-3 code is designed to generate initial conditions for transient fuel rod analysis by the FRAPTRAN computer code.

This document describes FRAPCON-3.4a, which is the latest version of FRAPCON-3, released April 13, 2010.

12. KEY WORDS/DESCRIPTORS *(List words or phrases that will assist researchers in locating the report.)*

Nuclear fuel performance code
Fission gas release
Rod internal gas pressure
Fuel centerline temperature
Cladding hoop strain
High burnup licensing analysis

13. AVAILABILITY STATEMENT

unlimited

14. SECURITY CLASSIFICATION

(This Page)

unclassified

(This Report)

unclassified

15. NUMBER OF PAGES

16. PRICE

PRINTED ON RECYCLED PAPER

Printed
on recycled
paper

Federal Recycling Program

UNITED STATES
NUCLEAR REGULATORY COMMISSION
WASHINGTON, DC 20555-0001

OFFICIAL BUSINESS